Scholar Commons
USF University of South Florida

University of South Florida
Scholar Commons

Graduate Theses and Dissertations | Graduate School

10-31-2003

Mass Transfer of Ionic Species in Direct and Reverse Osmosis Processes

Silvana Melania Stefania Ghiu
University of South Florida

Follow this and additional works at: https://scholarcommons.usf.edu/etd

 Part of the American Studies Commons

Scholar Commons Citation
Ghiu, Silvana Melania Stefania, "Mass Transfer of Ionic Species in Direct and Reverse Osmosis Processes" (2003). *Graduate Theses and Dissertations.*
https://scholarcommons.usf.edu/etd/1371

This Dissertation is brought to you for free and open access by the Graduate School at Scholar Commons. It has been accepted for inclusion in Graduate Theses and Dissertations by an authorized administrator of Scholar Commons. For more information, please contact scholarcommons@usf.edu.

Mass Transfer of Ionic Species in Direct and Reverse Osmosis Processes

by

Silvana Melania Stefania Ghiu

A dissertation submitted in partial fulfillment
of the requirements for the degree of
Doctor of Philosophy
Department of Civil and Environmental Engineering
College of Engineering
University of South Florida

Major Professor: Robert P. Carnahan, Ph.D.
Marilyn Barger, Ph.D.
Venkat R. Bhethanabotla, Ph.D.
Kenneth A. Buckle, Ph.D.
Robert W. Flynn, Ph.D.
Noreen D. Poor, Ph.D.

Date of Approval:
October 31, 2003

Keywords: RO membranes, nanofiltration, diffusion, Spiegler-Kedem model,
Kimura-Sourirajan model, ion hydration

©Copyright 2003, Silvana M.S. Ghiu

DEDICATION

To my mother who has constantly urged for excellence, to my brother who had many answers to my questions throughout my years in school, and to my father who always has been a restless engineer.

ACKNOWLEDGEMENTS

I would like to express my everlasting gratitude to Dr. Robert Carnahan for providing me the ideal environment to carry on this doctoral program. I am very grateful to Dr. Carnahan for ensuring the financial support and for the technical guidelines throughout the years. Dr. Carnahan has had many words of encouragement and appreciation for me, and that kept me going through the difficult moments. He represents the professor I would like one day to become.

Very special thanks to Dr. Marilyn Barger for continuous technical advice, and for promptly answering all my anxious emails, while I was jammed in a theory or a research experiment. I am very thankful to Dr. Barger for proofreading this dissertation and many other technical papers and for setting very high standards for my work.

Many thanks to Bob Smith and Tom Gage for manufacturing several components of my experimental apparatus and to Catherine High for her timely help whenever it was needed. Last but not least, I am grateful to my friends Cola, Danielly, and Maysson for cheering me up and making this effort more bearable. I thank the Calintaru family for giving me a hand when I needed most.

TABLE OF CONTENTS

LIST OF TABLES

LIST OF FIGURES

LIST OF SYMBOLS

A	Pure water permeability when the membrane skin layer faces the high pressure side
A'	Pure water permeability when the membrane skin layer faces the low pressure side
C	Membrane constant in the Free Energy Theory
ΔC	Difference in the salt concentration across the membrane
C_{avg}	Average concentration of salt in the membrane
C_{DI}	Concentration of salt in the DI chamber in DO experiments
$(C_{DI})_{mem}$	Concentration of salt at the membrane wall in the DI side in DO experiments
C_{feed}	Concentration of salt in the feed solution in RO experiments
C_{prod}	Concentration of salt in the product water in RO experiments
C_{mem}	Concentration of salt at the membrane wall
C_{mem}^{max}	Concentration of salt at the membrane wall at $\sigma_1=1$
C_{mem}^{k}	Concentration of salt at the membrane wall calculated from film theory and Sherwood correlation
C_S	Concentration of salt in the salt solution chamber in DO experiments
$(C_S)_{mem}$	Concentration of salt at the membrane wall in the salt solution side in DO experiments
d	Thickness of the concentration boundary layer
D	Diffusion coefficient in membrane
d_h	Hydraulic diameter
D_w	Diffusion coefficient of salt in infinitely dilute solution
$(D/K\delta)_{DO}$	Salt permeability in DO experiments

$(D/K\delta)_{RO}$	Salt permeability in Kimura-Sourirajan model in RO experiments
e_0	Electron charge
E_{mem}	Value of parameter E at the membrane – solution interface
E_S	Value of parameter E in the solution
$F_{i,k}$	Generalized forces in Spiegler-Kedem model
ΔG_S	Free energy in the solution
ΔG_{mem}	Free energy at the membrane-solution interface
$\Delta\Delta G$	Free energy parameter, $\Delta\Delta G = \Delta G_{mem} - \Delta G_S$
h	Height of the flow channel
ΔH	Enthalpy of hydration
J_{conv}	Salt convective flux
J_{diff}	Salt diffusive flux
J_i	Generalized fluxes in Spiegler-Kedem model
J_S	Flux of salt in RO experiments (equal to J_{total})
J_{total}	Salt total flux, $J_{total} = J_{dfff} + J_{conv}$
J_v	Flux of product water in RO experiments
$J_{w,\,DO}$	Pure water flux in DO experiments
k	Back diffusion coefficient
K	Partitioning coefficient solution-membrane
k^{RO}	Back diffusion coefficient in Kimura-Sourirajan model
l	Width of the flow channel
L	Length of the flow channel
L_{ik}	Phenomenological coefficients in the Spiegler-Kedem model
L_p	Membrane hydraulic resistance

M_S	Salt molecular weight
n	2 for 1:1 salts and 3 for 1:2 salts
ΔN	Number of moles transported in DO experiments
n_w	Hydration number
N_A	Avogadro's number
P	Operating pressure
$P_{RO}^{(1)}$	Salt permeability in the first case of the Spiegler-Kedem model
$P_{RO}^{(2)}$	Salt permeability in the second case of the Spiegler-Kedem model
$P_{RO}^{(3)}$	Salt permeability in the third case of the Spiegler-Kedem model
R	Rejection coefficient
R_e	Reynolds number
R_g	Gas constant
R_h	Hydrated radii
R_i	Ionic radii
Q_P	Flow of product water
Q_F	Flow of feed water
S	Membrane surface area
ΔS	Entropy of hydration
S_c	Schmidt number
T	Absolute temperature
v	Feed flow velocity in RO experiments
V_w	Water molar volume
V_{DI}	Volume of water in DI vessel in DO experiments
X_{mem}	Molar fraction of salt at the membrane wall

X_{prod}	Molar fraction of salt in the product water
Z_i	Ionic charge
BW	Brackish water membrane
DO	Direct Osmosis
KS	Kimura-Sourirajan model
NF	Nanofiltration membrane
RO	Reverse Osmosis
SK	Spiegler-Kedem model
SW	Seawater membrane
α	Slope of the plot of concentration vs. time for the salt solution chamber
α_i	Number of moles of ion "i" in one mole of ionized salt
β	Slope of the plot of concentration vs. time for the DI chamber
δ	Membrane thickness
Δ_{mem}	Value of Δ at the membrane-solution interface
Δ_S	Value of Δ in the solution
$\Delta\pi$	Difference in osmotic pressure across the membrane
ε_S	Dielectric constant of the solvent
ϕ	Osmotic pressure coefficient
Γ_{DI}	Conductivity of the DI solution in DO experiments
λ_{salt}	Salt specific conductivity
ω	Salt permeability in Spiegler-Kedem model
π_{DI}	Osmotic pressure in the DI chamber in DO experiments
π_p	Osmotic pressure of the product water

π_{mem}^{DO}	Osmotic pressure at the membrane wall in DO experiments
Θ	Rate of free energy released per unit volume in Spiegler-Kedem model
σ_1	Reflection coefficient in Spiegler-Kedem model
σ_2	Salt-water coupling coefficient in Spiegler-Kedem model
τ	Duration of the DO experiments
(1), (2), (3)	Cases of the Spiegler-Kedem model

MASS TRANSFER OF IONIC SPECIES IN DIRECT AND REVERSE OSMOSIS PROCESSES

Silvana Melania Stefania Ghiu

ABSTRACT

This dissertation investigates the importance of diffusional and convective fluxes for salts in reverse osmosis (RO) and nanofiltration (NF) membranes. Moreover, the physical and thermodynamic factors controlling the salt permeability are analyzed. The study utilizes direct osmosis (DO) experiments and RO experiments, the later using both flat sheet and spiral wound membrane configurations. The salts considered are chlorides and acetates of alkali metals and alkaline earth metals.

The equation governing the salt transport in DO experiments is derived and a phenomenon inverse to concentration polarization in RO is observed. The salt permeability in DO is equal to the salt permeability calculated for the valid cases of the used RO models. DO is suggested as an alternative method in characterizing the salt transport in membranes. The method can be more advantageous than RO due to the lower costs and simplicity of the apparatus.

The models used to calculate the salt transport parameters in RO experiments are Spiegler-Kedem model, which considers both diffusion and convection of salt, and Kimura-Sourirajan model, which considers only diffusion of salt. It is found that diffusion is the dominant mechanism of transport in both RO and NF membranes. The percentage of the salt diffusional flux of the total flux is highest for seawater membranes and it is approximately equal for brackish water and nanofiltration membranes. The salt diffusive flux contribute more to the total flux for the 1:2 salts than for 1:1 salts. The two RO models are found equivalent in determining the salt permeability for only the seawater membranes. The

Kimura-Sourirajan model overestimates the salt permeability coefficient for salts with rejection coefficient lower than 86%.

The permeation rates for studied salts follow the lyotropic series regardless the membrane type (RO or NF), the membrane configuration (flat sheet or spiral wound), the process (DO or RO), or the models used for the calculations. This order of salt permeability is explained by the hydration of the cations, which is quantified by the enthalpy and entropy of hydration. The relative free energy theory can also be used to predict the salt permeability in a membrane based on preliminary data.

CHAPTER 1

INTRODUCTION

1.1 Importance of the research problem

In 1798, Samuel Taylor Coleridge wrote in The Rime of the Ancient Mariner “Water, water every where, Nor any drop to drink”. The old lyrics seem to be outdated by the present times, when reverse osmosis (RO) technology offers an efficient method of producing drinking water from seawater. With salty water constituting more than 97% of the Earth’s water resources, and in the context of world-wide increasing demands on fresh water supplies, the reverse osmosis solves the equation “salty water- salt = water” by using a non-polluting and sustainable method.

Reverse osmosis has been researched since 1940’s, but it was not until 1959 that the practicality of the RO process was demonstrated. In 1959, two students at UCLA, S. Loeb and S. Sourirajan, produced the first synthetic RO membrane from cellulose acetate polymer which was capable of rejecting the salt while passing the fresh water at reasonable flow rates. This discovery marked the beginning of the desalination industry using RO membranes. Similar membranes were later adopted in other fields, such as food industry, electronics, and pharmaceuticals.

Not all the salt is rejected in the RO processes. In the case of seawater desalination, a membrane rejection coefficient as high as 97%, which means that only 3% of the total salt passes through the membrane, is actually too low to produce water at the drinking water standards. For that reason, it is important to understand which transport mechanisms and what salt properties determine even very small amounts of salt to go through the membrane. Identifying the salt transport mechanism will not only provide reliable information for the RO

plant design, but it will benefit the development of membranes with superior selectivity. Moreover, recognizing the salt properties controlling the salt rejection makes possible to estimate the rate of salt permeability with a minimum amount of experimental work.

1.2 Research objectives and approach

Despite the early research developments conducted in the RO desalination field, and even though the RO processes are well implemented in practical applications, the mechanism of salt and water separation in RO membranes is not well understood. There is controversy over the importance of the salt diffusive flux, which is due to a concentration gradient across the membrane, and the salt convective flux, which is caused by the salt-water coupling effect.

The objectives of this dissertation are first, to identify what transport mechanism is dominant in hyperfiltration membranes, and second, to confirm the physical and thermodynamic factors controlling the permeation rate of salts through hyperfiltration membranes. The approach considered in answering the first research question is outlined below:

- Compare the salt permeability coefficient in the direct osmosis (DO) process, for which there is no convective salt flux, with the salt permeability in RO process, for which both diffusional and convective salt fluxes may occur. A new equation for the salt transport in DO needs to be developed;
- Calculate the percentage of salt diffusional flux of the total flux in RO using the Spiegler-Kedem model, which quantifies both the diffusive and the convective salt fluxes. Identify the consequences of model simplification which often occurs in the literature;
- Compare the salt permeability obtained from two RO models, the Spiegler – Kedem model, which quantifies both the diffusive and the convective salt

fluxes, and Kimura-Sourirajan model, which assumes that diffusion is the only mechanism of salt transport in hyperfiltration membranes;

- Perform the above calculations and comparisons for three types of hyperfiltration membranes: seawater membrane, brackish water membrane and nanofiltration membranes. Also, the salt transport is studied for three 1:1 salts and three 1:2 salts. It is expected that the importance of the salt diffusional flux depends on the membrane type and the salt valence.

In order to address the second research question, the approach is as follows:

- For the salts with common anion, the relationship between the salt permeability and physical and thermodynamic properties of the cations is investigated. The physical properties of the cations are ionic radii and hydrated radii, and the thermodynamic properties are ionic enthalpy and entropy of hydration. The values of the cation ionic and hydrated radii, as well as ionic enthalpy and entropy of hydration are taken from the literature.
- The salt permeability of both chlorides and acetates is compared to the salt diffusivity in infinitely dilute solution, which is calculated based on ions diffusivity coefficients and the ionic charge.
- The relative free energy parameter is calculated according to the literature for each chloride salt and the exponential relationship between the salt permeability and the relative free energy parameter is verified.

1.3 Dissertation outline

Chapter 2 of this dissertation is divided in two parts. The first part presents general information related to hyperfiltration membranes as well as direct osmosis and reverse osmosis processes. The second part of this chapter presents a critical review of the previous

research in the area related to this dissertation. The need for additional research is highlighted.

Chapter 3 presents the experimental apparatus, the operating conditions and operating procedure for direct reverse osmosis experiments, along with a description of the instrumentation and the membrane manufacturer specifications. For reverse osmosis experiments, two membrane configurations are used: flat sheet and spiral wound.

In Chapter 4 of this dissertation, the results obtained for direct osmosis are presented, followed by the results from the RO flat sheet membrane and the results from the RO spiral wound membranes. The section on the direct osmosis experiments presents first the derivation of the equation used in calculating the salt permeability coefficient, $(D/K\delta)_{DO}$, along with the values obtained for $(D/K\delta)_{DO}$ in the case of two seawater membranes, one brackish water and one nanofiltration membrane. The results from the RO flat sheet membrane experiments are interpreted from the perspective of two models: the Spiegler-Kedem (SK) model and the Kimura-Sourirajan (KS) model. The KS model is used to determine the salt and water transport parameters in the case of RO spiral wound membrane experiments. The transport parameters for the salt and pure water are compared with the transport parameters obtained from the RO flat sheet membrane experiments.

Chapter 5 discusses the experimental results and their implications. The first section presents a correction of the equation derived in the previous chapter for the salt transport in direct osmosis experiments. It addresses the concentration at the membrane wall as well as the transport of pure water in direct osmosis assuming that the salt and the water fluxes do not interact within the membrane. The second section of this chapter discusses the salt transport parameters $P_{RO,}$ σ_1 and σ_2 as well as the importance of the salt diffusive flux in the Spiegler-Kedem model. The third section compares the two models, the Spiegler-Kedem model and

the Kimura-Sourirajan model. The comparison addresses both the salt and the water transport parameters and defines the situations when the two models can be used interchangeably. The fourth part of this chapter brings together the salt permeability from the direct osmosis experiments and the reverse osmosis experiments. It is shown that the salt permeability is the same in direct osmosis and reverse osmosis, therefore it does not depend on the operating pressure applied.

The last part of the Chapter 5 analyzes what physical and thermodynamic parameters control the salt permeability in RO and NF membranes. There is a certain pattern of variation for the salt permeation among the six studied salts regardless the membrane type (RO or NF), the membrane configuration (flat sheet or spiral wound), the type of the experiment (DO or RO), or the model used in calculating the salt permeability (Spiegler-Kedem or Kimura-Sourirajan). This pattern is explained by any of the parameters measuring the degree of the hydration for the cations (hydrated radii, enthalpy and entropy of hydration). The relative free energy can be used to predict the permeability of salts in a certain membrane based on known values of the several other salt permeabilities in the membrane. Chapter 6 draws the conclusions and the implications of this research and Chapter 7 presents a set of recommendations for continuation of this research.

CHAPTER 2

RO MEMBRANE FILTRATION: INTRODUCTION AND RELEVANT PREVIOUS RESEARCH

This Chapter is divided in two main parts. The first part presents general information related to membrane reverse osmosis (RO) filtration. It introduces the hyperfiltration membranes and the direct and reveres osmosis processes, it describes the two RO models used in this dissertation and discusses the importance of concentration polarization.

The second part presents a critical review of research undertaken to date on the topics addressed in this research. The previous studies on salt and water transport in direct osmosis are presented first. The controversy in the existing literature on the distribution of the salt flux (diffusive and convective) is described next. A comparison of the transport parameters for two RO models, the solution-diffusion model and the Kedem-Katchalsky model, is addressed. Last, previous work in identifying the factors controlling the salt permeability in hyperfiltration membranes is described briefly.

2.1. Background information

Information similar to that presented in this section can be found in numerous publications describing hyperfiltration membranes and processes. References are made only occasionally and mainly when information is specific to a source.

2.1.1 Hyperfiltration membranes

A membrane is defined as a thin film which acts as a separation barrier to the transport of matter. All types of membranes have one common characteristic: limited the passage of some chemical species while allowing others to pass through. Membranes are

more often defined by what they do rather than what they are. According to the solute exclusion size, the pressure driven membranes used in liquid-liquid separation are divided in microfiltration, ultrafiltration, nanofiltration and reverse osmosis membranes.

Hyperfiltration membranes refer to membranes used in reverse osmosis (RO) and nanofiltration (NF) processes. The two processes are based on the same principles and they are often treated together. Nanofiltration membranes are the same as RO membranes, except that the network structure of the membrane polymer is more open in the NF membranes. Reverse osmosis membranes are further divided in sweater and brackish water membranes. Most NF membranes have a net negative charge on the surface which influences the membrane rejection.

The RO and NF membranes typically reject species with radii as small as 10^{-10} m (ionic range), or in terms of molecular weight, they reject low molecular weight solute such as inorganic salts and small organic molecules like glucose and sucrose (Mulder, 2003). A summary of the characteristics of the two types of membranes is presented in Table 2.1.

Table 2. 1. Comparison of the characteristics of RO and NF membranes (Baker, 1991).

Characteristics	Reverse Osmosis (RO)		Nanofiltration (NF)
	Seawater (SW)	Brackish Water (BW)	
Typical water source	Oceans and Seas	Surface Water Groundwater	Surface Water Groundwater
Source solution concentration (%)	1-5	0.2-0.5	0.05
Rejection NaCl	99.5	97	60
Rejection $MgCl_2$	99.9	99	89
Operating pressure (psi)	800-100	300-500	100-150

According to membrane morphology, the vast majority of the hyperfiltration membranes used in currently practice are anisotropic. They consist of a very thin and dense

layer, called the skin layer, and a support layer, which is thicker and more porous. The thickness of the skin layer represents about 1% of the thickness of the support layer. The support layer functions only as mechanical support for the skin and it has a negligible resistance to mass transfer (Mallevialle et al., 1996).

The anisotropic membranes are divided in asymmetric and thin film composite membrane (TFC). A schematic drawing of the two anisotropic membrane types is presented in Figure 2.1. The layers in asymmetric membranes are made of the same material. Conversely, for the thin film composite membranes, the skin and the support layers are made of different materials.

The most common configurations of the hyperfiltration membranes for industrial practices are spiral wound and hollow fine-fiber, while flat sheet membranes are commonly used in laboratory studies. The spiral-wound membranes are manufactured by rolling membrane envelopes that are glued to a center tube which collects the product water. The membrane envelopes are made by folding a flat sheet membrane over a permeate carrier mesh, with the skin layer of the membrane facing outside of the fold. A diagram of a spiral wound membrane is presented in Figure A.7. The hollow fine-fiber membranes consists of a bundle of fine tubes which are folded into an U-shape and the free ends are epoxy-casted in one end of a pressure tube.

The skin layer of RO and NF membranes is typically made of organic polymers such as cellulose acetate (CA) and cellulose acetate derivatives such as cellulose triacetate, polyamide (PA) and polyamide derivatives. The CA membranes are more hydrophilic than PA membranes and present higher resistance to fouling. However, they are susceptible to hydrolysis, especially at pH outside the range 4 to 6.5, and biological degradation. They compact under high operating pressure. The PA membranes have lower flux permeability

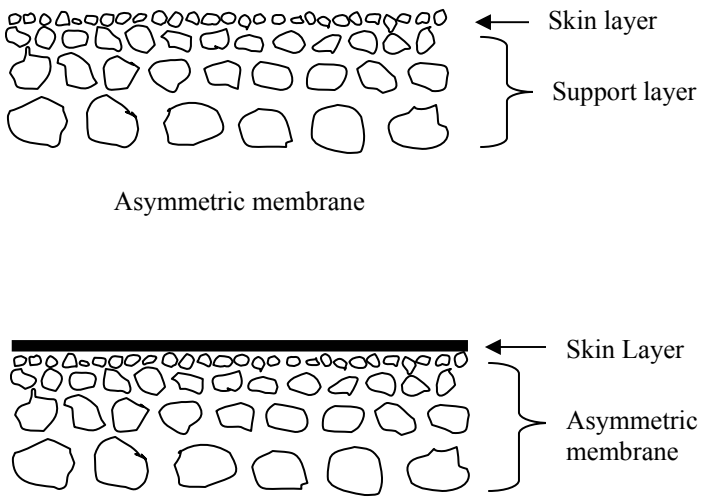

Figure 2. 1. Schematic drawing of anisotropic membranes (Mallevialle et al., 1996).

than the CA membranes but they have superior selectivity. They also can be operated at wider pH range and are more stable to biological degradation. However, PA membranes are susceptible to oxidative degradation. Their compaction at high operating pressure is reduced.

2.1.2 Direct and reverse osmosis processes

Figure 2.2 presents the solvent (water) and solute (salt) fluxes in direct osmosis (DO) and reverse osmosis (RO). The membrane is permeable to the solvent and ideally, impermeable to the solute. In DO, due to the differences in the chemical potential across the membrane, the solvent from the low concentration side diffuses to the high concentration side until the equilibrium of chemical potential is reached. Practically, a small amount of the solute is transported through the membrane via diffusion, in DO, and due to diffusion and convection, in RO. The real difference in the osmotic pressure across the membrane in DO is not $\Delta\pi$ but $\sigma\Delta\pi$, where σ is the reflection coefficient which accounts for the membrane

permeability to solutes. The reflection coefficient is discussed in Section 2.1.3.1. When an external pressure, ΔP, larger than the modified osmotic pressure, $\sigma\Delta\pi$, is applied to the high concentration side, the direction of the solvent flux is reversed. In practical applications, ΔP has to be at least two times higher than $\sigma\Delta\pi$. It ranges from 150 psi to 350 psi for NF processes and from 200 psi to 1200 psi for RO processes, depending on the solute concentration.

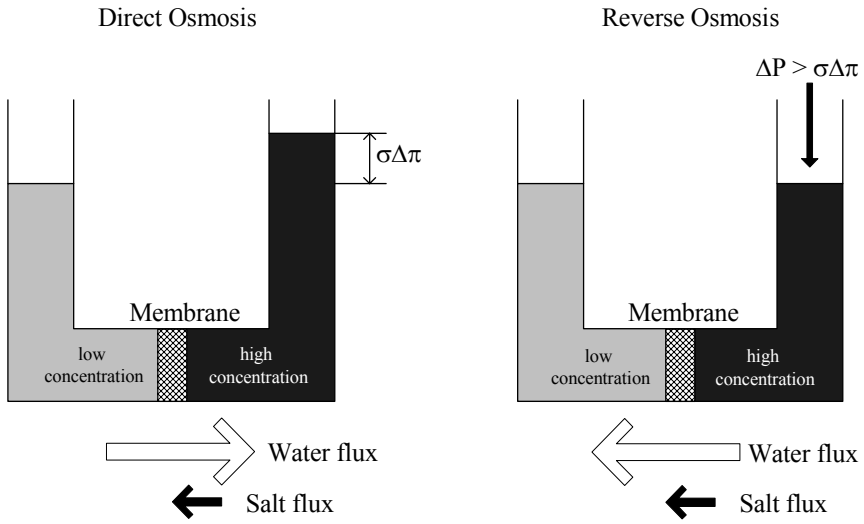

Figure 2. 2. Schematic drawing of water and salt fluxes in direct and reverse osmosis.

Direct osmosis has not been studied to a large extent due to the limited number of practical applications of this process. Some studies has shown the application of DO in concentrating liquid food and in food concentrate for emergency supply of drinking water in lifeboats (Kessler and Moody, 1976; Petrotos et al., 1998; Petrotos et al., 1999; Petrotos and Lazarides, 2001). Direct osmosis does have importance for research in determining the osmotic pressure and the transport coefficients through a membrane (Rautenbach and Albrecht, 1989).

Alternatively, reverse osmosis has been studied intensively for more than 50 years and has a large spectrum of applications. About 50% of the RO systems currently installed produce drinking water from seawater and brackish water (such as ground water and surface water). Another 40 % produce ultrapure water for electronics, pharmaceutical and power generation industries. The remaining 10% of the RO systems are involved in special applications such as wastewater treatment and food processing (Baker, 2000). Since hyperfiltration membranes reject toxic and biologic agents, the RO and NF processes are also used by the military. Nanofiltration membranes are used in special applications such as color removal and water softening.

2.1.3 Reverse osmosis models

Although the RO processes have been studied for more than 40 years and have been well implemented in practical applications for 20 years, the mechanism of solute separation from the solvent in the membrane is still a matter of controversy. The two models presented in this Chapter are selected based on the credibility they have among the researchers as well their domination in practical applications. The two models are conceptually different. The Spiegler-Kedem model is based on irreversible thermodynamics and introduces the explicit terms ω and σ as coefficients to characterize the transport of salt due to diffusion and convection. Alternately, the Kimura-Sourirajan model is a mechanistic membrane model which considers that the solute is transported through the membrane solely by diffusion. It defines the salt permeability coefficient, $(D/K\delta)$, starting from Fick's law of diffusion applied to membranes.

2.1.3.1 Spiegler-Kedem (SK) model

The SK model is based on irreversible thermodynamics. Since the membrane structure and the mechanism of transport within the membrane are not known, the membrane is considered a "black box" which separates two phases in non-equilibrium states. The system is divided in small subsystems for which local equilibrium exists. The rate of free energy released per unit volume is given by Equation 2.1

$$\Theta = \sum_{i=1}^{n} J_i F_i \tag{2.1}$$

where Θ is the free energy dissipated per unit volume, and J_i and F_i are the generalized fluxes and forces, respectively. For sufficiently slow processes taking place in membranes, the fluxes are linearly proportional to the conjugated and non-conjugated forces, as expressed in Equation 2.2:

$$J_i = \sum_{k=1}^{n} L_{ik} F_k \qquad (i = 1, 2, ..., n) \tag{2.2}$$

where L_{ii} are the "straight" coefficients of proportionality for the conjugated forces and L_{ik} are the "cross" coefficients of proportionality for the non-conjugated forces. Substituting Equation 2.2 in 2.1 yields to Equation 2.3 which can be satisfied if $L_{ii} \geq 0$ and $L_{ii} \cdot L_{kk} \geq (L_{ik})^2$ (Bitter, 1991):

$$\Theta = \sum_{i=1}^{n} \left(\sum_{k=1}^{n} L_{ik} F_k \right) F_i > 0 \tag{2.3}$$

The SK model leads to Equations 2.4 and 2.5 which describe the fluxes of product water and of salt through the membranes:

$$J_v = L_p(\Delta P - \sigma_1 \Delta \pi) \tag{2.4}$$

$$J_S = \omega \Delta \pi + (1-\sigma_2) J_v C_{avg} \tag{2.5}$$

$$C_{avg} \equiv \frac{C_{mem} + C_{prod}}{2} \tag{2.6}$$

where J_v is the product water flux ($mL \cdot cm^{-2} \cdot s^{-1}$), L_p is the membrane hydrodynamic resistance ($mL \cdot cm^{-2} \cdot s^{-1} \cdot psi^{-1}$), ΔP is the operating pressure (psi), σ_1 is the reflection coefficient, $\Delta\pi$ is the difference in the osmotic pressure across the membrane (psi), J_S is the total flux of salt permeating the membrane ($mol \cdot cm^{-2} \cdot s^{-1}$), ω is the salt permeability coefficient ($mol \cdot cm^{-2} \cdot s^{-1} \cdot psi^{-1}$), σ_2 is the coefficient of coupling between salt and water, and C_{avg} is the average salt concentrations across the membrane ($mol \cdot L^{-1}$), defined by Equation 2.6 (Mason and Lonsdale, 1990).

The coefficient σ_1 is the Staverman reflection coefficient defined by Equation 2.7 and describes how effective the salt is in developing an osmotic pressure across the membrane. It is a indicator of the membrane selectivity and has values between 0 and 1. A reflection coefficient of 1 corresponds to ideal membranes where there is no solute transport (or rejection coefficient equal unity), and 0 for entirely unselective membranes (Spiegler, 1966).

$$\sigma_1 \equiv \lim_{J_v \to 0} \left(\frac{\Delta P}{\Delta \pi} \right) \tag{2.7}$$

The coefficient σ_2 is zero for perfect coupling (solute convective transport is dominant) and it is unity when there is no coupling solute-solvent (pure diffusive solute transport). The large majority of the research papers considers $\sigma_1 = \sigma_2$, based on the validity of Onsager reciprocal relationship. However, the equality of $\sigma_1$and σ_2 has to be proven experimentally for each separation system.

The first term in Equation 2.5 represents the flux of salt due to diffusion ($J_{diff} \equiv \omega \cdot \Delta\pi$) whereas the second term ($J_{conv} \equiv (1-\sigma_2)J_v C_{avg}$) is the flux of salt due to convection. Since the the osmotic pressure is given by $\pi = \phi n R_g T \Delta C$, the term $\omega\Delta\pi$ can be expressed as $P_{RO}\Delta C$, where $P_{RO} \equiv \omega \Delta\phi n R_g T$. The term $\Delta\phi$ is the difference in the osmotic coefficient ϕ across the membrane, n is the sum of salt valences, R_g is the gas constant, and T is the absolute temperature. The coefficient P_{RO} is introduced in this research for the purposes of an easier comparison of the salt transport coefficients in the Spiegler-Kedem model and Kimura-Sourirajan model. The units for P_{RO} are ($cm \cdot s^{-1}$). Substituting ω for P_{RO} in Equation 2.5 yields to Equation 2.8:

$$J_S = P_{RO}\Delta C + (1-\sigma_2)J_v C_{avg} \tag{2.8}$$

The parameters of transport which need to be determined in the Spiegler–Kedem model are L_P, σ_1, σ_2 and P_{RO}. Equations 2.4 and 2.8 can be rearranged as Equations 2.9 and 2.10, respectively, which allow the calculations of the transport parameters using a graphical method. For example, L_P and σ_1 are the intercept and the slope, respectively, of the line represented by the Equation 2.9. Similarly, P_{RO} and σ_2 are the slope and the intercept of the line represent by Equation 2.10.

$$\frac{J_v}{\Delta P} = L_P - \sigma_1 \frac{\Delta\pi}{\Delta P} \tag{2.9}$$

$$\frac{J_S}{J_v C_{avg}} = \frac{\Delta C}{J_v C_{avg}} P_{RO} + (1-\sigma_2) \tag{2.10}$$

The Spiegler-Kedem model has the main advantage of quantifying both the diffusional and the convective fluxes of the salt through the membrane. The disadvantage of this model is that in does not provide any information on the actual mechanism of separations in hyperfiltration membranes.

2.1.3.2 Kimura-Sourirajan model (Preferential sorption-capillary flow model)

The preferential sorption-capillary flow model was introduced in 1970 by Kimura and Sourirajan. It is also referred in the literature and in this dissertation as Kimura-Sourirajan model. This model assumes that the solvent and the solute fluxes do not interact with each other and are transported through the membrane by different mechanisms. The membrane skin layer is assumed to be microporous and heterogeneous and the mechanism of separation is governed partly by surface phenomena and partly by fluid transport under pressure through capillary pores. When a pressure is applied to the system, salt and water tend to permeate through the micropores but water is adsorbed into the pores whereas salt is rejected (preferential adsorption of water on the membrane surface due to the physicochemical nature of the surface layer). The water is transported through the capillary pores in a viscous flow whereas the salt is transported due to pore diffusion. The pore size, their shape and number, together with the composition of the surface layer are critical parameters in the separation process. The model uses the film theory to calculate the back diffusion coefficient, k (Appendix E).

The expressions for water and salt fluxes through the membrane are given by Equations 2.11 and 2.12:

$$J_v = A\,(\Delta P - \Delta\pi) \tag{2.11}$$

$$J_S = \left(\frac{D}{K\delta}\right)_{RO} \Delta C \tag{2.12}$$

where J_v is the product water flux ($mL \cdot cm^{-2} \cdot s^{-1}$), A is the pure water permeation ($mL \cdot cm^{-2} \cdot s^{-1} \cdot psi^{-1}$), ΔP is the operating pressure (psi), $\Delta\pi$ is the difference in the osmotic pressure across the membrane (psi), J_S is the flux of salt permeating the membrane ($mol \cdot cm^{-2} \cdot s^{-1}$), $(D/K\delta)_{RO}$ is the salt permeability coefficient ($cm \cdot s^{-1}$), and ΔC is the difference in salt

concentration across the membrane ($mol \cdot L^{-1}$). The salt permeability coefficient takes into account the diffusivity coefficient of the salt through the membrane, D, the partitioning of salt concentration between the bulk solution and the membrane, K, and the membrane thickness, δ. The model considers $(D/K\delta)_{RO}$ as an intrinsic parameter which is not calculated by dividing the diffusivity coefficient to the product of the partitioning coefficient times the membrane thickness.

The algorithm proposed by Sourirajan (1970) to calculate the salt permeability is described by the Equations 2.13 through 2.15:

$$J_v = \frac{Q_{prod}}{S\left(1 + \frac{C_{feed}(1-R)M_S}{1000}\right)} \tag{2.13}$$

$$\pi_{mem} = P + \pi_{prod} - \frac{J_v}{A} = \phi n R_g TC_{mem} \tag{2.14}$$

$$\left(\frac{D}{K\delta}\right)_{RO} = \frac{J_v}{\left(\frac{1-X_{prod}}{X_{prod}}\right)\left(C_{mem}X_{mem} - C_{prod}X_{prod}\right)} \tag{2.15}$$

where J_v is the water flux ($mL \cdot s^{-1} \cdot cm^{-2}$) which cannot be measured when the feed is a salt solution, Q_{prod} is the measured product flow ($mL \cdot s^{-1}$), S is the membrane surface area (cm^2),R is the rejection coefficient defined by $R \equiv 1\text{-}C_{feed}/C_{prod}$, M_S was the salt molecular weight (g/mol), X_{mem} and X_{prod} are the salt mole fraction given by $X_i = C_i /(C_i + 55.5)$ at the membrane wall and in the product, respectively. The salt concentration at the membrane wall, $C_{mem,}$ as well as the mole fraction, $X_{mem,}$ in Equation 2.15 are obtained from Equation 2.14. One of the advantages of this model is the explicit dependence of pure water permeation and solute permeability on operating conditions such as temperature and pressure. The main

disadvantage of the model is that it assumes diffusion being the only mechanism of salt transport.

2.1.4 Concentration polarization

Concentration polarization occurs in any pressure driven membrane separation process. It describes an increase in the concentration at the membrane wall due to the rejection of ionic species transported there by the convective flux, J_{feed}. Figure 2.3 shows the solute fluxes in the bulk solution (J_vC_{feed}) and permeating in a direction perpendicular to the membrane (J_S), as well as the velocity and concentration polarization profiles between two parallel membranes. It is an undesirable phenomenon which results in the increase of the osmotic pressure at the membrane wall and consequently, a reduction in the product flux and the membrane rejection coefficient. In the polarized layer, the concentration of sparingly soluble salts such as $CaCO_3$ and $CaSO_4$ in a feedwater can increase so much locally that they exceed their solubility limit, precipitate and form a scale on the membrane surface.

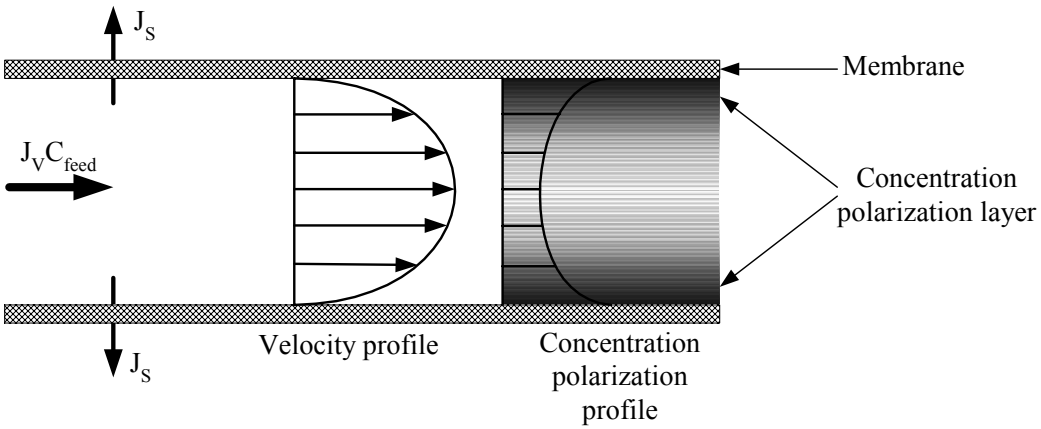

Figure 2. 3. Fluid flow and concentration polarization between two parallel membranes.

The concentration gradient at the membrane wall (Figure 2.3) controls the diffusion of the rejected species back into the bulk solution. The thickness of this boundary layer is established at the equilibrium of three fluxes: the salt convective flux, the salt flux through the membrane, and the salt back diffusive flux. The concentration at the membrane wall is calculated in the literature either by using the resistance layers approach or more often, by combining the film theory with the correlations for the back diffusion coefficient, k (Baker, 2000). Details of the later method are given in Appendix E.

2.2 Previous research on the transport parameters in hyperfiltration membranes

This section presents the findings of an extensive search on the previous relevant work performed in the past 40 years. Despite the progress made in the RO separation field in the past 20 years, the older information is found to be just as valuable as more recent ones. The relevant subjects for this dissertation are the salt and water transport in direct and reverse osmosis, as well as the factors controlling the salt rejection and permeability in hyperfiltration membranes.

2.2.1 Salt and water transport in direct osmosis

The literature of membrane separation is scarce when in the area of salt and water transport in direct osmosis processes. In most of the research papers, transport parameters in direct osmosis are addressed in parallel to and compared with the transport parameters in reverse osmosis. This approach is consistent with one of the objectives of this dissertation.

The research on direct and reverse osmosis conducted by Sherwood et al. (1967) has an historical importance. In 1967, RO was not yet commercialized and the two models later to become classic models, Spiegler-Kedem and Kimura-Sourirajan, were not yet largely used. The authors used the solution-diffusion-imperfection model, which assumes that both salt and

water are transported through the membrane by parallel processes of diffusion and pore flow in RO, and by diffusion in pores and polymer matrix, in DO. The DO experimental apparatus consisted of a diffusion cell with two chambers separated by a cellulose acetate membrane. Individual NaCl and $CaCl_2$ solutions were recirculated through one chamber and DI water was recirculated through the other chamber, both at high circulations rate to assure a good mixing.

The water and salt permeability were determined graphically and compared with the manufacturer specifications for RO. The concentration at the membrane wall was considered equal to the concentration in the bulk solution. The manufacturer specifications for RO were found 1 to 4 times lower than in DO for water permeability and 18 to 23 times lower than in DO for salt permeability. The differences were attributed to the membrane compaction under high operating pressure in reverse osmosis.

Lonsdale et al. (1971) has studied the salt and water transport in a DO experiment by using a stirred Plexiglass cell with two chambers separated by a lab-made symmetrical cellulose acetate membrane. One chamber was filled with a NaCl 5 wt -% salt solution and the other chamber contained DI water. The authors determined the salt permeability from the steady–state transport and Equation 2.12 (referred in the literature as time lag method), using the conductivity readings in the DI water chamber. The pure water permeation was determined based on the water flux measured by collecting the overflow from the NaCl chamber, and using Equation 2.11 with $\Delta P = 0$. The authors considered the salt concentration at the membrane wall equal to the salt concentration in the bulk solution.

The transport parameters determined in the DO experiments were compared with the transport parameters determined from a classic lab-scale RO experiment, when the operating pressure was 1500 psi. The Kimura-Sourirajan model was used to calculate the salt and water

permeability in the RO experiments. The salt rejection coefficient was found 98.6%. The thickness of the membrane, measured with a Federal Products Corporation Thickness gauge, was of 70 μm. A good agreement was found between the transport parameters in DO and RO. The authors concluded that the salt-water coupling is not of fundamental importance for the transport of NaCl through the membrane.

A different set of DO experiments were conducted by Matsuda and Kamizawa (1984). The authors used a countercurrent type cell which assured a constant difference in the concentration across the membrane. The pure water flux was reduced to zero by using NaCl solution on one side of the cell and sucrose solutions (which is highly rejected) on the other side of the cell. The concentration of NaCl was adjusted so that the two solutions had the same osmotic pressure. The salt permeability was calculated using Equation 2.5 from the Spiegler-Kedem model, taking J_v equal zero. The pure water permeability was calculated by applying Equation 2.4 for the systems NaCl-DI water and sucrose-DI water. Ten lab-made asymmetric cellulose acetate membranes were used, with different rejection coefficients. The water and salt permeability from DO were compared to the salt and water permeability in RO, calculated also from Spiegler-Kedem model. The authors reported very good agreement of the transport parameters in DO and RO for membranes with rejection coefficients higher than 94%.

Mori et al. (2000) performed experiments with NaCl solutions and lab-made symmetric cellulose acetate membranes using a DO experimental setup similar to the one described above for Lonsdale's research. The diffusivity coefficient, determined using the time lag method, increased with the increase in the salt concentration, and the extrapolated value of diffusivity at zero salt concentration was taken to determine the salt permeability in DO. The salt permeability in DO was calculated as the product of the diffusivity and the

distribution coefficient, determined in an independent adsorption experiment. The values of the salt permeability in DO experiments were in good agreement with the values of the salt permeability in RO experiments calculated from Spiegler-Kedem model.

Another comparison of the salt transport parameters in DO and RO processes was performed by Chaudry (2002). He used a symmetric lab-made RO cellulose acetate membrane and 0.025 to 0.2 $mol \cdot L^{-1}$ feed solutions of NaCl and KCl. In DO experiments, the salt permeability was calculated as the product of the diffusion coefficient with the salt distribution coefficient, defined as the inverse of the salt partitioning coefficient K from the Kimura-Sourirajan model. The diffusion coefficient was calculated from the time lag method whereas the salt distribution coefficient was calculated from the limiting transport numbers of the cations and anion, respectively. In RO experiments, the salt permeability was calculated using the Spiegler-Kedem model. He found that the salt permeability in RO was almost twice as much as the salt permeability in DO. Further experiments with crystal violet Millipore filter paper has proved that this difference can not be attributed to the leaks in the membrane. He concluded that the differences in the salt permeability in DO and RO were a result of the high convective flux of salt (38 %) in the cellulose acetate membrane.

2.2.2 Salt and water transport in reverse osmosis

The literature describing theory and practice of reverse osmosis is abundant. Each topic addresses its own niche of interest, whether it regards membrane transport properties, calculations of concentration polarization and back diffusion coefficients, scaling and fouling, design of RO systems or manufacturing of novel membranes. The topic of interest for this research is the importance of diffusional and convective fluxes of salt in hyperfiltration membranes. This section is divided in two parts. The first part presents the previous work on quantification of the salt diffusive and convective fluxes. The second part summarizes a

research study which compared the Kedem-Katchalsky model with the solution-diffusion model.

2.2.2.1 Diffusion and convection in hyperfiltration membranes

In a review of the reverse osmosis membrane and transport made by Soltanieh and Gill (1981), it is concluded that since the diffusion of salt through the membrane is slow, the contribution of pore flow, and therefore the convective flux, is significant. The developments in the membrane manufacturing technology resulted in the production of pore-free membranes (actually, with pores size < 1nm), with improved rejection coefficients. In a more recent book edited by Malleviale et al. (1996), hyperfiltration membranes (reverse osmosis and nanofiltration) are referred to as diffusion controlled membranes.

The Spiegler-Kedem model allows one to estimate the importance of the salt diffusive flux by calculating the percentage of the salt diffusive flux of the salt total flux. The calculation of the salt flux distribution is simple once the transport coefficients L_p, P_{RO}, σ_1 and σ_2 are determined. A rough estimation of the importance of the diffusive flux is given by the salt –water coupling coefficient, σ_2. Some authors concluded that diffusion is the dominant transport process whenever the calculated salt-water coupling coefficient, σ_2, is close to unity, without carrying out the calculations to determine the salt flux percentages (Marinas and Selleck, 1992; Urama and Marinas, 1997).

Gilron et al. (2001) studied the transport of 1500 ppm and 15,000 ppm NaCl in commercial polypiperazine nanofiltration membrane. According to the manufacturer, the rejection of NaCl by this membrane is 70%. The feed flux varied approximately between 20 $Lm^{-2}h^{-1}$ to 100 $Lm^{-2}h^{-1}$. The Spiegler-Kedem model was used to calculate the relative distribution of the salt flux through the membrane. The authors found that at least half of the salt flux is due to convective coupling, with the diffusive flux decreasing with the increase in

the feed flux. The relative distribution of NaCl flux in a commercial RO membrane (FT 30 produced by FilmTec) was studied by Bhanushali et al. (2002), who found a very low contribution of the salt convective flux to the salt total flux.

Chaudry (2002) used the Spiegler-Kedem model to calculate the percentage of diffusive and convective fluxes in symmetric lab-made cellulose acetate membranes. He found that 62.9% of the total flux for KCl and 57% for NaCl is attributed to diffusion transport. He calculated that less than 1% of the total salt flux is due to ion-exchange capacity of the membrane and concluded that the rest of about 38.5% is due to the salt convective flux. The average values of σ_2 found by Chaudry at 25 ^{o}C were 0.931 for NaCl and 0.954 for KCl. There is no indication in this research paper whether the concentration polarization was considered or not in the application of the Spiegler-Kedem model.

2.2.2.2 Comparison of RO models

McCray et al. (1991) had compared the salt and water transport properties in asymmetric cellulose acetate membranes with different acetyl content using two RO models. The first model, named the Kedem-Katchalsky model, is derived from irreversible thermodynamics and provides an identical set of transport equations as the Spiegler-Kedem model described in Section 2.1.3.1. The second model, named the solution-diffusion model, assumes no convective salt flux, and it provides an identical set of transport equation with the Kimura-Sourirajan model, described in Section 2.1.3.2.

The authors varied the acetyl content of the cellulose acetate membranes by hydrolyzing commercial reverse osmosis cellulose acetate membranes. They found that both water and salt permeabilities increased, and the rejection coefficient and the salt-water coupling coefficient decreased with the decrease in the membrane acetyl content. The calculated water permeability was the same for both models regardless the membrane acetyl

content. The calculated salt permeability was the equal for the two models only for unhydrolyzed membranes, when the salt-water coupling coefficient was closed to unity. As the membranes underwent hydrolysis, the membrane rejection coefficient decreased and the salt-water coupling increased. Consequently, the differences in the salt permeabilities from the two models increased, with a higher salt permeability for the solution –diffusion model than for the Kedem-Katchalsky model. The differences were attributed to the increase in the salt convective flux which is not accounted for in the solution-diffusion model.

2.2.3 Factors controlling the selectivity of salts in hyperfiltration membranes

Taniguchi and Kimura (2000) have calculated the permeability in a commercial RO spiral wound membrane for different 1:1 and 1:2 chloride and sulfite salts as well as for the boric acid. The authors compared the permeability of the ions with their diffusivity in water. They found that except for the boric acid, the ion permeability increased with the increase in the ion diffusion coefficient in water.

Several research papers have studied the dependence of the rejection coefficient for inorganic salts with common anion on the physical and thermodynamic properties of the cations. Johnson (1975) considered the rejection of chloride salts of eighteen heavy metal in lab-made cellulose acetate RO membranes. The author reported that the percentage of the metal removal increases with the decrease in the cation free energy of hydration and with the increase in the cation entropy at infinite dilution. Also, the cation partial molal volumes at infinite dilution were directly correlated to the metal rejections. The author concluded that thermodynamic solution properties were the controlling factors for the selective rejection of the heavy metal.

Similar results were reported by (Fang and Chian, 1975; Fang and Chian, 1976). They studied the rejection of several alkali and alkali-earth halogen salts in cellulose acetate

and aromatic polyamide membranes. The rejection of ions with the same valence increased with the decrease in the ionic radii and with the increase in the cation entropy of hydration. It was concluded that the enthalpy of hydration of an ion could be used as a single parameter to determine the ionic rejection in a membrane.

Matsuura et al. (1975) and Dickson et al. (1975) introduced the relative free energy of a salt as the parameter which controls the salt permeability in both cellulose acetate and aromatic polyamide RO membranes. The relative free energy of an ion is the difference in the free energy of the ion at the membrane surface and in the bulk solution. The sign of the relative free energy determines whether an ion is attracted or repelled by the membrane. The permeability of a salt varies exponentially with the weighted sum of the relative free energy parameter of the salt ions.

2.2.4 Conclusions on the previous relevant research

The result reported in the literature on the comparison of salt permeability in RO and DO are controversial. Sherwood et al. (1967) has found larger permeation rate in the DO experiments than in the RO experiments, whereas Chaudry (2002) reported lower salt permeability in DO than in the RO. Finally, Lonsdale et al. (1971), Matsuda and Kamizawa, (1984), and Mori et al. (2000) calculated equal salt permeability coefficients for the two processes. Several methods of calculating the salt permeability in DO are used in the literature, which might be the source of the contradictory results. Moreover, most of the research conducted in DO disregards the phenomena of salt dilution occurring at the membrane surface.

In 1981, Soltanieh and Gill summarized the findings of the current research at that time and concluded that since the diffusion of salt though the membrane is slow, the contribution of the convective flux is significant. Fifteen years later, Mallevialle et al. (1996)

referred to hyperfiltration membranes (which are RO and nanofiltration membranes), as diffusion controlled membranes. Gilron et al. (2001) has found that in a nanofiltration membrane with a rejection coefficient of 70%, at least half of the salt total flux is due to convection. Chaudry (2002) determined that the salt diffusion fluxes in RO membranes contributed by 57% to 63% to the total salt flux. Opposing, Bhanushali et al. (2002) reported that the convective salt flux in RO membranes is insignificant. According to McCray et al. (1991), the solution-diffusion model and the Kedem-Katchalsky model provided the same salt permeability only for membranes and salts with a rejection coefficient larger than 94%. These contradictions on the importance of the salt diffusive and convective fluxes originate in improper, simplified usage of the theoretical models.

The rejection of several inorganic salts in RO processes has been reported to increase with the increase in the cation hydration radii and increase in the cation enthalpy and entropy of hydration. The relative free energy has been introduced in 1975 as a parameter that controls the solute permeability in hyperfiltration membranes. These theories can be useful in predicting the salt permeability in hyperfiltration membranes and need to be verified for the new types of commercial available membranes.

CHAPTER 3

METHODOLOGY

This chapter describes the technical procedure utilized in performing the experimental part of this research. The chemical preparation and the instrumentation are described first followed by the experimental procedures. The types of experiments are:

- a direct osmosis (DO) study
- a reverse osmosis study (RO) using a flat sheet membrane
- a reverse osmosis study (RO) using a spiral wound membrane

For each experiment type, a diagram of the equipment set-up is shown with each component briefly described. The details of the test cells are presented in this chapter and the detailed drawings of the cells are included in Appendix A. The description of each type of experiment contains a summary table of the membranes used for that stage and their manufacturer specifications, as well as the salts solutions used as feedwater, their concentration and the system operating parameters. The operation of each experimental set-up is described in separate subsections. The sampling and the measurement protocols, as well as the procedure for the replicate runs are presented for each type of experiment.

3.1 Chemicals Preparation

The feedwater for all the experiments is prepared using deionized (DI) water and analytical grade salts from Fisher Scientific. DI water is produced from tap water using a lab scale RO unit. The conductivity of the product is 20±5 μS. Only simple binary solutions are considered in this research. The concentration of the solutions is calculated from the conductivity measurements using specific conductance for each salt at specific temperature

and concentration. The specific conductance for the salts is taken from the Handbook of Chemistry and Physics (1967).

3.2 Instrumentation

The instrumentation used is presented in Table3.1 together with calibration requirements, manufacturer, readings range and accuracy. The sensors presented in Table 3.1 are connected to a computer for data collection and analysis using a LabPro interface and a LoggerPro software acquired from Vernier Software & Technology.

Table 3. 1 Instrumentation and its specifications.

Nr.	Instrument	Manufacturer	Model	Calibration Required	Range	Accuracy
1	Analytical Balance	Mettler Toledo	Delta Range AE 260	No	0-81g	0.1mg
2	Digital Caliper	Fowler	ProMax	No	0-150mm	±0.02 mm
3	Conductivity Probe	Vernier Software &Technology	Conductivity Probe	Yes	0-200µS/cm 0-20000µS/cm	± 1%
4	Conductivity Meter &Probe	Cole-Parmer	Field Cole-Parmer Conductivity Meter/	Yes	0-2 µS/cm 0-20 µS/cm 0-200 µS/cm 0-2000 µS/cm	± 0.2% ± 0.15% ± 0.1% ± 0.15% ± 0.30%
5	Flowmeter	McMillan	Model 111	No	20-200 mL/min 100- 2000 mL/min	± 3%
6	Pressure Gauge	Wika	13x.53	No	0-1000 psig	± 0.15%
7	Pressure Transmitter	Cole-Parmer	Economical ±0.25% Accuracy Pressure Transmitter	No	0-1000 psig	± 0.25%
8	Stopwatch	Cole-Parmer	Easy-Grip Stopwatch	No	24 h	±1.5 s/day
9	Electronic Toploading Balance	Ohaus	Adventurer	No	0-3100g	±0.1g

Table 3. 1 (Continued) Instrumentation and its specifications.

Nr.	Instrument	Manufacturer	Model	Calibration Required	Range	Accuracy
10	Thermistor	Vernier Software &Technology	Stainless Steel Temperature Probe	No	-25 ^{O}C to 125^{O}C	±0.3%
11	Voltage Probe	Vernier Software &Technology	Voltage Probe	No	-10 to 10V	± 0.05%
12	Volumetric Flask	Kimble	Serialized and Certified Class A with Stopper	No	0-10 mL	±0.2%
13	Volumetric Flask	Kimble	Serialized and Certified Class A with Stopper	No	1000 mL	±0.03%

3.3 Direct osmosis experiments

The diffusion experiments are conducted under controlled laboratory conditions at the ambient temperature of 23±0.5 ^{o}C. The diffusion apparatus consists of a diffusion cell, a peristaltic pump, DI and salt solution vessels, magnetic stirrers, tubing and the instrumentation. A diagram of the direct osmosis experimental set-up is presented in Figure 3.1.

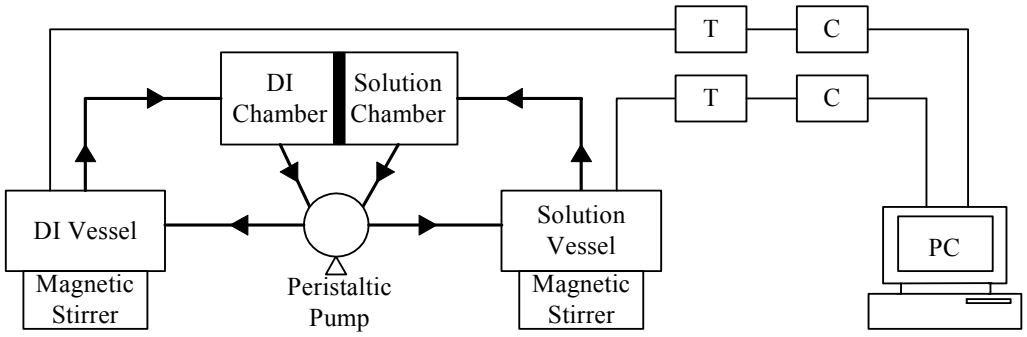

Figure 3. 1 Experimental set-up for the direct osmosis experiments.

The diffusion cell is machined from stock (acrylic) in the University of South Florida, College of Engineering Shop. It consists of two chambers, the salt solution chamber (Figure A.1) and the DI water chamber (Figure A.2). The dimensions of the cell body are 18.9 cm x 14 cm x 5.8 cm. The height of the flow channel is of 0.2 cm in both chambers. The membrane separates the two chambers and has an effective surface area of 88.7 cm^2. The skin layer of the membrane faces the solution chamber and the support layer faced the DI chamber. A spacer is placed in the flow channel of each chamber. The spacer is a diamond shaped mesh made of polypropylene with dimensions of 7 cm x 12.6 cm.

The circulation of DI water and salt solution is maintained at constant flowrate of 187 mL/min using a two head peristaltic pump (model Masterflex®L/S from Cole-Parmer®). DI water and salt solution vessels are covered 4.7 liters Nalgene® cylindrical jar baths. Holes are drilled in the cover of each solution vessel to allow the insertion of tubes and instrumentation. Each vessel sits on a magnetic stirrer and one magnetic stir bar is introduced in each vessel to maintain complete mixing throughout the run. The tubing used is flexible Tygon®Lab from Norton. All the piping is 1/4". A set of conductivity and stainless steel temperature probes is inserted in each of the two solution vessels. The data is recorded by a PC for further analysis using a computer interface and a software, as described in Section 3.2.

3.3.1 Diffusion cell operation

DI water is pumped from the DI water vessel to the DI water chamber and back to the DI water vessel whereas the salt solution is pumped from the salt solution vessel to the salt solution chamber and back to the salt solution vessel. Initially, 2 liters of salt solution is prepared as described in Section 3.1 and poured into the salt solution vessel and also 2 liters of DI water is poured in the DI water vessel.

Both the DI water vessel and the salt solution vessel are weighted in the beginning of each run. The DI water vessel and the salt solution vessel are weighted again at the end of each run to determine the volume of water that diffused through the membrane from the DI vessel to the solution vessel. The weight measurements for the DI water vessel and the salt solution vessel at the end of the runs is performed after both chambers of the diffusion cell and the tubing are emptied and the emptied water is pored back to the corresponding vessels.

The difference in the mass of water lost from the DI vessel and the mass of water gained in the solution vessel is due to evaporation. Half of the total evaporated water m_{evap} is considered to come from the DI vessel and half from the solution vessel. The total water mass considered to diffuse to the solution vessel is calculated as the sum of two terms: 1) the difference in the weight of the solution vessel between the beginning ($m_{w,\,t=0}$) and the end of the run and ($m_{w,\,t=\tau}$) 2) half of the total water evaporated. The water flux $J_{w,\,DO}$ is calculated by dividing mass of the total water diffused by the duration of a run τ (600 minutes) and by the active surface area of the membrane S (88.7 cm^2), as shown in Equation 3.1. It represents an average of the pure water flux over the duration of a run.

$$J_{w,DO} = \frac{\left(m_{w,t=\tau} - m_{w,t=0}\right) + \frac{1}{2} m_{evap}}{S\tau} \tag{3.1}$$

The membranes studied in the direct osmosis experiments are presented in Table 3.2, together with their characteristics and manufacturer specifications. Four flat sheet membranes are considered in this study: a seawater aromatic polyamide membrane (AD), a seawater aromatic polyamide -thin film composite membrane (SE), a brackish water cellulose acetate membrane (CG), and a nanofiltration cellulose acetate membrane (CG), all produced

by GE Osmonics. The membranes are selected based on their differences in the product flux and salt rejection: the cellulose acetate (CA) is a high water production but low rejection membrane whereas the polyamide (PA) is a low water production but high rejection membrane. The membrane types are representatives of the two general categories of RO membranes used in practice today. Each membrane is cut from a one square foot sheet (929 cm^2) in order to fit the diffusion cell and stored for 24 hours in fresh DI water at room temperature to keep the membrane saturated.

Table 3. 2 Manufacturer specifications for the membranes used in the direct osmosis experiments.

Membrane Manufacturer Name and Application	Membrane Polymer	pH Range	Typical Product Flux gfd @ psi ($mL \cdot m^{-2} \cdot min$ @ atm)	Rejection %
AD -Seawater	PA	4-11	15 @ 800 (425 @ 54)	99.5
CG -Brackish Water	CA	2-8	30 @ 420 (849 @ 29)	92
CK -Nanofiltration	CA	2-8	28 @220 (792 @ 15)	92 for divalent
SE -Seawater	TFC	2-11	22 @ 425 (623 @ 29)	98.9

Note: The typical product flux and the rejection are given for 2000 $mg \cdot L^{-1}$ NaCl feed solution at 25°C.

The salt solutions and their concentrations for the direct osmosis runs are presented in Table 3.3. The solutions are prepared as described in Section 3.1. The conductivity probes are calibrated before each run using two standard solutions provided by Oakton. Conductivity and temperature measurements are automatically taken every minute for duration of 10 hours corresponding to each run. The data is stored in a computer and used for further analysis. Concentrations are evaluated from the conductivity readings. The system is cleaned after each

Table 3. 3 Salt solutions and their concentrations in the direct osmosis experiments.

Salts	Salts Concentration ($mol \cdot L^{-1}$)			
	SE	AD	CG	CK
LiCl	0.01, 0.02, 0.05, 0.1, 0.15, 0.2	0.05	0.05	0.05
NaCl				
KCl				
$MgCl_2$	0.02, 0.05, 0.1			
$CaCl_2$				
$BaCl_2$	0.05			
LiAc	0.05, 0.1			
NaAc				
KAc				
$MgAc_2$				
$CaAc_2$				

Note: Ac represents the acetate ion CH_3COO^-.

run by rinsing the diffusion cell and the tubing with DI water until the conductivity of the effluent water is the same as the conductivity of the DI water.

Duplicates for the direct osmosis runs for each membrane type are conducted by replacing the membrane with a new piece cut from the same one square foot sheet used in the first run. Duplicate salt solutions are run in the same order as for the first run for each particular membrane.

3.3.2 Determination of pure water permeability coefficient, A'

A very similar apparatus with the one described in Section 3.4 is used to determine the pure water permeability A' for the membranes used in the direct osmosis experiments. The only difference is that the RO flat sheet membrane cell is replaced by a replica cell made in the University of South Florida, College of Engineering Shop. The replica cell accommodates membranes with the same dimensions as the membranes used in the direct osmosis experiments (active surface area of 88.7 cm^2).

After the direct osmosis runs are finished for all the salts for a membrane, the membrane is rinsed with DI water and placed in the replica cell, with the skin layer facing the permeate side of the cell. The membranes are not conditioned for these runs. The feed water

is DI water. The operating pressures for all four membranes are 300 psi, 250 psi, 200 psi, 150 psi and 100 psi, respectively. The pulse dampener is set at half the operating pressure. The product sampling and the measurements of the product flowrate are performed at each operating pressure as described in Section 3.4.1.

3.4 Reverse osmosis flat sheet membrane experiments

A conventional lab scale RO apparatus is used to carry out the reverse osmosis experiments. The apparatus consists of a flat sheet membrane cell, a high-pressure pump, a pulsation dampener, a feedwater tank, a refrigerated recirculator, needle valves, and instrumentation. A diagram of the apparatus is presented in Figure 3.2. The flat sheet membrane cell is made of stainless steel and it is manufactured by Osmonics (model Sepa CF). The cell body dimensions are 16.5 cm x 21.3 cm x 5.2 cm. Diagrams of the bottom and top side of the cell are presented in Figure A.4 and Figure A.5, respectively. The bottom side of the cell is referred as the high pressure of feed side and the top side is referred as the low pressure or permeate side. The cell is held in a steel holder which with 6 steel bolts to seal the membrane compartments. The holder is made in the University of South Florida, College of Engineering Shop. The active surface area of the membrane is 139 cm^2. The feed channel height is 0.2 cm. No feed spacer is used in the flat sheet runs.

The bottom side of the cell is fed by a high-pressure diaphragm pump model M-03-E, made by Hydra-cell which provides a flow of 8.3 $L{\cdot}min^{-1}$. Flexible stainless steel tubing is used to connect the pump to the cell. Braided PVC tubes are used for the rest of the piping. All the piping is 1/4" except for the permeate side of the cell for which the piping is 1/8". A bypass valve installed after the pump is used to maintain the feed flowrate for the cell at 2 $L{\cdot}min^{-1}$. A Blacoh H1020B pulsation dampener is installed between the pump and the cell to smooth the flow from the pump. The dampener is initially pressurized at 200 psi using an air

hand pump and then gradually depressurized so that dampener bladder pressure is always maintained half the system operating pressure. A Nalgene HDPE 20 liters tank is used to hold the feed solution. A general purpose mixer from Cole-Parmer is used to keep the solution in the feedwater tank completely mixed. The temperature in the feed tank is maintained at 23±0.2°C by using a refrigerated recirculator (Cole-Parmer® Polystat model).

The temperature in the feed tank is measured and recorded using a stainless steel temperature probe described in Table 3.1. Conductivity of the feed solution is measured and recorded using a conductivity probe also described in Section 3.2. The operating pressure is adjusted at the desired value by using the bypass needle valve and the concentrate needle valve located downstream the cell, on the concentrate side (Figure 3.2). The concentrate flowrate is measured and recorded using a digital flowmeter described in Section 3.2. Since the product flowrate represented less than 1% of the concentrate flowrate, the feed flowrate

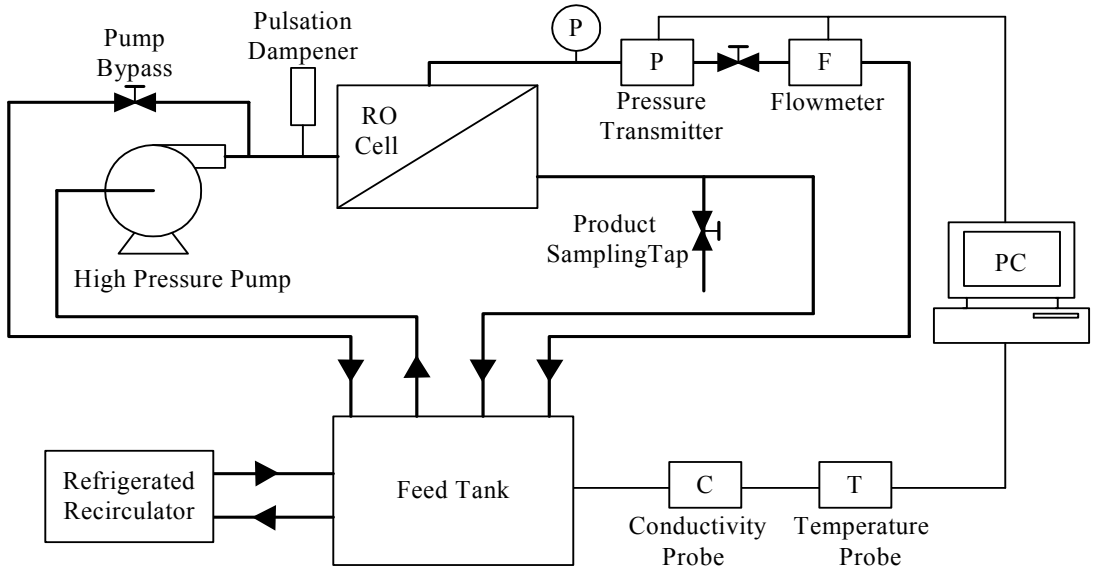

Figure 3. 2 Experimental set-up for the RO flat sheet membrane experiments.

can be approximated as the measured concentrate flowrate. The operating pressure is monitored using a pressure gauge and it is recorded using a pressure transmitter (Section 3.2).

The concentrate and the product are directed to the feed tank. When samples are taken from the product, they are poured back into the feed tank after conductivity measurements.

3.4.1 RO flat sheet membrane operation

The membranes used in these experiments are presented in Table 3.4. They are the same membranes used in the direct osmosis study except for the SE membrane which is only used for the direct osmosis experiments. The manufacturer specifications are presented in Table 3.2. The membrane pieces are cut from a 1 square foot sheet in order to fit the flat sheet cell and stored for 24 hours in fresh DI water at room temperature to keep the membrane

Table 3. 4 Membranes, salt solution and their concentrations, and the operating pressure for the RO flat sheet membrane experiments.

Membrane Name	Salts	Feed Concentration ($mol \cdot L^{-1}$)	Operating Pressure (psi)
AD	LiCl, NaCl, KCl $MgCl_2$, $CaCl_2$, $BaCl_2$	0.05	400, 350, 300, 250, 200, 150
CG			400, 350, 300, 250, 200, 150
CK			350, 300, 250, 200, 150

saturated. Then the membrane is placed in the cell with the skin layer facing the high pressure side and conditioned in the cell by feeding 0.05M KCl for 5 hours at 450 psi.

The system is further flushed with tap water and finally finished with DI water. After that, the feed solutions of LiCl, NaCl, KCl, $MgCl_2$, $CaCl_2$, and $BaCl_2$ are tested sequentially, at the operating pressures presented in Table 3.4. The feedwaters are prepared as described in the Section 3.1 at a concentration of 0.05 $mol \cdot L^{-1}$ for all the runs. The concentrations are calculated form the measured conductivity. For each salt solution and each membrane, the system is first operated at the highest pressure (400 psi for the AD and CG membranes, and 350 for the CK membrane) and let reach equilibrium. After setting the pressure, it takes

approximately 60 minutes for the product flowrate to reach a constant value. The conductivity of the product steadily declined and the equilibrium is reached when it decreases by less than 2% over 30 minutes. Three product samples are consecutively collected at the equilibrium state corresponding to the highest pressure. The product flowrate is determined volumetrically by recording the time to fill a 10 mL volumetric flask. The conductivity of the product is measured using the auto temperature correction probe from Cole-Parmer (Table 3.1) and the product concentration is determined from the product conductivity measurements.

Next, the pressure is decreased by 50 psi and the system is allowed to re-equilibrate. Three samples of the product are again taken as described earlier. This procedure continued for all the pressures listed on Table 3.4 for each membrane. Tap water and DI water are used to flush the system between runs of different salt solution. After all the salt solution runs are completed with one membrane, the procedure cycle is repeated using DI as feedwater. In this case, the equilibrium is declared when the increase of the product flow is less than 2% over 30 minutes. The duplicates of the RO flat sheet runs for a certain membrane are perform by repeating the sequence of procedures described in this section with a new piece of membrane of the same type.

3.5 Reverse osmosis spiral wound membrane experiments

The reverse osmosis experiments carried out with a spiral wound membrane are very similar to those carried out with a flat sheet membrane. The diagram of the experimental set-up is shown in Figure 3.3. The membrane element is manufactured by Dow FilmTec (SW30-2514 model). The main differences from the RO-flat sheet cell are the membrane configuration and the membrane surface area. The membrane characteristics are presented in Table 3.5 and a drawing of the membrane configuration is shown in Apendix A, Figure A.7.

The membrane element dimensions are 6.35 cm (2.5") diameter and 35.56 cm (14") length, and the total surface area is 5574 cm^2 (6 ft^2). The feed channel height is 1.65 mm.

The membrane pressure vessel is made of reinforced fiberglass and has a rated maximum operating pressure of 1000 psi. The pressure vessel is produced by Crans Engineering. The high pressure pump, pulsation dampener, refrigerated recirculator and the instrumentation are identical with those used for the flat sheet cell (Section 3.4). Due to the large surface area of the membrane, there is no need to bypass any of the pump flow as is done in the RO flat sheet membrane experiments. The pump capacity is 8.33 $L \cdot min^{-1}$ (2.2 $gal \cdot min^{-1}$). The pulsation dampener is precharged at 130 psi which is half of the system pressure. A Nalgene 114 liters HDPE tank is used to hold the feedwater. The product flowrate is sufficiently large to be measured by a digital flowmeter (model 111 from McMillan) which is places in the product line (Figure 3.3). Conductivity and temperature probes are also inserted in the product line. Temperature of the feedwater is maintained constant at $23 \pm 0.2^{o}C$.

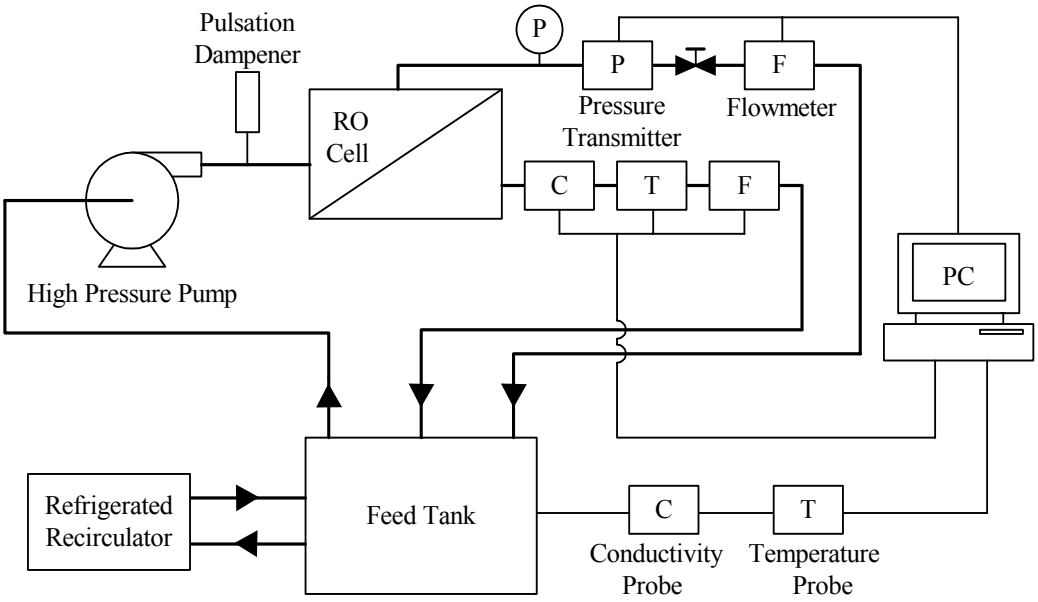

Figure 3. 3 Experimental set-up for the RO spiral wound membrane experiments.

Table 3. 5 Manufacturer specifications for the spiral wound membrane, the salt solutions and their concentrations for the RO spiral wound membrane experiments.

Membrane Manufacturer Name and Application	Membrane Polymer	Salts	Salts Concentration ($mol \cdot L^{-1}$)	pH Tolerance	Product Flux (gfd@psi)	Rejection (%)
SW30-2514 Seawater	TFC	LiCl NaCl KCl $MgCl_2$ $CaCl_2$ $BaCl_2$	0.05	2-11	16.7 @ 800psi	99.4

3.5.1 Spiral wound membrane operation

The salt solutions and their concentration are identical to those used for the RO flat sheet cell runs. All the RO spiral wound runs are performed at 260 psi. Product sampling is not necessary for the spiral wound runs because all the necessary readings are automatically performed by the probes and recorded by a PC.

The membrane is conditioned with a 0.05 mol·L^{-1} KCl for 5 hours at 260 psi. The system is further flushed with tap water and finally flushed with DI water. After that, the feed solutions of LiCl, NaCl, KCl, $MgCl_2$, $CaCl_2$, and $BaCl_2$ are tested successively at 260 psi. The run for each salt solution is finished when the product water conductivity and flowrate are at equilibrium.

The equilibrium is based on the same criteria as that of RO flat sheet membrane experiments (Section 3.4.1). The system evolution to the equilibrium state can be visualized on the PC screen by monitoring the product flowrate and the product conductivity. At the end of the runs, the pure water permeability coefficient, A, is determined using DI water. Duplicate runs are performed using the same membrane.

CHAPTER 4

RESULTS

This chapter presents the results obtained from the three types of experiments described in Chapter 3. First, the results obtained from the direct osmosis experiments are presented, followed by the results from the RO flat sheet membrane experiments and finally, the results from the RO spiral wound membrane experiments. For each type of the experiments, the results are presented first for the salt transport and next, for the pure water transport. The differences among several types of membranes (seawater, brackish water and nanofiltration) in the transport of the 1:1 and 1:2 salts as well as the order of salt permeation rate for the twelve studied salts are emphasized throughout this chapter.

The direct osmosis (DO) experiments results section presents the derivation of the equation used in calculating the salt permeability coefficient $(D/K\delta)_{DO}$ and the values obtained for $(D/K\delta)_{DO}$ for four membranes AD (seawater), CG (brackish water), CK (nanofiltration), and SE (seawater) . For the seawater membrane SE, the effect of the salt solution concentration is shown together with the differences in the salt permeation for pairs of salts with common cation but different anions. The differences in the pure water flux and pure water permeation for the four membranes are presented next. The effect of the salt solution concentration on the pure water flux is highlighted.

The results from the RO flat sheet membrane experiments are presented from the perspective of two models: the Spiegler-Kedem (SK) model and the Kimura-Sourirajan (KS) model. The parameters characterizing the salt transport in the SK model are P_{RO}, σ_1 and σ_2 which represent the salt permeability, the reflection coefficient and the salt-water coupling coefficient, respectively. The parameters P_{RO} and σ_1 are calculated for three cases: 1) the

concentration polarization is neglected; 2) the concentration polarization is calculated at $\sigma_1 = 1$; and 3) the concentration polarization is calculated by combining the thin film theory with the Sherwood correlation. Multiple comparisons are made for the salt transport parameters obtained in the three cases for each of the three membranes AD, CG, and CK.

The values of the salt permeability obtained from the SK model, P_{RO}, are compared with the values of the salt permeability obtained from the KS model, $(D/K\delta)_{RO}$, as well as with the values of the salt permeability from the direct osmosis experiments, $(D/K\delta)_{DO}$. The pure water transport results are also compared from the perspective of the two models. The KS model is also used to determine the salt and water transport parameters in the case of RO spiral wound membrane experiments. The transport parameters obtained with the spiral wound membrane are compared with the transport parameters obtained with the RO flat sheet membrane.

4.1 Salt and water transport in the direct osmosis (DO) experiments

This Section is divided in two parts. The first part (Section 4.1.1) presents the results obtained for the salt permeation coefficient, $(D/K\delta)_{DO,}$ whereas the second part (Section 4.1.2) presents the results obtained for the transport of pure water.

4.1.1 Salt transport in the direct osmosis experiments

The equation governing the transport of salts across the membrane assumes that the salt flux and the pure water flux are not coupled within the membrane. The salt is transported through the membrane due to the differential concentration across the membrane. Therefore, the salt transport in direct osmosis is diffusion controlled.

Fick's law of diffusion characterizes the diffusive transport of ionic species in porous materials and it relates the diffusion flux to the differential concentration of the species across

the porous material. Details of the derivation of Equation 4.1 are presented in Appendix B. Equation 4.2 represents the definition of the molar flux.

$$J_S = \left(\frac{D}{K\delta}\right)_{DO} \left((C_S)_{mem} - (C_{DI})_{mem}\right) \tag{4.1}$$

$$J_S \equiv \frac{dN}{S\,dt} \tag{4.2}$$

J_S represents the number of moles which diffuses through the surface area S in unit time ($cm{\cdot}min^{-1}{\cdot}cm^{-2}$), D is the diffusion coefficient in the membrane ($cm^2{\cdot}s^{-1}$), K is the partitioning (solubility) coefficient between membrane and solute which is considered the same on both sides of the membrane, δ is the membrane thickness (cm), $(C_S)_{mem}$ is the concentration of the salt solution at the membrane surface ($mol{\cdot}L^{-1}$), and $(C_{DI})_{mem}$ is the concentration of DI water at the membrane surface ($mol{\cdot}L^{-1}$). The quantity $(D/K\delta)_{DO}$ represents the salt permeability coefficient for diffusion and is considered as an intrinsic parameter. In Equation 4.2, dN is the number of moles of solute transported in time dt through the surface S.

The salt solution concentration at the membrane surface $(C_S)_{mem}$ is approximated by the bulk concentration of the salt solution C_S. This approximation is based on the fact that the concentration polarization is insignificant in the direct osmosis experiments due to the following: 1) the system run in cross-flow filtration, 2) no pressure is applied on the salt solution side, 3) DI water diffuses across the membrane in the opposite direction of the salt (due to the osmotic pressure) impeding the formation of salt layer on the membrane surface, 4) the use of spacers as turbulence promoters on both sides of the membrane, and 5) the relative short duration of each run which is followed by cleaning with DI water. The concentration of the DI water at the membrane surface $(C_{DI})_m$ is equal to the bulk concentrations of the solution in the DI side, C_{DI}. Therefore Equation 4.1 becomes:

$$J_S = \left(\frac{D}{K\delta}\right)_{DO}\left(C_S - C_{DI}\right) \tag{4.3}$$

The experimental results show with a regression coefficient of 0.98 that salt concentration on both sides of the membrane vary linearly with time. The decrease in the salt solution concentration is represented by Equation 4.4 and the increase of the concentration in the DI water is represented by Equation 4.5:

$$\left(C_S\right)_t = \left(C_S\right)_{t=0} - \alpha t \tag{4.4}$$

$$\left(C_{DI}\right)_t = \left(C_{DI}\right)_{t=0} + \beta t \tag{4.5}$$

In these equations, α and β are the slopes and $(C_s)_{t=0}$ and $(C_{DI})_{t=0}$ the intercepts of the plot of concentration vs. time. The values of α, β, $(C_S)_{t=0}$ and $(C_{DI})_{t=0}$ are specific to each salt solution, concentration, and membrane. Their values are determined graphically by plotting the concentration versus time from t = 0 (beginning of the run) to t = τ (end of the run). The salt permeability, $(D/K\delta)_{DO}$, is calculated using Equation 4.6, which is obtained by integrating Equation 4.1 over the duration, τ, of each run and substituting Equations 4.2, 4.4 and 4.5 into 4.3. Details of the calculations are provided in Appendix B. In this approach, $(D/K\delta)_{DO}$ is considered independent of the solution concentration C_S because C_S varied by less the 5% from start to finish for each run.

$$\left(\frac{D}{K\delta}\right)_{DO} = \frac{\Delta N}{S\tau}\,\frac{1}{\left[\left(C_s\right)_{t=0} - \left(C_{DI}\right)_{t=0}\right] - 0.5(\alpha+\beta)\tau} \tag{4.6}$$

The salt permeability coefficient $(D/K\delta)_{DO}$ is calculated using Equation 4.6 for LiCl, NaCl, KCl, $MgCl_2$, $CaCl_2$ and $BaCl_2$ at 0.05 mol·L^{-1} for all four membranes. The calculated

coefficients are presented in Table C.1. The salt permeates at the lowest rates for the seawater membranes AD (average of 1.5 x10^{-7} cm·s^{-1}) and SE (average of 5.9 x 10^{-7} cm·s^{-1}). The salt permeates at higher rates for the brackish water membrane CG (average of 54.7 x 10^{-7} cm·s^{-1}) and nanofiltration membrane CK (average of 100.1 x 10^{-7} cm·s^{-1}). Figure 4.1 illustrates the differences in the salt permeability, $(D/K\delta)_{DO}$, for the four membranes and for the 1:1 and 1:2 salts. The $(D/K\delta)_{DO}$ is plotted on a logarithmic scale to illustrate the differences in the salt permeability for seawater membranes and nanofiltration membranes.

The 1:1 salts permeated at a higher rate than the 1:2 salts for all four membranes. The smallest variation between the average permeability of 1:1 salts and the average permeability of 1:2 salts occurs in the seawater membrane SE (22%). The differences between the average permeability of 1:1 salts and the 1:2 salts for the AD, CG and CK are 57%, 64% and 56% respectively. Among the 1:1 salts, LiCl has the slowest permeation rate for each of the four membranes while $MgCl_2$ has the slowest permeation rate for each of the four membranes among the 1:2 salts. The order of permeation in direct osmosis experiments is Mg < Ca < Ba < Li < Na < K in each of the four membranes except for the AD for which the order is Mg < Li < Ca < Ba < Na < K.

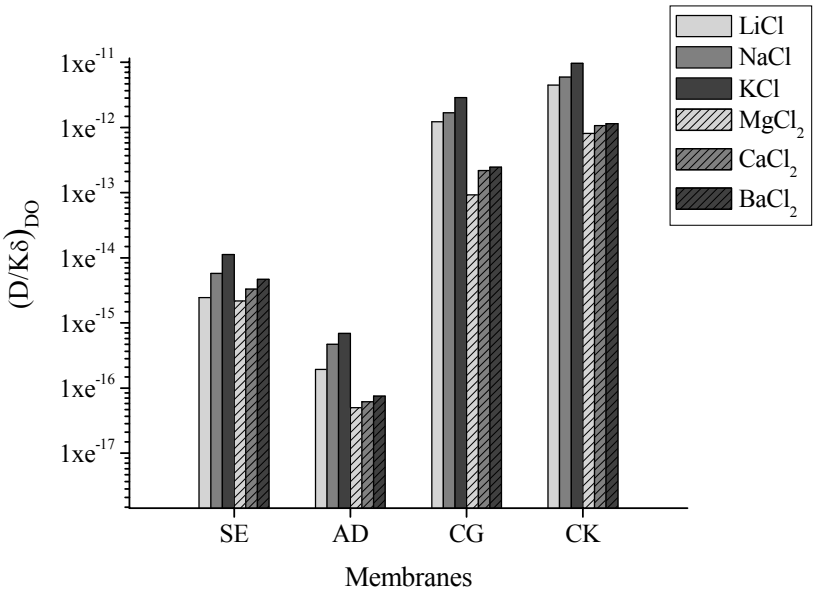

Figure 4. 1 Salt permeability for the different membranes at 0.05 mol·L^{-1} in the direct osmosis experiments.

Figures 4.2 and Figure 4.3 present the variation of the salt permeability coefficient with the salt solution concentration C_s for the SE membrane. The values of salt permeability coefficients in these plots are tabulated in Tables C.2 and C.3. The salts having different cations but the common anion Cl^- are referred as chlorides and the salts having different cations but the common anion Ac^- are referred as acetates. The salt permeability decreases with the increase in the salt solution concentration for both chlorides (Figure 4.2) and acetates (Figure 4.3).

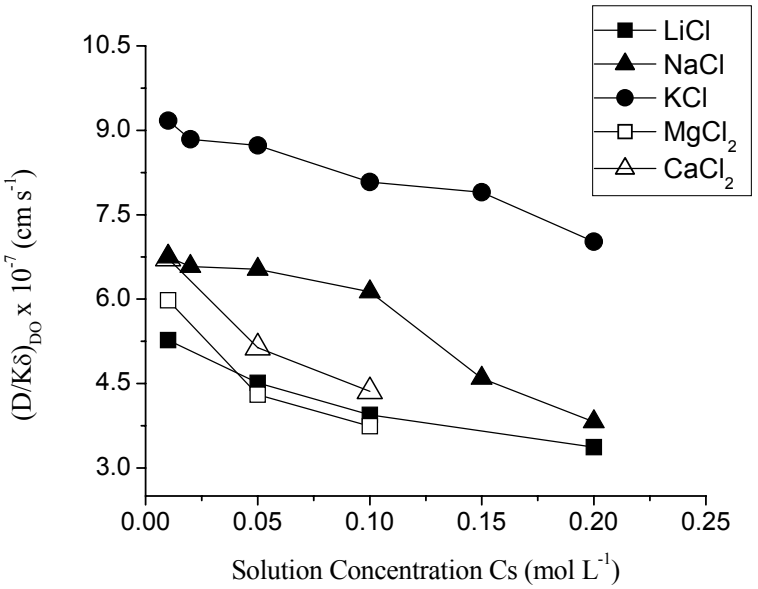

Figure 4. 2 Variation of salt permeability with concentration for chlorides in SE membrane in direct osmosis experiments.

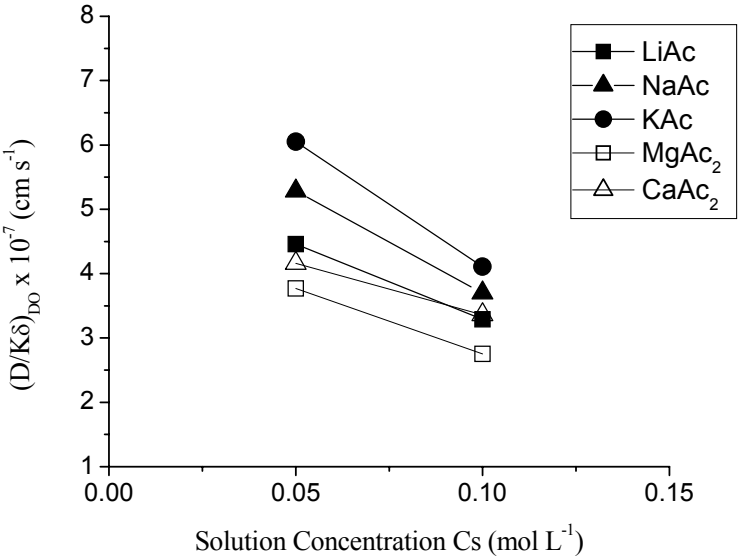

Figure 4. 3 Variation of salt permeability with concentration for acetates in SE membrane in direct osmosis experiments.

Figure 4. 4 and Figure 4. 5 present the salt permeability for pairs of salts which have a common cation but different anion (such as the pair LiCl and LiAc or the pair $MgCl_2$ and $MgAc_2$) for the SE membrane. The values of salt permeability coefficient are tabulated in Table C.4. The acetates permeate slower than the chlorides at both concentrations (Figure 4.4 at 0.05 mol$\cdot L^{-1}$ and Figure 4.5 for 0.1 mol$\cdot L^{-1}$) and for all the studied ions.

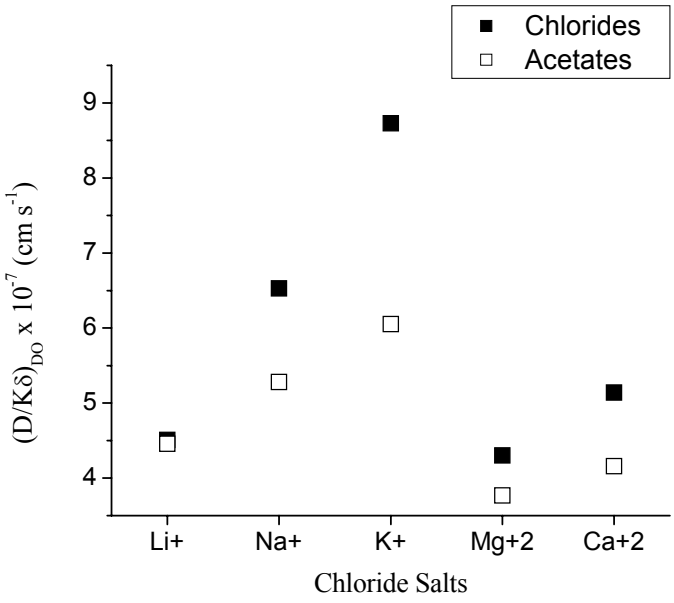

Figure 4. 4 Comparison of salt permeability for chlorides and acetates at 0.05 mol$\cdot L^{-1}$ in direct osmosis experiments.

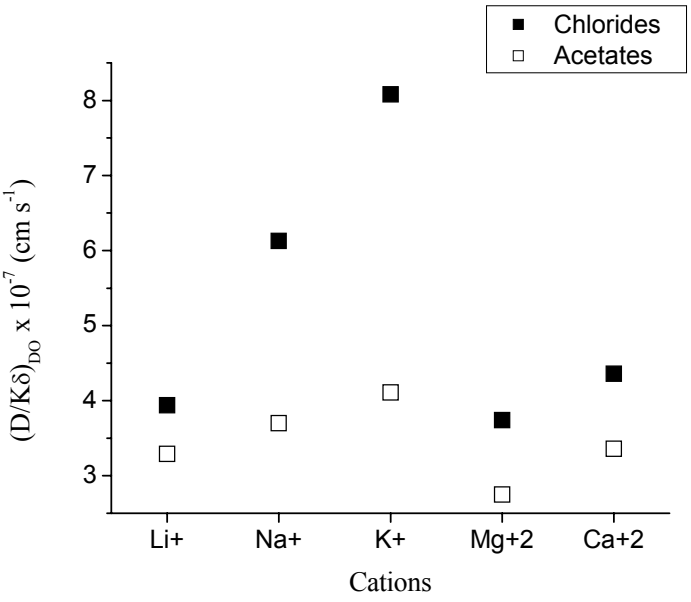

Figure 4. 5 Comparison of salt permeability for chlorides and acetates at 0.1 molL^{-1} in direct osmosis experiments.

4.1.2 Pure water transport in the direct osmosis experiments

Table 4.1 shows the average values of the pure water parameter, A', determined as described in Section 3.3.2 at different operating pressures. The two seawater membranes, SE and AD, have close values for the pure water permeability A' (A' is 22% higher for SE than for AD) whereas for the brackish water membrane, CG, and the nanofiltration membrane, CK, the pure water permeability is considerably higher.

Table 4. 1 Pure water permeability.

Membrane	SE	AD	CG	CK
A' x 10^{-6} ($g \cdot s^{-1} \cdot cm^{-2} \cdot psi^{-1}$)	0.44	0.34	2.60	3.78

The pure water flux $J_{w, DO}$ is calculated for each salt and each membrane using Equation 3.1. The pure water flux for the four membranes studied when the salt solution

concentration is 0.05 mol·L^{-1} is presented in Figure 4.6 and the data is tabulated in Table C.6. The water flux averaged over all the six salts studied is the lowest for the SE membrane (6.0 x 10^{-6} g·s^{-1}·cm^{-2}) and the largest for the brackish water membrane CG (24.7 x 10^{-6} g·s^{-1}·cm^{-2}).

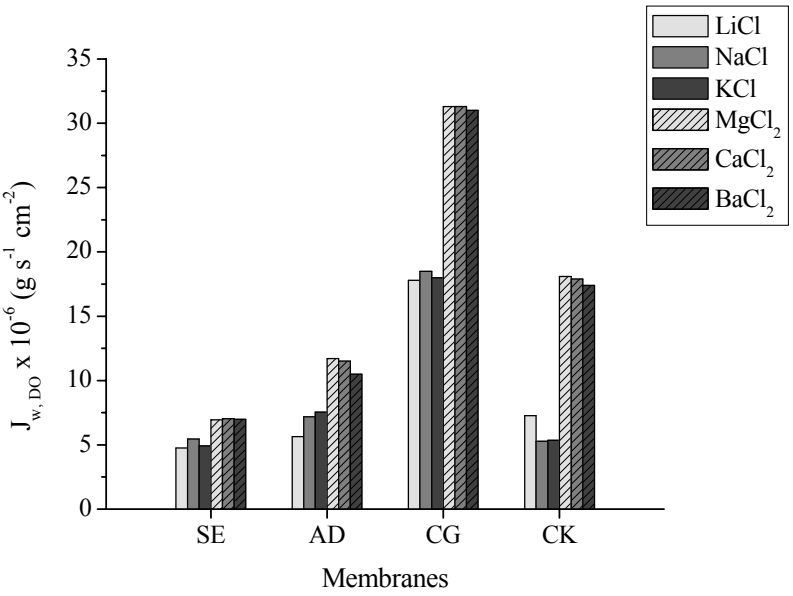

Figure 4. 6 Pure water flux for different membranes at 0.05 mol·L^{-1} in the direct osmosis experiments.

The pure water flux is higher for the 1:2 salts than for the 1:1 salts for all the membranes. The difference between the 1:1 and 1:2 salts is lowest for the SE membrane (28%) and largest for the CK membrane (66%). The pure water flux varies within 10% for the 1:1 salts averaged over the four membranes and within 1% for the 1:2 salts averaged over the four membranes. Details of the calculations are presented in Table C.6.

Figure 4.7 and Figure 4.8 present the variation of the pure water flux with solution concentration C_s for the SE membrane. The values of salt permeability coefficient in these figures are tabulated in Tables C.7 and C.8. The pure water flux increased with the increase of the solution concentration for all chlorides (Figure 4.7) and acetates (Figure 4.8).

Figure 4.9 presents the comparison of the pure water flux for pairs of salts which have a common cation but different anion for the SE membrane. The differences in the pure water flux for 1:1 salts, including chlorides and acetates, are less than 7% at 0.05 mol·L^{-1} and less than 1% at 0.1 mol·L^{-1} (Table C.8). The differences in the pure water flux for the 1:2 salts, including chlorides and acetates, are less than 1% for both concentrations of 0.05 mol·L^{-1} and 0.1 mol·L^{-1} (Table C.8).

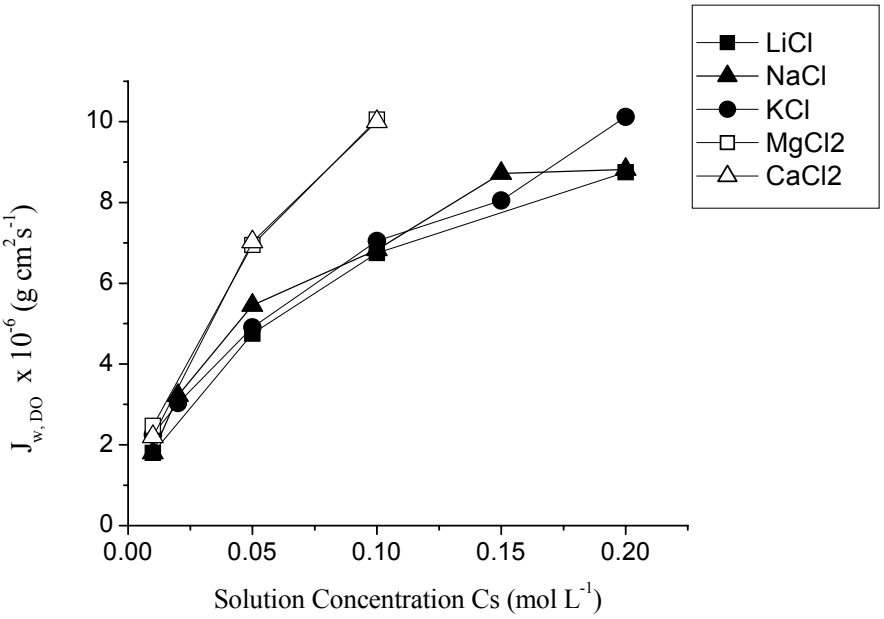

Figure 4. 7 Variation of pure water flux with concentration for chlorides in SE membrane in direct osmosis experiments.

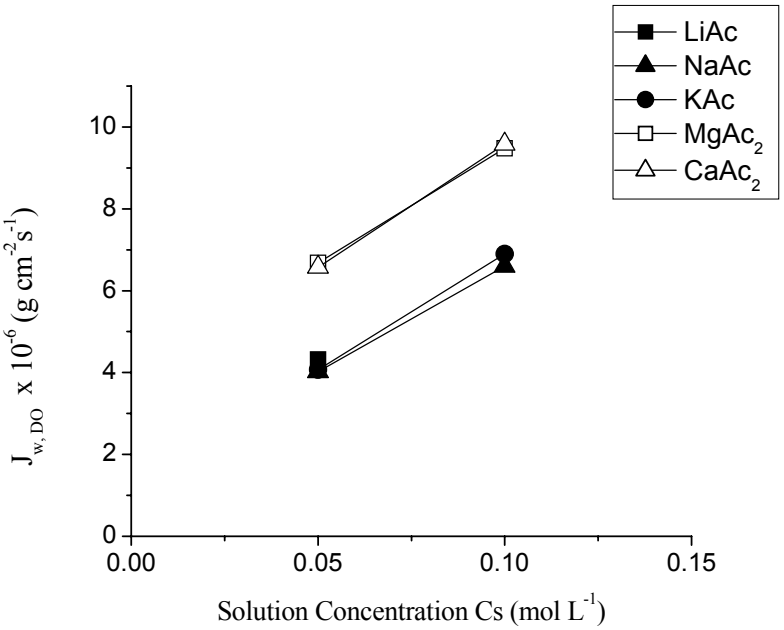

Figure 4. 8 Variation of pure water flux with concentration for acetates in SE membrane in direct osmosis experiments.

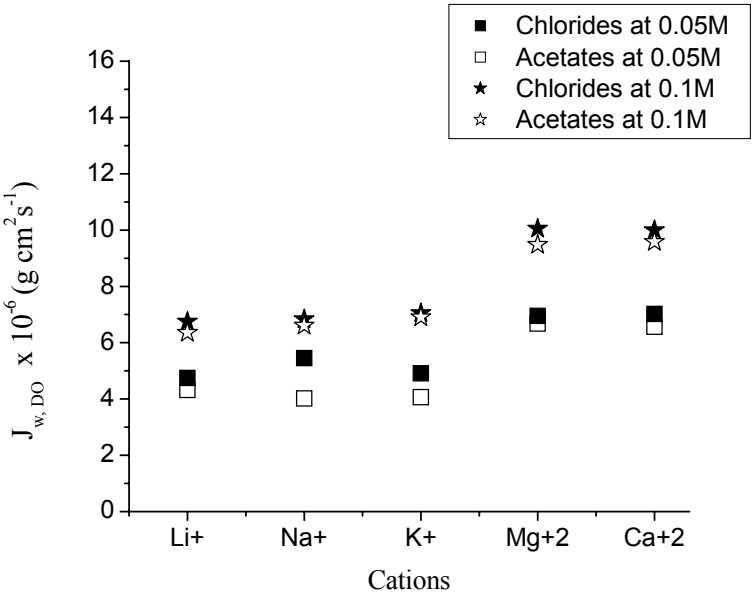

Figure 4. 9 Comparison of the pure water flux for chlorides and acetates at two concentrations in SE membrane in direct osmosis experiments.

4.2 Salt and water transport in the RO flat sheet membrane experiments

Two conceptually different models are used in calculating the salt and water parameters of transport for the RO flat sheet cell experiments. The models are described in detail in Chapter 2, Section 2.1.3. Finally, the salt permeability coefficients determined for the RO flat sheet membrane experiments are compared with the salt permeability coefficients obtained in the direct osmosis experiments.

4.2.1 Salt permeability in the Spiegler-Kedem model - the absence of concentration polarization

The parameters of salt transport in the Spiegler-Kedem (SK) model are calculated for three cases. First, the concentration at the membrane wall is considered equal to the concentration of the bulk feed solution (i.e. concentration polarization is neglected); second, the concentration at the membrane wall is calculated taking $\sigma_1 = 1$; and third, the

concentration at the membrane wall is calculated by combining the film theory with Sherwood correlation. Although the parameter σ_1 characterizes the salt transport, it is presented in Section 4.2.3 together with the results for the water transport.

In the first case, the salt permeability, P_{RO}, and the salt-water coupling coefficient, σ_2, are calculated using Equation 2.10 from Chapter 2. The results are presented in Table 4.2, together with the salt diffusive flux, J_{diff}, as percentage of the total salt flux, J_S. The salt permeability coefficient for the direct osmosis experiments $(D/K\delta)_{DO}$ is also listed in the Table 4.2 for a better comparison with the salt permeability $P_{RO.}$

When the concentration polarization is neglected, the salt permeated at a higher rate in the RO flat sheet membrane experiments than in the direct osmosis experiments for all three membranes studied. The differences are the smallest for the seawater membrane, AD, and the highest for the nanofiltration membrane, CK. The $(D/K\delta)_{DO}$ is on average, three times less than P_{RO} for the seawater membrane, five times less for the brackish water membrane and nine times less for the nanofiltration membrane .

Similar to the results from the direct osmosis experiments, the 1:2 salts have a lower permeability coefficient than the 1:1 salts for all three membranes. The order of the permeation rate for the studied salts in the RO flat sheet membrane is the same as the order of permeation rate shown in the direct osmosis study. According to the P_{RO}, the order of permeability is given by Mg < Ca < Ba < Li < Na < K for all three membranes.

As described in Section 4.2.3, Chapter 2, the salt-water coupling coefficient, σ_2, is zero for no coupling salt-water and one for the perfect coupling of the salt-water transport. An estimation of the strength of the salt-water coupling is actually given by $1-\sigma_2$. In the first case of SK model, the strength of the salt-water coupling is lowest for the seawater membrane AD (0.013 on average), followed by the brackish water membrane CG (0.162 on

average) and by the nanofiltration membrane CK (0.421 on average). For all three membranes, the strength of the coupling salt-water is lower for the 1:2 salts than for 1:1 salts. The differences in the salt-water coupling coefficient between 1:2 salts and 1:1 salts are the highest for the nanofiltration membrane CK (70 %) and lowest for the seawater membrane AD (0.9 %). The strength of the coupling salt-water increases is the same order as the salt permeability coefficient P_{RO} increases, which is Mg < Ca < Ba < Li < Na < K.

When concentration polarization is neglected in the SK model, the flux of salt permeating the membrane due to diffusion J_{diff} represents, on average, 29% of the total salt flux J_{total} for the AD membrane. For the CG membrane, J_{diff} is, on average, 38% from the total salt flux, and for the CK membrane, J_{diff} is on average 22% from the total salt flux. The diffusive flux has a higher contribution to the total flux for the 1:2 salts than for the 1:1 salts for the CG and CK membranes. The diffusive flux has a lower contribution for the 1:2 salts than for the 1:1 salts in the case of AD membrane. The values of J_{diff}/J_S do not show any order for the six salts for any of the three membranes.

Table 4. 2 Salt transport parameters and the percentage of the diffusion flux for the SK model in absence of concentration polarization in RO flat sheet membrane experiments.

Seawater membrane AD				
Salt	$(D/K\delta)_{DO}$ x 10^{-7} ($cm \cdot s^{-1}$)	P_{RO} x 10^{-7} ($cm \cdot s^{-1}$)	σ_2	J_{diff}/J_{total} (%)
LiCl	1.5	4.95	0.984	34
NaCl	2.2	6.63	0.983	27
KCl	2.6	10.9	0.981	43
$MgCl_2$	0.83	1.19	0.993	25
$CaCl_2$	0.91	1.23	0.992	22
$BaCl_2$	1.0	1.42	0.991	24
Brackish water membrane CG				
	$(D/K\delta)_{DO}$ x 10^{-7} ($cm \cdot s^{-1}$)	P_{RO} x 10^{-7} ($cm \cdot s^{-1}$)	σ_2	J_{diff}/J_{total} (%)
LiCl	67.1	359	0.773	29
NaCl	77.1	409	0.769	31
KCl	96.9	557	0.756	38
$MgCl_2$	21.9	134	0.913	43
$CaCl_2$	31.6	149	0.908	43
$BaCl_2$	33.4	158	0.906	43
Nanofiltration membrane CK				
	$(D/K\delta)_{DO}$ x 10^{-7} ($cm \cdot s^{-1}$)	P_{RO} x 10^{-7} ($cm \cdot s^{-1}$)	σ_2	J_{diff}/J_{total} (%)
LiCl	118	896	0.437	12
NaCl	133	1141	0.429	13
KCl	165	1612	0.416	15
$MgCl_2$	56	520	0.761	34
$CaCl_2$	63	550	0.718	29
$BaCl_2$	65	561	0.710	28

4.2.2 Salt permeability in the Spiegler-Kedem model - concentration polarization

The salt permeability coefficient, the salt-water coupling coefficient and the percentage of the diffusive flux of the total salt flux are calculated using Equation 2.10 when the phenomenon of concentration polarization is considered. The concentration of the feed is replaced by the concentration at the membrane wall, C_{mem}. The concentration at the membrane wall is determined first at $\sigma_1 = 1$, and next, by combining the film theory with the Sherwood correlation (see Appendix E).

4.2.2.1 C_{mem} at $\sigma_1 = 1$

Concentration at the membrane wall C_{mem} when $\sigma_1 = 1$ is calculated at each pressure using Equation 4.7. In this case, the concentration at the membrane wall is denoted C_{mem}^{max}. The reflection coefficient, σ_1, reaches its maximum value of 1 for a perfect membrane which does not allow any fraction of the salt to permeate (coefficient of salt rejection, R =1). This is, of course, an ideal situation. In practice, the coefficient of salt rejection and σ_1 are always less than 1. Calculating the concentration at the membrane wall from $J_v = L_p(\Delta P - \sigma_1 \Delta\pi)$ when $\sigma_1=1$ results in the maximum value of the concentration polarization, C_{mem}^{max}. According to Equation 4.7, for a given salt and a given membrane, at constant feed concentration and constant feed temperature, C_{mem}^{max} depends on the operating pressure. The averaged values of C_{mem}^{max} over the pressure range are presented in Table 4.3.

$$C_{mem}^{max} = \frac{P + \pi_P - \frac{J_v}{AP}}{\phi n R_g T} \qquad \text{where} \quad \begin{cases} n = 2 \text{ for } 1:1 \text{ salts} \\ n = 3 \text{ for } 1:2 \text{ salts} \end{cases} \tag{4.7}$$

Table 4. 3 Average concentrations at the membrane wall for $\sigma_1 = 1$ for feed concentration of 0.05 mol·L^{-1} in RO flat sheet membrane experiments.

Salt	C_{mem}^{max} (mol·L^{-1})		
	AD (seawater)	CG (brackish water)	CK (nanofiltration)
LiCl	0.169	0.078	0.073
NaCl	0.142	0.074	0.071
KCl	0.134	0.073	0.064
$MgCl_2$	0.179	0.082	0.097
$CaCl_2$	0.169	0.081	0.094
$BaCl_2$	0.142	0.080	0.088

The normalized values of C_{mem}^{max} to the feed concentration C_{feed} are presented in Figure 4.10 for the three membranes. The C_{mem}^{max} is on average three times higher than the feed

concentration for the AD membrane and on average 1.6 times higher for the CG and CK membranes. For all three membranes, the 1:2 salts present a higher membrane concentration than the 1:1 salts. The maximum concentration at the membrane wall increases in the order K < Na < Li and Ba < Ca < Mg for all three membranes.

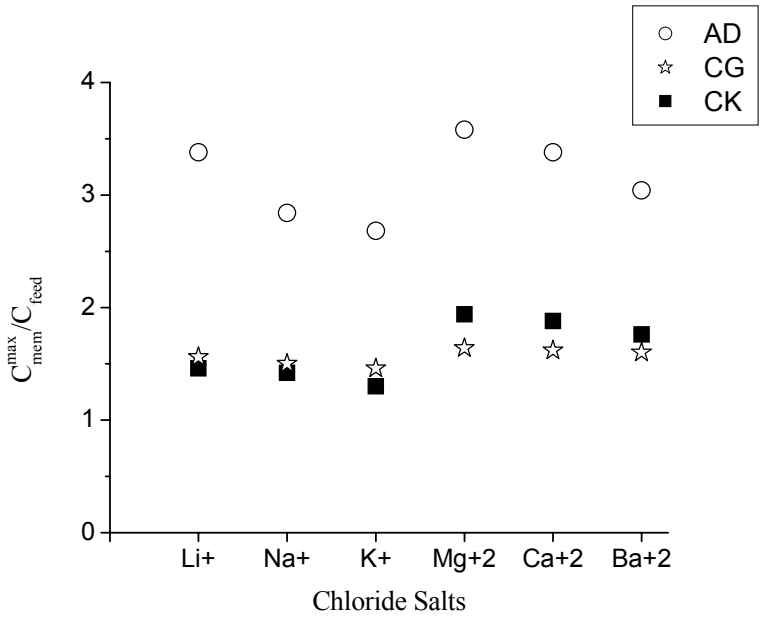

Figure 4. 10 Concentration at the membrane wall normalized to the feed concentration for $\sigma_1 = 1$ in RO flat sheet membrane experiments.

Table 4.4 presents the parameters of the salt transport when the concentration at the membrane wall is calculated using $\sigma_1 = 1$. In this case, the transport parameters, P_{RO} and σ_2, and the percentage of the diffusive flux of the total flux, J_{diff}/J_{total}, are modified from the first case of SK model when the concentration polarization is neglected.

In the two cases of SK model, the salt permeability P_{RO} varies slightly for the RO membranes AD and CG (by 15% on average) and becomes on average 121% for the nanofiltration membrane CK. As for the first case of SK model, the 1:2 salts have again a lower permeation rate than the 1:1 salts for all three membranes. The order of permeation rate

Table 4. 4 Salt transport parameters and the percentage of the diffusion flux for the SK model when concentration polarization is calculated for $\sigma_1 = 1$ in RO flat sheet membrane experiments.

Seawater membrane AD			
	$P_{RO} \times 10^{-7}$ ($cm \cdot s^{-1}$)	σ_2	J_{diff}/J_{total} (%)
LiCl	3.96	0.999	91
NaCl	5.92	0.999	89
KCl	9.55	0.999	97
$MgCl_2$	1.24	0.999	89
$CaCl_2$	1.34	0.999	68
$BaCl_2$	1.44	0.999	77
Brackish water membrane CG			
	$P_{RO} \times 10^{-7}$ ($cm \cdot s^{-1}$)	σ_2	J_{diff}/J_{total} (%)
LiCl	444	0.893	56
NaCl	499	0.885	57
KCl	616	0.880	63
$MgCl_2$	163	0.995	87
$CaCl_2$	177	0.985	86
$BaCl_2$	190	0.978	82
Nanofiltration membrane CK			
	$P_{RO} \times 10^{-7}$ ($cm \cdot s^{-1}$)	σ_2	J_{diff}/J_{total} (%)
LiCl	2878	0.829	65
NaCl	3004	0.803	54
KCl	3258	0.731	54
$MgCl_2$	732	0.991	95
$CaCl_2$	882	0.981	93
$BaCl_2$	919	0.959	85

for the studied salts when concentration at the membrane wall is calculated for $\sigma_1 = 1$ remains the same as when the concentration polarization is neglected (Section 4.2.1).

When the concentration at the membrane wall is calculated for $\sigma_1 = 1$, the strength of the coupling salt-water $1-\sigma_2$ is reduced for all the salts, however it remains the lowest for the AD membrane (0.001 on average), followed by the CG membrane (0.064 on average) and CK membrane (0.118 on average). For the CG and CK membranes, the salt-water coupling coefficient remains higher for the 1:2 salts than for 1:1 salts. The strength of the coupling salt-water increases in the same order as the salt permeability coefficient P_{RO} increases, which

is Mg<Ca<Ba<Li<Na<K. There is no difference in the salt-water coupling coefficients for the 1:1 and 1:2 salts for the AD membrane.

Comparing to the first case of the SK model, the contribution of the diffusive salt flux to the total salt flux has increased from 29% to 85% for the AD seawater membrane, from 37% to 72% for the CG brackish water membrane and from 22% up to 72% for the CK nanofiltration membrane. The percentage of the diffusive flux remains higher for the 1:2 salts than for the 1:1 salts.

4.2.2.2 C_{mem} from the film theory combined with Sherwood correlation

The third case considered for the SK model implies the calculation of the concentration at the membrane wall by combining the film theory with the Sherwood correlation. The Sherwood correlations provides the back diffusion coefficient k (Equation 4.8) which is further used in the film theory (Equation 4.9) to determine the concentration at the membrane wall (denoted C_{mem}^{k} in this case). Details of the calculation for k from Equation 4.8 are shown in Appendix E. The values of k and the concentration at the membrane wall C_{mem}^{k} are presented in Table 4.5.

$$k = 0.186\left(Re\,Sc\,\frac{d_h}{L}\right)^{0.33} \tag{4.8}$$

$$\frac{C_{mem}^{k} - C_{prod}}{C_{feed} - C_{prod}} = \exp\left(\frac{J_v}{k}\right) \tag{4.9}$$

According to the Equation 4.8, the back diffusion coefficient k does not depend on the membrane type, however it depends on the cell geometry, the feed flowrate and the salts diffusivity coefficient in the bulk solution. The values of k are higher for the 1:2 salts than for the 1:1 salts and the order k increases is given by Mg < Ca < Ba < Li < Na < K.

Table 4. 5 Back diffusion coefficient calculated from Sherwood correlation and the concentration at the membrane wall calculated from the film theory in RO flat sheet membrane experiments.

Salt	k x 10^{-3} ($m \cdot s^{-1}$)	C^k_{mem} ($mol \cdot L^{-1}$)		
		AD	CG	CK
LiCl	2.16	0.059	0.071	0.069
NaCl	2.40	0.059	0.069	0.069
KCl	2.78	0.061	0.064	0.062
$MgCl_2$	1.93	0.062	0.070	0.071
$CaCl_2$	1.98	0.065	0.069	0.069
$BaCl_2$	2.03	0.059	0.069	0.072

The average over the six salts for C^k_{mem} is 22% higher than the concentration in the feed for the AD membrane and 37% higher than the concentration in the feed for the CG and CK membranes. The C^k_{mem} is 2.6 times lower than C^S_{mem} for the AD membrane, 12% lower for the CG membrane and 15% lower for the CK membrane. Figure 4.11 presents C^k_{mem} normalized to the feed concentration for the three membranes studied. The differences in C^k_{mem} among the three membranes are lower than in the case of $\sigma_1 = 1$. Similar to C^{max}_{mem}, the concentration C^k_{mem} is higher for the 1:2 salts than for the 1:1 salts for all three membranes. However, there is no trend in the variation of C^k_{mem} among either the 1:1 salts or the 1:2 salts.

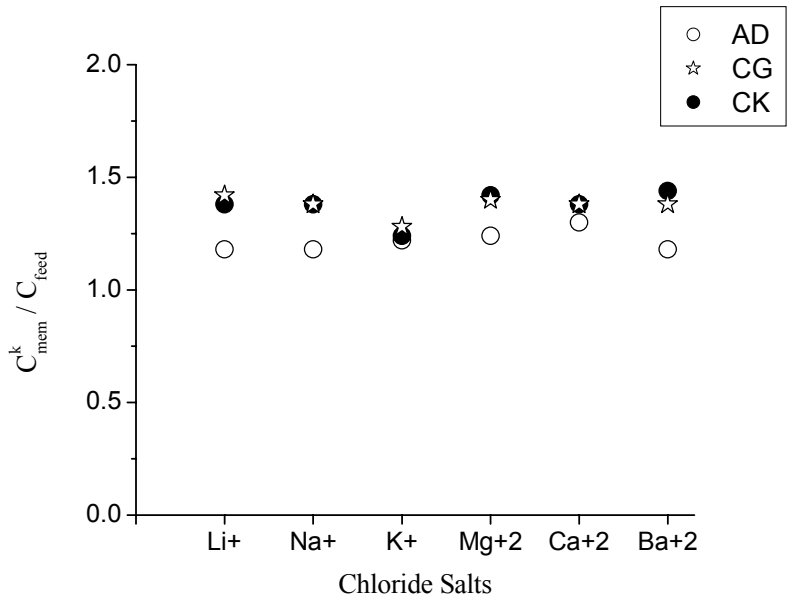

Figure 4. 11 Concentration at the membrane wall normalized to the feed concentration from Sherwood correlation and thin film theory in RO flat sheet membrane experiments.

The transport parameters, P_{RO} and σ_2, and the percentage of the salt diffusive flux of the salt total flux are presented in Table 4.6 for the third case of the SK model. For the AD and CG membranes, the salt permeability P_{RO} has increased on average by 28% in comparison with the salt permeability for the case when the concentration polarization was neglected. For the CK membrane, the increase is on average 144%. These increases are higher compared to the increases of P_{RO} and σ when the concentration at the membrane wall is calculated at $\sigma_1 = 1$ (Section 5.2.2.1). The order of permeation rate for the studied salts is the same as the order of permeation rate when the concentration polarization is neglected (Section 4.2.1) or when the concentration at the membrane wall is calculated at $\sigma_1 = 1$.

Table 4. 6 Salt transport parameters and percentage of the diffusion flux for the SK model in the case of concentration polarization calculated from film theory and Sherwood correlation in RO flat sheet membrane experiments.

Seawater membrane AD			
	P_{RO} x 10^{-7} ($cm \cdot s^{-1}$)	σ_2	J_{diff}/J_{total} (%)
LiCl	5.96	0.989	48
NaCl	7.71	0.988	49
KCl	13.1	0.988	60
$MgCl_2$	1.41	0.995	35
$CaCl_2$	1.49	0.994	33
$BaCl_2$	1.70	0.994	34
Brackish water membrane CG			
	P_{RO} x 10^{-7} ($cm \cdot s^{-1}$)	σ_2	J_{diff}/J_{total} (%)
LiCl	529	0.901	62
NaCl	587	0.894	61
KCl	753	0.891	67
$MgCl_2$	167	0.969	74
$CaCl_2$	184	0.964	72
$BaCl_2$	196	0.961	77
Nanofiltration membrane CK			
	P_{RO} x 10^{-7} ($cm \cdot s^{-1}$)	σ_2	J_{diff}/J_{total} (%)
LiCl	2796	0.755	54
NaCl	3310	0.733	60
KCl	3965	0.717	52
$MgCl_2$	907	0.951	82
$CaCl_2$	924	0.922	72
$BaCl_2$	976	0.907	71

A comparison of the salt permeability coefficient, P_{RO}, for the three cases of the SK model (absence of concentration polarization, concentration polarization calculated at $\sigma_1 = 1$ and concentration polarization calculated from combination of film theory and Sherwood correlation) is shown in Figure 4.12, each plot corresponding to one membrane. In all three cases of the SK model, the differences in the P_{RO} are lower for the 1:2 salts than for the 1:1 salts for any of the three membranes.

(a)

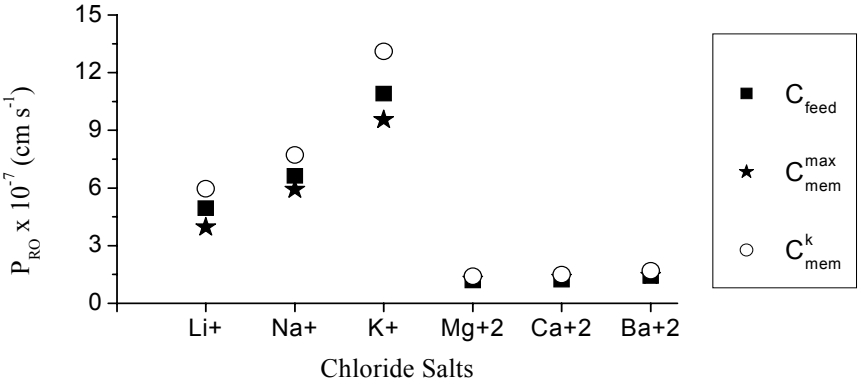

(b)

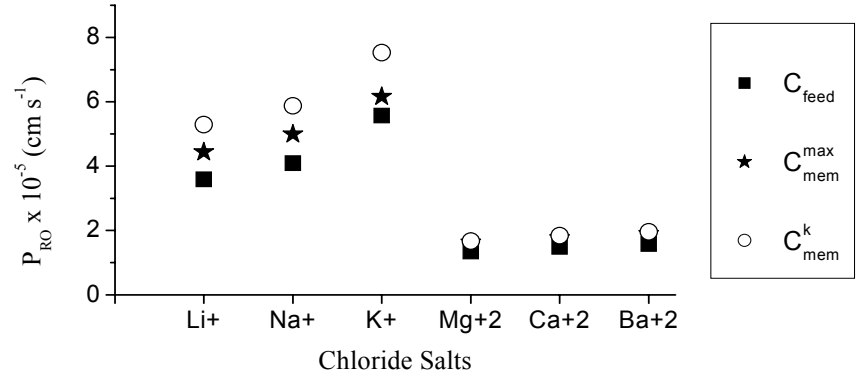

(c)

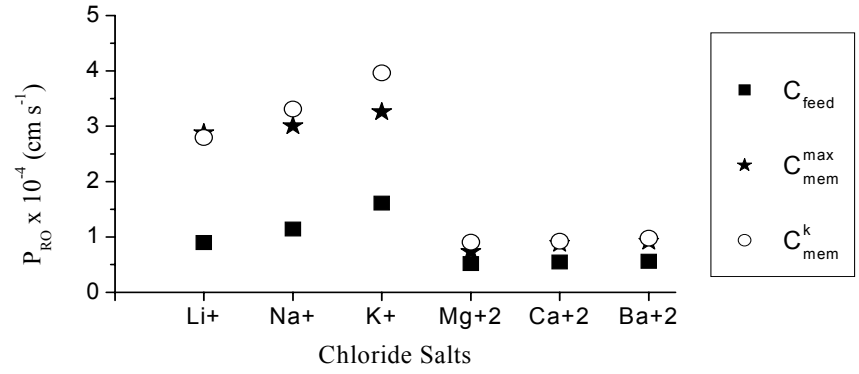

Figure 4. 12 Comparison of the salt in the SK model at different concentration at the membrane wall for (a) AD membrane; (b) CG membrane; and (c) CK membrane. in RO flat sheet membrane experiments.

The strength of the coupling salt-water $1-\sigma_2$ is also presented in Figure 4.13 for the three cases of the SK model. For the third case when concentration polarization is calculated using the Sherwood correlation and the thin film theory, the strength of the coupling salt-water, $1-\sigma_2$, is reduced for all the salts and all the membranes when compared with $1-\sigma_2$ in the absence of concentration polarization. It remains the lowest for the AD membrane (0.009 on average), followed by the CG membrane (0.070 on average) and CK membrane (0.169 on average). These average values of $1-\sigma_2$ are higher when compared with $1-\sigma_2$ for $\sigma_1 = 1$. For all the membranes, $1-\sigma_2$ is lower for the 1:2 salts than for the 1:1 salts in all three cases of the SK model. The magnitude of $1-\sigma_2$ increase in the same order for the six salts regardless how the concentration at the membrane wall is calculated. The order is Mg < Ca < Ba < Li <Na < K. The differences in $1-\sigma_2$ for the two methods of calculating the concentration polarization are lower for the CG and CK membranes than for the AD membrane.

The percentage of the diffusive flux of the total flux is presented in Figure 4.14 for the three cases of concentration at the membrane wall. In the third case of the SK model, the contribution of the diffusive flux to the total flux represented on average 43% for the AD membrane, 69% for the CG membrane and 65% for the CK membrane. The percentages of the diffusive flux of the total flux are lower than in the case of $\sigma_1 = 1$. The differences between J_{diff}/J_{total} at $\sigma_1 = 1$ and combined theory approach are largest for the AD membrane (49%), followed by the CK membrane (12%) and CG membrane (4%). In all three cases of the SK model, the percentage of the diffusion flux is higher for the 1:2 salts than for the 1:1 salts for the CK and CG membrane, whereas for the AD membrane the percentage of the diffusion flux is lower for the 1:2 salts than for the 1:1 salts.

(a)

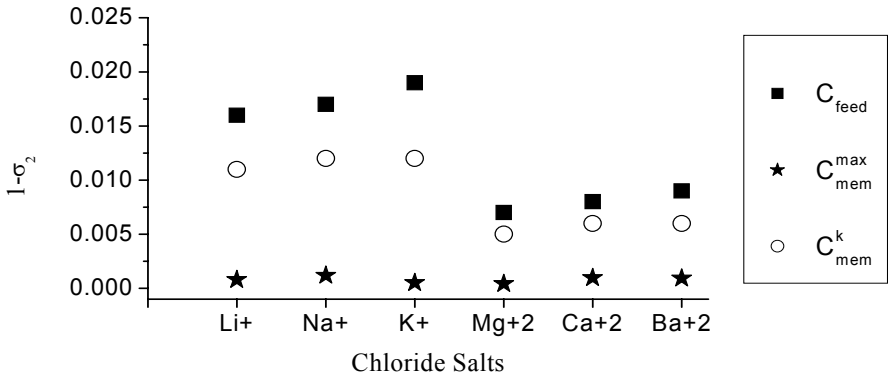

(b)

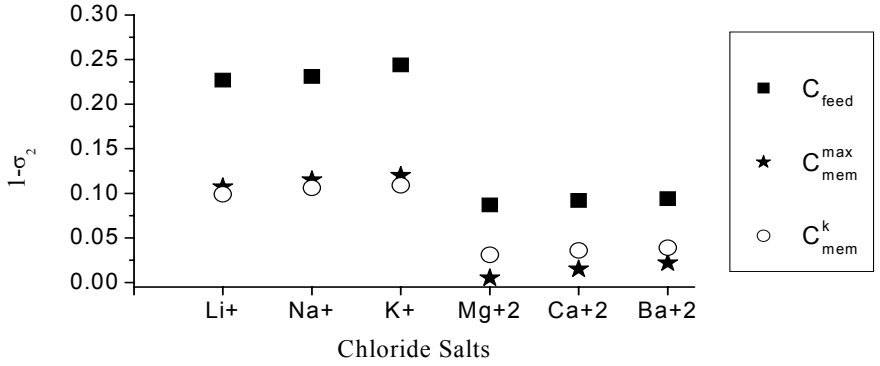

(c)

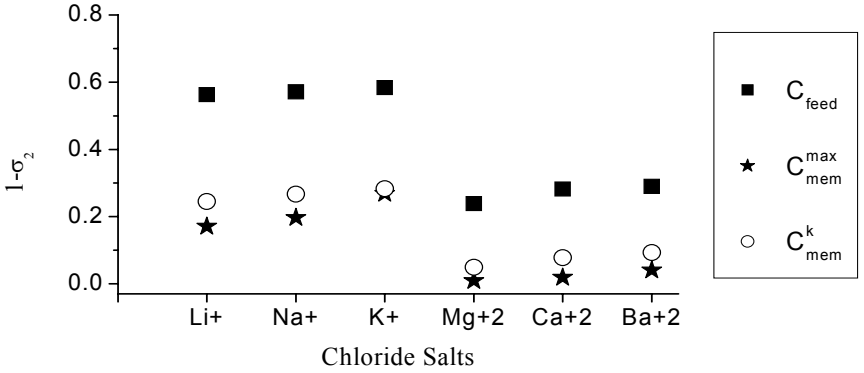

Figure 4. 13 Comparison of the strength of the salt-water coupling in the SK model at different concentration at the membrane wall for (a) AD membrane, (b) CG membrane, (c) CK membrane CK membrane in RO flat sheet membrane experiments.

(a)

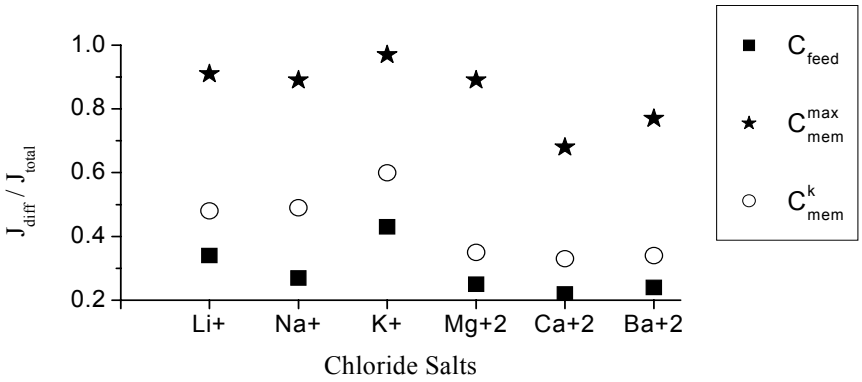

(b)

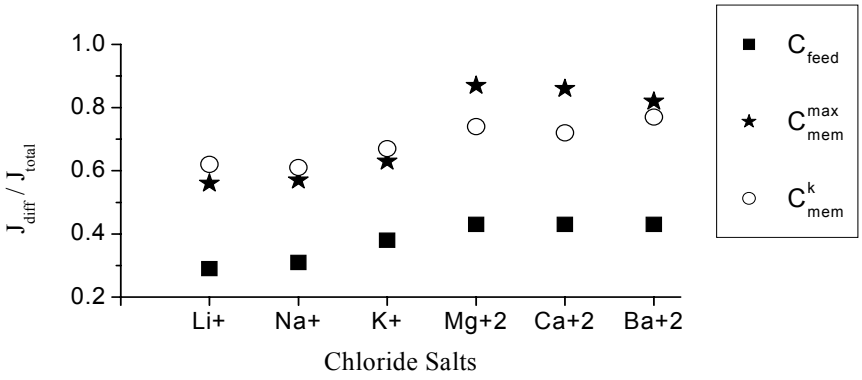

(c)

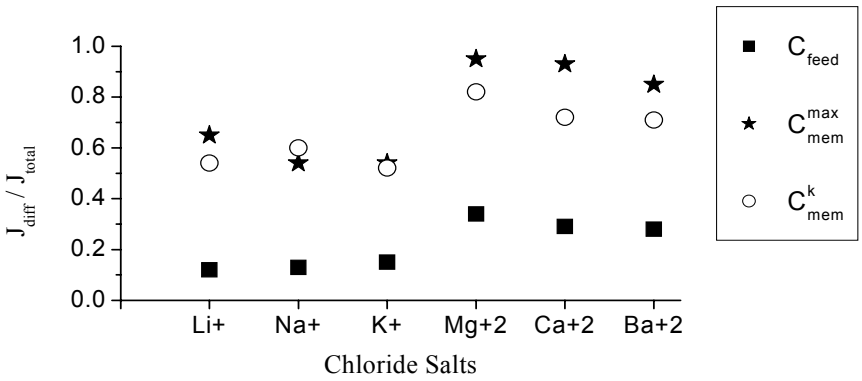

Figure 4. 14 Comparison of the percentage of the diffusive flux of the total flux in the SK model at different concentration at the membrane wall for (a) AD membrane, (b) CG membrane, (c) CK membrane in RO flat sheet membrane experiments.

4.2.3 Pure water transport in the Spiegler-Kedem model

As in the case of the transport parameters for the salts, the transport parameters for pure water are analyzed using the two models, Spiegler-Kedem (SK) and Kimura-Sourirajan (KS). The results of the pure water transport parameters are presented first for the SK model and next for the KS model.

The same three cases of the SK model considered in calculating the salt transport are used in calculating the parameters for the water transport. As described before, the three cases are: 1) neglecting the concentration polarization; 2) calculating the concentration polarization for $\sigma_1 = 1$; and 3) calculating the concentration polarization by combining the film theory with the Sherwood correlation. The transport of pure water is characterized in the SK model by the parameter L_p. Although the reflection coefficient, σ_1, characterizes the salt transport, it appears only in the equation describing the product water flux $J_v = L_p(\Delta P - \sigma_1 \Delta\pi)$. Therefore, it is included in the results for the water transport. The L_p and σ_1 are determined graphically from plotting Equation 2.9 at various operating pressure.

$$\frac{J_v}{\Delta\pi} = \frac{\Delta P}{\Delta\pi} L_p - L_p \sigma_1 \tag{2.9}$$

The results are presented in Table 4.7 for the first case of the SK model when concentration polarization is neglected. The reflection coefficient σ_1 has values close to the salt-water coupling coefficient σ_2 when the concentration polarization is not considered. The differences between σ_1 and σ_2 are on average less than 2% for any of the three membranes.

Table 4. 7 Pure water permeability and reflection coefficient in the SK model in the absence of concentration polarization in RO flat sheet membrane experiments.

Salt	AD (seawater)		CG (brackish water)		CK (nanofiltration)	
	L_p x 10^{-6} ($g \cdot s^{-1} \cdot cm^{-2} \cdot psi^{-1}$)	σ_1	L_p x 10^{-6} ($g \cdot s^{-1} \cdot cm^{-2} \cdot psi^{-1}$)	σ_1	L_p x 10^{-6} ($g \cdot s^{-1} \cdot cm^{-2} \cdot psi^{-1}$)	σ_1
LiCl	1.49	0.956	3.26	0.781	4.16	0.431
NaCl	1.65	0.950	3.21	0.776	4.48	0.414
KCl	1.70	0.943	3.28	0.750	4.37	0.412
$MgCl_2$	1.70	0.993	2.90	0.924	3.73	0.752
$CaCl_2$	1.72	0.991	2.93	0.909	3.71	0.732
$BaCl_2$	1.79	0.989	3.01	0.901	3.87	0.698

The average of hydraulic permeability L_P for the seawater membrane AD is 1.68 x 10^{-6} ($g s^{-1} cm^{-2} psi^{-1}$), for the brackish water membrane CG is 3.10 x 10^{-6} ($g s^{-1} cm^{-2} psi^{-1}$), and for the nanofiltration membrane CK is 4.05 x 10^{-6} ($g s^{-1} cm^{-2} psi^{-1}$). Comparing to the pure water permeability for the AD membrane, the pure water permeability for the brackish water membrane CG is 85% larger and 148% for the nanofiltration membrane CK.

For the second case of the SK model, σ_1 is considered to be 1 and L_p is determined experimentally when the feed water is DI water. In this case equation $J_v = Lp(\Delta P - \sigma_1 \Delta \pi)$ becomes $J_w = Lp \Delta P$ and L_p is equal to the pure water permeability, A, which is presented later in this Chapter (Table 4.10). Comparison of $\sigma_1 = 1$ with σ_2 from the Table 4.4 shows differences smaller than 4% for all salts in the seawater membrane as well as for the 1:2 salts for the brackish water and nanofiltration membrane. The values for σ_1 are up to 12% smaller than σ_2 for the 1:1 salts in the brackish water membrane and as much as 27% higher than σ_2 for the 1:1 salts in the nanofiltration membrane.

For the third case of the SK model, the calculation of the concentration at the membrane wall uses a combination of the film theory and Sherwood correlation in Equation 4.10 to express $\Delta \pi$. The resulting transport coefficients L_p and σ_1 are presented in Table 4.8.

Table 4. 8 Pure water permeability and reflection coefficient in the SK model when the concentration at the membrane wall is calculated from film theory and Sherwood correlations in RO flat sheet membrane experiments.

Salt	AD (seawater)		CG (brackish water)		CK (nanofiltration)	
	$L_p \times 10^{-6}$ ($g \cdot s^{-1} \cdot cm^{-2} \cdot psi^{-1}$)	σ_1	$L_p \times 10^{-6}$ ($g \cdot s^{-1} \cdot cm^{-2} \cdot psi^{-1}$)	σ_1	$L_p \times 10^{-6}$ ($g \cdot s^{-1} \cdot cm^{-2} \cdot psi^{-1}$)	σ_1
LiCl	1.49	0.965	3.44	0.846	4.34	0.609
NaCl	1.65	0.959	3.36	0.836	4.64	0.516
KCl	1.73	0.950	3.40	0.799	4.46	0.466
$MgCl_2$	1.80	0.999	3.20	0.969	4.17	0.843
$CaCl_2$	1.81	0.999	3.23	0.944	4.07	0.811
$BaCl_2$	1.89	0.999	3.31	0.958	4.03	0.724

The hydraulic permeability L_P increases slightly comparing with the first case of the SK model (by 3% on average for the AD, by 7% on average for the CG and by 6% for the CK). The differences between σ_1 and σ_2 in the third case of the SK model are very small for the AD and CG membrane (1.3% and 4.3% respectively). For the CK membrane, σ_1 is on average smaller than σ_2 by 14% for the 1:2 salts and by 28% for the 1:1 salts.

4.2.4 Salt permeability in the Kimura-Sourirajan model

The second model considered in calculating the salt transport parameters is the Kimura-Sourirajan (KS) model. In the case of KS model, the salt permeability as well as the back diffusion coefficient, k, depend on the operating pressure and the membrane. The salt permeabilities, $(D/K\delta)_{RO}$, and the back diffusion coefficients, k_{RO}, are shown for each membrane in Table 4.9.

Table 4. 9 Salt permeability and back diffusion coefficient in the KS model in RO flat sheet membrane experiments.

Seawater membrane AD		
Salt	$(D/K\delta)_{RO}$ x 10^{-7} ($cm \cdot s^{-1}$)	k_{RO} x 10^{-4} ($cm \cdot s^{-1}$)
LiCl	4.40	2.74
NaCl	6.65	3.49
KCl	9.96	3.93
$MgCl_2$	1.37	2.63
$CaCl_2$	1.65	2.92
$BaCl_2$	1.74	2.99
Brackish water membrane CG		
Salt	$(D/K\delta)_{RO}$ x 10^{-7} ($cm \cdot s^{-1}$)	k_{RO} x 10^{-4} ($cm \cdot s^{-1}$)
LiCl	788	16.1
NaCl	916	20.4
KCl	991	24.1
$MgCl_2$	184	11.8
$CaCl_2$	212	12.9
$BaCl_2$	231	14.3
Nanofiltration membrane CK		
Salt	$(D/K\delta)_{RO}$ x 10^{-7} ($cm \cdot s^{-1}$)	k_{RO} x 10^{-4} ($cm \cdot s^{-1}$)
LiCl	3701	16.6
NaCl	4887	20.1
KCl	6630	25.5
$MgCl_2$	762	6.6
$CaCl_2$	960	7.0
$BaCl_2$	1068	7.6

The values of the salt permeability $(D/K\delta)_{RO}$ in the KS model are larger than values of the salt permeability, $(D/K\delta)_{DO}$, obtained in the direct osmosis experiments for all the membranes. The differences are the smallest for the seawater AD membrane, followed by the brackish water membrane CG and the nanofiltration membrane CK. Thus, the values of the salt permeability $(D/K\delta)_{DO}$ are on average, three times less than the values of the salt permeability, $(D/K\delta)_{RO}$, for the seawater membrane AD, nine times less for the brackish water membrane CG and thirty times less for the nanofiltration membrane CK.

Similar to the results obtained in the direct osmosis study as well as the results obtained in the RO flat sheet membrane study-SK model, the 1:2 salts present a lower permeability coefficient than the 1:1 salts for all three membranes. The order of permeation rate for the studied salts remained the same as the order of permeation rate calculated in the direct osmosis study and in the RO study-SK model. According to the $(D/K\delta)_{RO}$ coefficient, the order of permeation is Mg < Ca < Ba < Li < Na < K for all three membranes.

The values of the back diffusion coefficient, k_{RO}, for the three membranes are presented in Figure 4.15 together with the values of the back diffusion coefficient, k, calculated from the Sherwood correlation. The seawater membrane AD presents on average over all salts the lowest k_{RO} (3.1 $cm{\cdot}s^{-1}$), followed by the nanofiltration membrane CK (13.9 $cm{\cdot}s^{-1}$) and the brackish water membrane CG (16.6 $cm{\cdot}s^{-1}$). The back diffusion coefficient is lower for the 1:2 salts than for the 1:1 salts for all three membranes. The differences between the 1:2 salts and the 1:1 salts are 16% on average for the AD membrane, 36% on average for the CG membrane and 66% on average for the CK membrane. The order the coefficient increases is Li < Na < K and Mg < Ca < Ba in all the cases.

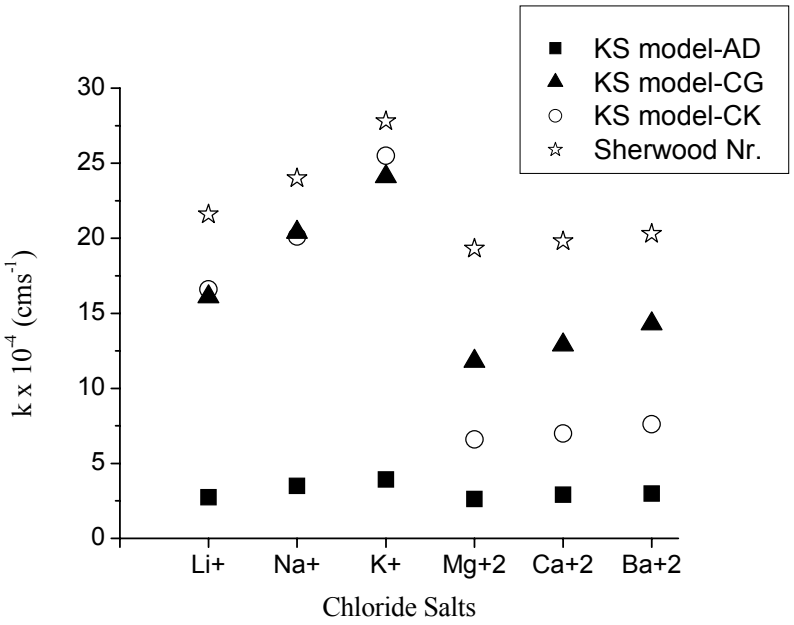

Figure 4. 15 Comparison of the back diffusion coefficient for all membranes in the KS model and from the Sherwood correlation (same for all membranes) in RO flat sheet membrane experiments.

4.2.5 Pure water transport in the Kimura-Sourirajan model

The pure water transport is characterized in the Kimura-Sourirajan (KS) model by the parameter, A, called the pure water permeability which is a characteristic of the membrane. It is determined experimentally by running dematerialized water as feedwater. Table 4.10 presents the average of A over the pressure range for the three membranes. The pure water permeability L_p is also presented for comparison.

The seawater membrane AD presented the smallest pure water permeability among the three membranes. The pure water permeability is 65% larger for the brackish water membrane CG and by 148% larger for the nanofiltration membrane CK. The differences between A and L_p [(1)] are of 4% for the AD membrane, 8% for the CG membrane and 7% for the CK membrane. The differences between A and L_p [(3)] are of 1% for the AD and CK membrane and of 13% for the CG membrane.

Table 4. 10 Pure water parameters of transport in RO flat sheet membrane experiments.

Membrane	A x 10^{-6} ($g \cdot s^{-1} \cdot cm^{-2} \cdot psi^{-1}$)	L_p [(1)] x 10^{-6} ($g \cdot s^{-1} \cdot cm^{-2} \cdot psi^{-1}$)	L_p [(3)] x 10^{-6} ($g \cdot s^{-1} \cdot cm^{-2} \cdot psi^{-1}$)
AD	1.75	1.68	1.73
CG	2.88	3.10	3.32
CK	4.34	4.05	4.29

Notes: [(1)] Denotes the averaged values obtain in the first case of the SK model (absence of concentration polarization).
[(3)] Denotes the averaged values obtain in the third case of the SK model (when the concentration polarization is calculated from film theory and Sherwood correlation).

4.3 Salt and water transport in the RO spiral wound membrane experiments

The results from the RO spiral wound membranes are determined using only the Kimura-Sourirajan model. The parameters of salt and water transport in the KS model are presented in Table 4.11 for the seawater membrane element SW30 used in the RO-spiral wound membrane experiments. The concentration at the membrane wall calculated from at $\sigma_1 = 1$ is also shown in Table 4.11.

Table 4. 11 Salt and water transport parameters in the KS model in the RO spiral wound membrane experiments.

Salt	$(D/K\delta)_{RO}$ x 10^{-6} ($cm \cdot s^{-1}$)	k_{RO} x 10^{-4} ($cm \cdot s^{-1}$)	C_{mem}^{max} ($mol \cdot L^{-1}$)	A x 10^{-6} ($g \cdot s^{-1} \cdot cm^{-2} \cdot psi^{-1}$)
LiCl	1.91	9.65	0.084	2.41
NaCl	2.00	10.7	0.080	
KCl	2.26	11.5	0.078	
$MgCl_2$	1.28	6.50	0.101	
$CaCl_2$	1.34	6.63	0.102	
$BaCl_2$	1.44	6.79	0.100	

In the case of the RO spiral wound membrane experiments, the salts permeate the membrane in the same order as in the case of the direct osmosis experiments and the RO flat sheet membrane experiments. The order the salt permeability increases is given by Mg<Ca<Ba<Li<Na<K. On average, the salt permeability for the seawater membrane element

SW30 is four times larger than the salt permeability for the seawater membrane AD used in the flat sheet experiments.

The back diffusion coefficient k_{RO} is lower for the 1:2 salts than for the 1:1 salts for the spiral wound membrane element SW30 by 37% on average. The order the coefficient increases is given by and Mg<Ca<Ba< Li<Na<K. On average, the back diffusion coefficient for the spiral wound membrane SW30 is three times larger than the back diffusion coefficient for the seawater membrane AD used in the flat sheet experiments.

The set of values $(D/K\delta)_{RO}$, k_{RO}, C_{mem}^{max} , and A for the seawater membrane SE is in between the corresponding set of values for the seawater membrane AD and brackish water CG used in the RO flat sheet membrane experiments. The salt permeability $(D/K\delta)_{RO}$ and the back diffusion coefficient k_{RO} are closer to the seawater membrane AD whereas the C_{mem}^{max} and A are closer to the brackish water membrane CG.

CHAPTER 5

DISCUSSION OF RESULTS

This chapter analyses the results presented in Chapter 4. Comparisons to the analogous findings presented in the literature are made throughout the chapter. The discussion is divided in five sections. The first section presents a correction of the equation derived in the previous chapter for the salt transport in direct osmosis experiments. It discusses the concentration at the membrane wall as well as the transport of pure water in direct osmosis assuming that the salt and the water fluxes do not interact within the membrane.

The second section of this chapter discusses the salt transport parameters: the salt permeability, $P_{RO,}$ the reflection coefficient, σ_1, and the salt-water coupling coefficient, σ_2. This section also discusses the importance of the salt diffusive flux in the Spiegler-Kedem model. The differences in the salt transport parameters are analyzed for three cases of the model. In the first case, the increase in the concentration at the membrane wall is neglected whereas for the second and the third cases, the effects of concentration polarization are considered. The concentration at the membrane wall is calculated in the second case by taking $\sigma_1=1$ and in the third case, by combining the film theory with the Sherwood correlation. It is shown that the concentration polarization cannot be neglected (case one) and that the diffusion is the dominant mechanism of salt transport in both RO and NF membranes (case two and three).

The third section compares the two most common models used in calculating the salt permeability in RO and NF membranes: the Spiegler-Kedem model and the Kimura-Sourirajan model. The comparison regards both the salt and the water transport parameters

and defines the situations when the two models can be used interchangeably. The fourth part of this chapter brings together the salt permeability from the direct osmosis experiments and the reverse osmosis experiments, both from Spiegler-Kedem and Kimura-Sourirajan model. It is shown that for the salt permeability is the same in direct osmosis and reverse osmosis, therefore it dose not depend on the operating pressure applied.

The last part of the chapter analyzes what physical and thermodynamic parameters control the salt permeability in RO and NF membranes. There is a certain pattern of variation for the salt permeation among the six studied salt regardless the membrane type (RO or NF), the membrane configuration (flat sheet or spiral wound), the type of the experiment (DO or RO), or the model used in calculating the salt permeability (Spiegler-Kedem or Kimura-Sourirajan). This pattern is explained by any of the parameters correlated to the degree of the hydration for the cations (hydrated radii, enthalpy and entropy of hydration). The relative free energy can be used to predict the permeability of salts in a certain membrane based on known values of the several other salt permeabilities in the membrane.

5.1 Salt and water transport in the direct osmosis experiments

The objectives of this sections are 1) to determine the concentration at the membrane wall in the case of direct osmosis, 2) to derive the set of equations for water and salt fluxes in direct osmosis; and 3) to calculate the corrected salt water permeability coefficient, $(D/K\delta)_{DO}$.

The salt permeability coefficient in the direct osmosis experiments, $(D/K\delta)_{DO}$, is calculated using Equation 4.6 and considering that the concentration at the membrane wall is equal to the concentration of the salt solution in the bulk. The validity of this assumption has to be reconsidered in the context of having the salt flux and the pure water flux moving in opposite directions through the membrane. The opposing directions of the salt and water fluxes is observed experimentally from the measured increase in the salt concentration in the

DI water (due to the transport of salt) and the increase in the salt solution volume in the salt solution vessel (due to the transport of pure water).

5.1.1 Concentration at the membrane wall in the direct osmosis experiments

Assuming that the two fluxes do not interact with each other within the membrane (Rautenbach and Albrecht, 1989), the equation describing the transport of pure water in the direct osmosis experiments can be derived from Equation 2.11. A graphical representation of the Equation 2.11 is presented in Figure 5.1.

$$J_v = A(\Delta P - \Delta\pi) \tag{2.11}$$

It can be observed that when the difference in the applied pressure across the membrane ΔP is lower than the difference in the osmotic pressure across the membrane $\Delta\pi$, the direction of the pure water flux is reversed. In the direct osmosis experiments, the differential pressure ΔP is zero since there is no external pressure applied on the membrane. Therefore, Equation 2.11 becomes Equation 5.1.

$$J_{w,\,DO} = - A\Delta\pi \tag{5.1}$$

In direct osmosis experiments, the pure water permeates the membrane by flowing first through the support layer of the membrane and then through the skin layer. The pure water permeability is different from the pure water permeability, A, when the water flows first through the skin layer and next through the support layer, due to membrane asymmetry. The pure water permeability in the direct osmosis experiments is denoted A'.

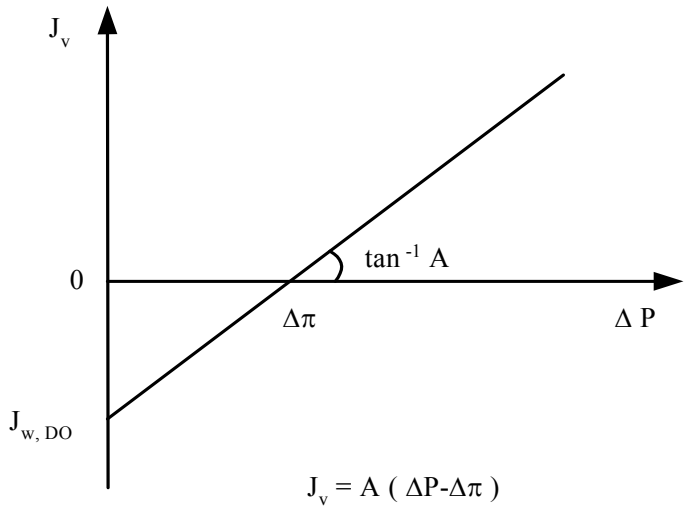

Figure 5. 1 Schematic diagram of the pure water flux as function of the applied pressure across membrane. Modified from Mulder (2003).

Since A' cannot be determined in a direct osmosis experiment, it is determined experimentally in a reverse osmosis experiment at a range of transmembrane pressures form 100 psi to 300 psi (Chapter 3, Section 3.3.2). In direct osmosis experiments, the pressure across the membrane is less than 54 psi, therefore lower than the pressure at which A' is determined. However, the variation of A' with pressure is less than 6% for the seawater membranes and less than 11% for both the brackish water and nanofiltration membranes. Hence, the use of A' determined in RO experiments for the DO experiments is adequate.

Disregarding the negative sign in Equation 5.1 which only reflects the change in direction of the pure water flux in direct osmosis, and considering the pure water permeability A' instead of A, Equation 5.1 becomes Equation 5.2. Combining Equation 5.2 with the expression of the osmotic pressure $\pi = \phi n R_g T C$, results in Equation 5.3 which allow the calculation of the concentration at the membrane wall in the direct osmosis experiments C_{mem}^{DO}.

$$J_{w,DO} = A'\Delta\pi = A'\left(\pi_{mem}^{DO} - \pi_{DI}\right) \tag{5.2}$$

$$C_{mem}^{DO} = \frac{J_{w,DO}}{A'\phi n R_g T} + C_{DI} \tag{5.3}$$

For a given membrane and salt solution, the concentration at the membrane wall, C_{mem}^{DO}, obtained from Equation 5.3 varies during a DO run due to variations of the concentration C_{DI}. The pure water flux, $J_{w,DO}$, is considered constant during a run (once the steady state in reached) and the rest of the terms in Equation 5.3 are constant for a given membrane and salt solution. Since C_{DI} increases linearly with time for the duration τ of a run (Equation 4.5), and the term $J_{w,DO}/ A'\phi nR_gT$ is a constant , it results that C_{mem}^{DO} increases linearly with time for the duration τ of a run. The slope of the line for the plot $C_{mem}^{DO} = f(t)$ is the same as the slope β for the plot $C_{DI} = f(t)$. The intercept is given by $(J_{w,DO}/ A'\phi nR_gT) + (C_{DI})_{t=0}$. Table 5.1 presents C_{mem}^{DO} averaged over the duration τ of a run for all four membranes when bulk salt solution concentration is 0.05 mol·L^{-1}. The C_{mem}^{DO} averaged over the duration τ of a run at different bulk salt solution concentrations is presented in Table F.1.

Table 5. 1 Pure water permeability and concentrations of the salt solution at the membrane wall for bulk salt solution concentration of 0.05 mol·L^{-1} in direct osmosis experiments.

Salts	C_{mem}^{DO} (mol·L^{-1})			
	SE	AD	CG	CK
LiCl	0.015	0.024	0.010	0.003
NaCl	0.017	0.030	0.010	0.002
KCl	0.016	0.031	0.010	0.003
$MgCl_2$	0.022	0.032	0.011	0.005
$CaCl_2$	0.022	0.032	0.011	0.005
$BaCl_2$	0.022	0.029	0.011	0.005

As shown in Table 5.1 and Table F.1, the concentration at the membrane wall is lower than the bulk salt solution concentration. Similar observations are made by Rautenbach and Albrecht (1989). The "dilution" phenomena at the membrane surface due to the counter water flux in the direct osmosis experiments is the opposite of the concentration polarization phenomena existing in the reverse osmosis experiments.

5.1.2 Salt transport in the direct osmosis experiments

Equation 4.4 describing the linear variation of the bulk salt solution concentration in time during a run is corrected for the concentration at the membrane wall C_{mem}^{DO} and becomes Equations 5.4. Consequently, Equation 4.6 becomes Equation 5.5 which is used to calculate the new salt permeability coefficients $(D/K\delta)_{DO}$. Figure 5.2 presents the salt permeability coefficients $(D/K\delta)_{DO}$ before and after correction.

$$\left(C_{mem}^{DO}\right)_t = \left(C_{mem}^{DO}\right)_{t=0} + \beta t \tag{5.4}$$

$$\left(\frac{D}{K\delta}\right)_{DO} = \frac{\Delta N}{S\tau}\,\frac{A'\phi n R_g T}{J_{w,DO}} \tag{5.5}$$

Figure 5.3 shows a significant increase of the salt permeability coefficient when the concentration from the bulk solution is replaced by the concentration at the membrane wall C_{mem}^{DO}. The increase of the salt permeability is lowest for the seawater membranes SE and AD (by 2.4 times in average over the six salts) and it is highest for the nanofiltration membrane CK (by 12.2 times in average over the six salts). The increase corresponds to the decrease in the salt solution concentration from the bulk value C_S to C_{mem}^{DO}, which is lowest for the seawater membranes SE and AD and highest for the nanofiltration CK (Table 5.1).

The order the salts permeate through the membranes remains the same as before the correction, which is $MgCl_2 < CaCl_2 < BaCl_2 < LiCl < NaCl < KCl$. After correction, the salt permeability for chlorides salts is lower than for acetates (Figure F.1 and F.2), which is the same as the finding before the correction (Figures 4.4 and 4.5). The order of the permeation rate among the six salts as well as the differences in the permeation for chlorides and acetates are discussed later in this Chapter (Section 5.5).

For the SE membrane, $(D/K\delta)_{DO}$ varies inverse proportionally to the concentration at the membrane wall, regardless whether the correction is made (Figures F.3 and F.4) or not (Figure 4.2 and 4.3). This is in agreement with the results reported by Heyde et al. (1974) who calculated the salt permeability based on conductivity measurements in a similar experimental set up.

Chaudry (2002) has calculated the salt diffusivity, D, in symmetric cellulose acetate membranes using kinetic conductance measurements and the equation of direct osmosis into and out of a semi-infinite slab (time lag method). Chaudry has found that D increases with the bulk salt concentration. On the other hand, theoretical and experimental studies on dependence of K on the concentration in the bulk solution show that K is independent of the concentration for both for cellulose acetate membranes

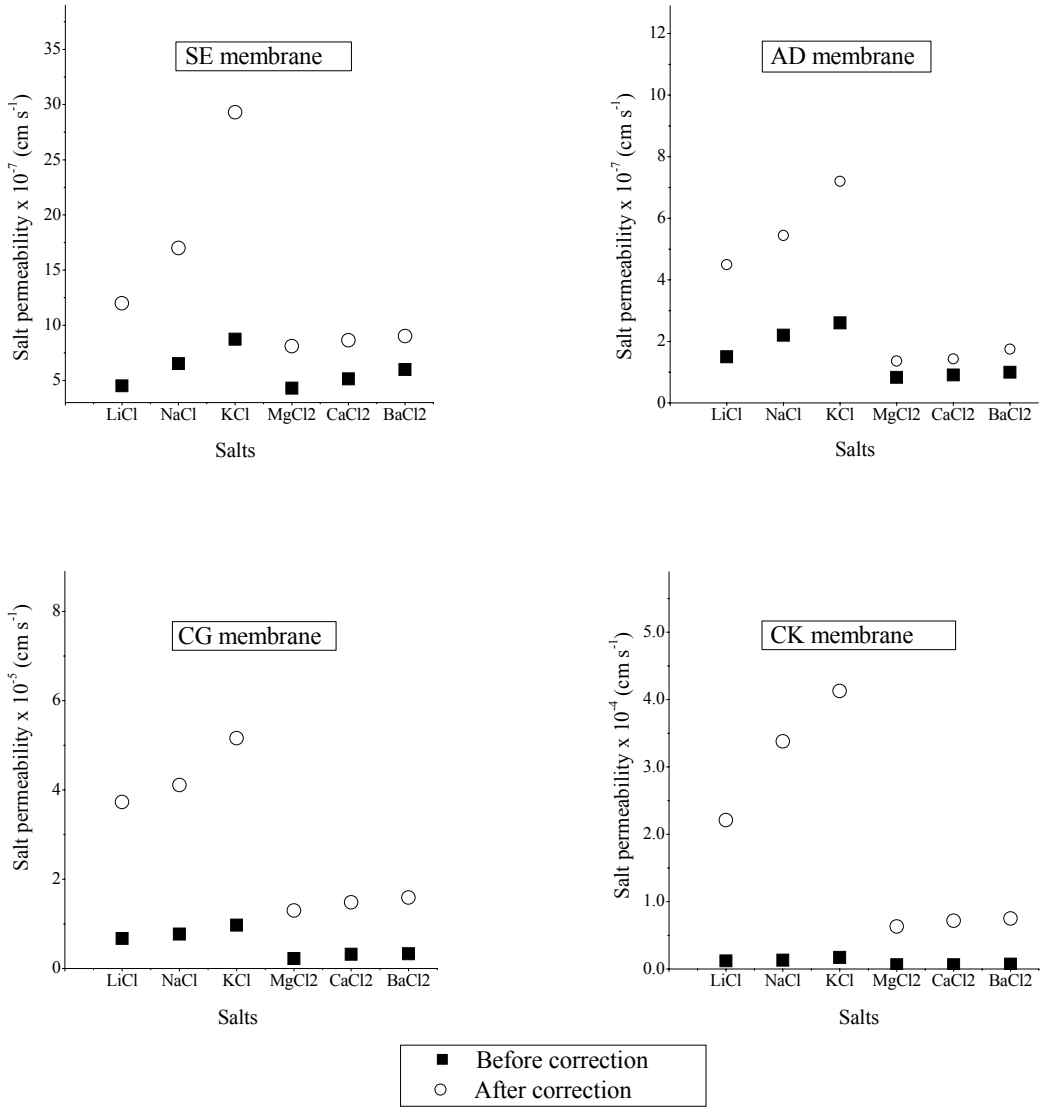

Figure 5. 2 Salt permeability before and after the correction of the membrane wall for SE, AD, CG and CK membranes in the direct osmosis experiments.

(Lonsdale et al., 1965; Heyde et al., 1974; Glueckauf, 1976) and for aromatic polyamide membranes (Frommer et al., 1973; Strathmann and Michaels, 1977). Assuming that K is independent of the concentration in Chaudry's research, and since δ is a constant, it results that $(D/K\delta)_{DO}$ increases with bulk concentration, which disagrees with Heyde's results and the results of this research. This contradiction can come from the assumption that K is independent of the bulk solution concentration or from the differences in evaluating the salt permeability coefficient.

5.1.3 Pure water transport in the direct osmosis experiments

As presented in Table 4.1, the order the pure water permeability A' increases is given by $A'_{SE} < A'_{AD} < A'_{CG} < A'_{CK}$. To date, there are no results found in the literature about the differences in the pure water permeability when the membrane is inverted. Assuming that by inverting the membrane the order of pure water permeability remains the same among the four membranes, the order A' increases for the four membranes is consistent with the order found in the literature, which is $A_{seawater} < A_{\text{brackish water}} < A_{\text{nanofiltration}}$ (Baker, 2000). The order is also the same for the order of A calculated in the KS model in the RO flat sheet membrane experiments (Table 4.9). The two parameters A' and A are presented in Figure 5.3.

As mentioned before, the pure water permeability A' is obtained when the skin layer faces the low pressure side whereas A is obtained when the membrane skin layer faces the high pressure side. When the skin layer faces the lower pressure side, the polysulfone support layer faces the high pressure side. In this configuration, the skin layer is subject to a lower pressure than if it were facing the high pressure side because there is additional resistance due to the support layer resistance. Jonsson and Benavente, (1992) has shown that 8% of the total hydraulic resistance of the membrane to the flow is due to the support layer. This explains that the pure water permeation when the skin layer faces the lower pressure side (A') is

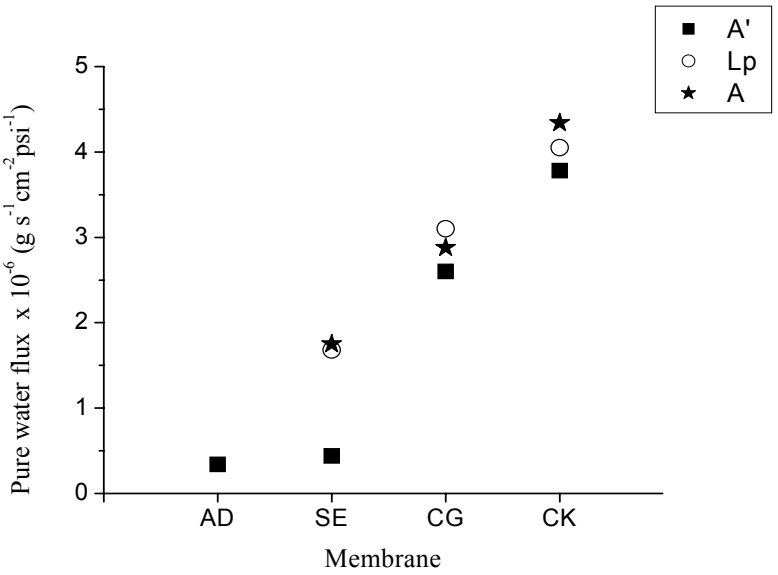

Figure 5. 3 Pure water permeability when the skin layer of the membranes faces the low pressure side (A') and high pressure side (L_p and A).

smaller than the pure water permeation when the skin layer faces the high pressure side (A). An illustration of the differences in the pressure across the skin layer for A and A' is presented in Figure 5.4, assuming that 8% of the total membrane resistance to the flow is due to the support layer.

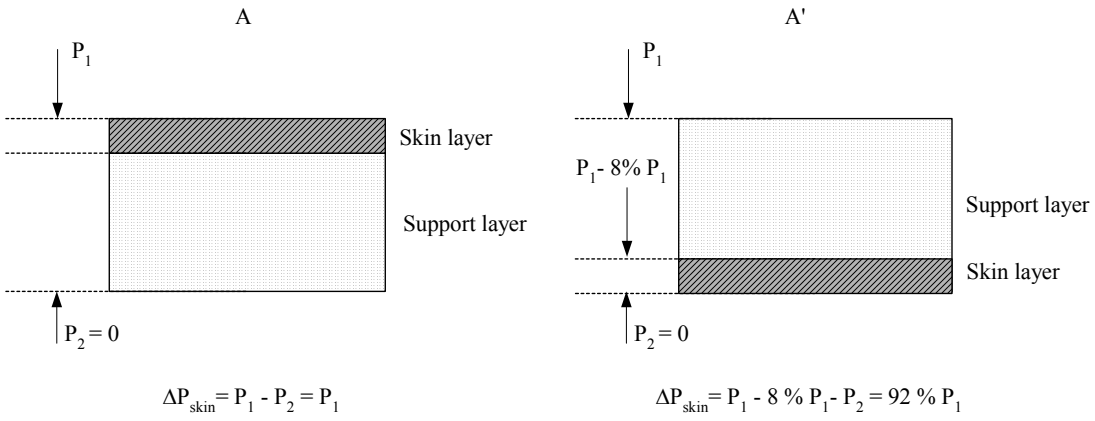

Figure 5. 4 Comparison of the differential pressure at the skin layer when the membrane is inverted.

According to the Table 4.2, the flux of pure water, $J_{w,DO}$, in the nanofiltration membrane, CK, is higher than in the seawater membranes but lower than in the brackish water membrane, CG. A larger pure water flux in a brackish water membrane than in a less "tight" membrane, such as the nanofiltration membrane, might seem surprising. According to the Equation 5.2, there are two factors controlling the flux of the pure water in direct osmosis: the pure water permeability, A', and the differential osmotic pressure, $\Delta\pi$. The order of A' among the four membranes is given by $A'_{AD} < A'_{SE} < A'_{CG} < A'_{CK}$, whereas the order of $\Delta\pi$ is $\Delta\pi_{CK} < \Delta\pi_{CG} < \Delta\pi_{SE} < \Delta\pi_{AD}$. Since the pure water flux is determined by the product $A'\Delta\pi$ (Equation 5.2), no ranking of the pure water flux can be established among the four membranes.

For all four membranes, the pure water flux is higher for the 1:2 salts than for the 1:1 salts. This can be explained by Equation 5.2 and considering that 1) the concentration at the membrane wall C_{mem}^{DO} is higher for the 1:2 salts than for 1:1 salts (Table 5.1); and 2) the concentration in the DI water side C_{DI} is negligible comparing to C_{mem}^{DO} (is less than 6%).

Equation 5.2 also explains the increase in the pure water flux with the increase in the salt concentration in the bulk solution (Figures 4.7 and 4.8). As presented in Table F.1, the increase in the bulk solution concentration determines an increase in the concentration at the membrane wall which results in higher pure water flux.

Moreover, Equation 5.2 explains that for a given membrane and for a given bulk solution concentration, the pure water flux is the same for all 1:1 salts (Figure 4.9). The pure water flux is also the same for all 1:2 salts in a given membrane at constant bulk solution concentration. As shown in Table F.1, at a given bulk solution concentration, the concentration at the membrane wall depends only on the valence of the cation and anion in the salt (ie 1:1 or 1:2). Since A' is constant for a membrane and C_{DI} is negligible comparing to

C_{mem}^{DO}, it results that at constant bulk solution concentration, the pure water flux depends only on the salt valence configuration. This result verifies the assumption that the water and salt fluxes do not interact with each other within the membrane in direct osmosis (Section 5.1.1).

5.1.4 Salt and water transport in the case of fluxes interaction in direct osmosis experiments

If the salt and water fluxes interact within the membrane, Equation 5.2 describing the transport of pure water and Equation 5.5 describing the transport of salt in the direct osmosis experiments have to be corrected with terms counting for the fluxes interaction. By analogy with the equations in the Spiegler-Kedem model (Chapter 2, Section 2.1.3.1), a possible way of correcting Equations 5.2 and 5.5 is given in Equations 5.7 and 5.8.

$$J_{w,DO} = L_p \sigma_1 \Delta\pi \tag{5.7}$$

$$J_s = \omega \Delta\pi - C_{avg}(1-\sigma_2) J_{w,DO} \tag{5.8}$$

Assuming that the concentration at the membrane wall C_{mem}^{DO} is known, the parameters L_p, σ_1, ω, and σ_2 can be determined by performing DO runs at several pressures lower than $\Delta\pi$ so that the water and salt flux have opposite directions. The coefficients ω and σ_2 can be determined graphically from Equation 5.8 whereas Lp and σ_1 can be determined graphically from $J_{w,DO} = L_p(\Delta P - \sigma_1 \Delta\pi)$. The key point here is to know C_{mem}^{DO}. The possibility of applying the film theory to determine C_{mem}^{DO} needs to be explored further and is beyond the purpose of this research.

5.2 Analysis of the transport parameters in the SK model

Several authors using the SK model in calculating the salt transport parameters assume that the concentration at the membrane wall is equal to the feed concentration in the bulk solution (Diawara, et al. 2003; Pontie et al. 2003; Schaep et al. 1998; Van Gauwbergen and Baeyens 1998). Moreover, a resulting salt-water coupling coefficient σ_2 close to 1 makes some authors conclude that the coupling salt-water is insignificant and the transport of salt is diffusion dominant (Marinas and Selleck, 1992; Urama and Marinas, 1997). Only a few authors have taken the next step to actually calculate the percentage of the diffusive flux of the total flux, J_{diff}/J_{total} (Gilron et al. 2001; Chaudry 2002).

The phenomenon of concentration polarization cannot be neglected a priori in any filtration processes using membranes, unless either measurements or calculations prove otherwise. In this research, concentration polarization is neglected in the first case of the SK model in order to analyze the implications in determining the salt and water transport parameters.

As presented in the previous chapter, Figures 4.15 and 4.16, significant differences in the salt transport parameters result when concentration at the membrane wall is replaced by the concentration polarization in the SK model. The objectives of this section are: 1) to analyze the changes in the salt permeability, $P_{RO,}$ the reflection coefficient σ_1, the salt-water coupling coefficient, σ_2, as well as J_{diff}/J_{total} when the concentration polarization is considered; 2) to compare the two methods of calculating the concentration polarization for the three membranes; 3) to compare the changes in water transport, L_P, as well as σ_1 and σ_2 when concentration polarization is considered; and, 4) to determine the most appropriate way of calculating the concentration at the membrane wall in the SK model.

First, the discussion addresses the transport of salt though the three membranes used in the RO flat sheet cell experiments. This part of the discussion is divided for each membrane type for an easier analysis. Next, the discussion addresses the transport of water in the same three membranes.

5.2.1 Salt transport in the seawater membrane AD

In the first case of the SK model when the concentration polarization is ignored, the results lead to contradictory conclusions for the AD membrane. As shown in Table 4.2, σ_2 has a minimum value of 0.981 which would correspond to uncoupled fluxes for salt and water ($\sigma_2 \approx 1$). However, the percentage of the diffusive flux of the total flux is lower than 43% (Table 4.2). It results that the salts are mainly transported through the seawater membrane in a convective flux, therefore the water and salt fluxes are strongly coupled. These contradictory results come from disregarding the concentration polarization at the membrane wall.

The second case of the SK model considers the concentration at the membrane wall when $\sigma_1=1$. Calculating the concentration at the membrane wall from $J_v = L_p(\Delta P - \sigma_1 \Delta\pi)$ when $\sigma_1=1$ results in the maximum value of the concentration polarization, C_{mem}^{max}. Since the seawater membrane has high rejection (R is higher than 0.995), C_{mem}^{max} represents a good approximation of the real concentration at the membrane wall.

C_{mem}^{max} is on average over six salts, 3.1 times higher than the concentration in the bulk solution. C_{mem}^{max} increases in the order $MgCl_2$<LiCl=$CaCl_2$<NaCl=$BaCl_2$<KCl which is consistent with the order reported in the literature (Srinivasan and Tien, 1970; Krinke, 1988). When the concentration of the bulk solution is replaced by C_{mem}^{max} in the SK model, the salt transport parameter P_{RO} remains unchanged (within the experimental error-Table G.6) but the

salt-water coupling coefficient σ_2 increases to 0.999 and becomes equal for all six salts. The equality of the salt-water coupling coefficients for all the salts is expected for high selective membranes (Mulder, 2003). The diffusive flux J_{diff} becomes dominant in the total flux for all salts. This is in agreement with the literature which refers RO and nanofiltration membranes as being diffusion-controlled processes (Mallevialle et al., 1996).

In the third case of the SK model, the concentration at the membrane wall, calculated from the film theory and Sherwood correlation is significantly lower than C_{mem}^{max} (Figures 4.7 and 4.8). It is on average over the six salts 1.4 times higher than the concentration in the bulk. Moreover, there is no specific order of developing concentration polarization among the six salts it this case. The salt permeability, P_{RO}, is 19% higher than P_{RO} calculated at the bulk solution concentration. The salt-water coupling coefficient σ_2 increases slightly and remains higher for the 1:2 salts than for the 1:1 salts. The salt convective flux is dominant (except for KCl) which, similar to the first case of the SK model, is an erroneous result.

The differences in the concentration polarization obtained when σ_1=1 and from combination of the film theory with the Sherwood correlation can come from multiple sources. First, the application of the film theory in its original form is criticized in the literature because 1) it assumes the membrane as being a non-porous smooth wall and 2) it assumes that a uniform concentration polarization layer is developed (Sutzkovere et al., 2000). Second, the Sherwood correlation might not be suitable because 1) there are differences in equipment geometry (Sablani et al., 2001); 2) the mass transfer coefficient, k, might not be strictly equal to D/δ (Bhattacharya and Hwang, 1997); and 3) the changes in the viscosity and diffusivity due to concentration polarization are ignored (Gekas and Hallstorm, 1987).

5.2.2 Salt transport in the brackish water membrane CG

When the concentration polarization is ignored for the CG membrane, σ_2 has a minimum of 0.756 which corresponds to a percentage of the diffusive flux of the total flux of 38%. The value of σ_2 shows a higher salt-water coupling effect than in the case of AD membrane and correspondingly, a convective flux dominant in the salt transport. The values of σ_2 and J_{diff}/J_{total} do not lead to contradictory results as in the case of AD membrane (for which at σ_2 =0.992, the J_{diff}/J_{total} is only 22%). However, it results that when the concentration polarization is ignored, the convection is the dominant term of the salt flux in the brackish water membrane. This result is in disagreement with the literature (Mallevialle et al., 1996).

In the second case of the SK model, the values of the concentration at the membrane wall calculated for σ_1=1, C_{mem}^{max}, are on average 1.6 times higher than the concentration in the bulk solution. The salt transport parameter is equal (within the experimental error) to the salt parameter when the concentration polarization is ignored and the salt-water coupling coefficient σ_2 increases on average by 12%. The order σ_2 increases among the six salts remains the same as when the concentration polarization was ignored. An existing order among σ_2 of the six salts is in agreement with findings from literature which suggest that in less selective membranes, an approximate relationship exists between σ_2 and the solute size (Mulder, 2003). In this research, it is observed that the higher the hydrated radii of the cations, the higher the σ_2. The hydrated radii of the cations are discussed later in Section 5.5.1.1. The diffusive flux J_{diff} becomes dominant in the total flux of salt for all salts (72% in average), although not as such high percentage as for the AD membrane (85%). The percentage of J_{diff}/J_{total} for the 1:2 salts are higher than the percentage of J_{diff}/J_{total} for the 1:1 salts. This can be explain by the stronger water-salt coupling for the 1:1 salts than for the 1:2

salts. The dominancy of the diffusion flux is in agreement with the results from the literature (Mallevialle et al., 1996).

In the third case of the SK model, the concentration polarization calculated from the film theory and Sherwood correlation, C_{mem}^{k}, is on average over all salts 1.4 times higher than the concentration in the bulk. Unlike for the seawater membrane, for the brackish water membrane C_{mem}^{k} is very close to C_{mem}^{max}. The values of the salt transport parameters, P_{RO} and $\sigma_{2,}$ as well as J_{diff}/J_{total} are very close to their corresponding values when concentration at the membrane wall is C_{mem}^{max}. The order σ_2 increases among the six salts is the same as for C_{mem}^{max} and the diffusive flux J_{diff} is dominant (68% on average over all salts), with higher percentages for the 1:2 salts than for the 1:1 salts.

Unlike for the seawater membrane, for the brackish water membrane the differences between the set of P_{RO}, σ_2 and J_{diff}/J_{total} are very small in the last two cases of the SK model (i.e. when the concentration polarization is calculated at σ_1 =1 and from film theory combined with Sherwood correlations). Moreover, both cases lead to the right conclusion that the diffusive flux is dominant in the brackish water membrane. This suggests that using the film theory combined with the Sherwood correlation is appropriate for the brackish water membrane, CG. Some possible explanations to the fact that the film theory combined with the Sherwood correlation is appropriate for the CG membrane but not for the AD membrane are 1) the CG membrane is made of cellulose acetate and has a smoother surface than the AD membrane made of polyamide (Elimelech et al., 1997) and 2) the variation of the viscosity and diffusivity due to concentration polarization are lower for the CG membrane than for the AD membrane since C_{mem}^{max} is 3 times higher than the bulk concentration for AD but only 1.6 times higher for CG.

5.2.3 Salt transport in the nanofiltration membrane CK

When the concentration polarization is ignored for the CK membrane, σ_2 has a minimum of 0.416 which corresponds to a percentage of the diffusive flux of the total flux of 15%. This shows the highest salt-water coupling effect among the three membranes studied. Correspondingly, the convective flux is dominant in the salt transport (more than 71%). This result is in disagreement with the literature (Mallevialle et al., 1996).

The concentration at the membrane wall when $\sigma_1 = 1$, C_{mem}^{max}, is on average over six salts the same as C_{mem}^{max} for the brackish water membrane (1.6 times the bulk concentration). The salt transport parameter P_{RO} and σ_2 increase significantly comparing to their values when concentration polarization is ignored (on average by 109% for P_{RO} and by 59% for σ_2). The order σ_2 increases among the six salts is the same as for the brackish water membrane. The diffusive flux J_{diff} is dominant and it is higher for the 1:2 salts than for the 1:1 salts. J_{diff}/J_{total} is almost the same as for the brackish water membrane (74% in average).

The values of concentration at the membrane wall calculated from the film theory and Sherwood correlation are on average the same as for the CG membrane (1.4 times the bulk concentration). In this case, the values of the salt transport parameters, P_{RO} and σ_2, are equal (within the experimental error –Table G.6) with the corresponding values when $\sigma_1 = 1$. The diffusive flux J_{diff} becomes almost as the same percentage as for the CG membrane (65% on average), with higher percentages for the 1:2 salts than for the 1:1 salts.

Just as in the case of the brackish water membrane, the results from the last two cases of the SK model are very similar for the nanofiltration as well. This shows that calculating the concentration at the membrane wall by combining the film theory and the Sherwood correlation is adequate for the nanofiltration membrane. Moreover, when the concentration

polarization is considered, the diffusive salt flux represents almost the same percentage of the total salt flux for the brackish water membrane, CG, and for the nanofiltration membrane, CK. For both CG and CK, σ_2 and J_{diff}/J_{total} are lower for the 1:1 salts and 1:2 salts. This shows the similarity in the transport mechanism for the two membranes. This is in agreement with the literature which refers nanofiltration membranes as "loose" RO membranes with high rejection for the 1:2 salts and low rejection for the 1:1 salts (Mallevialle et al., 1996).

5.2.4 Water transport in the SK model

The three cases of the SK model presented above for the discussion of the salt transport parameters are considered in analyzing the hydraulic permeability L_p. Also the discussion includes the investigation on the validity of the Onsager reciprocal relation $\sigma_1 = \sigma_2$.

The hydraulic permeabilities, L_p, are equal within the experimental error (Table G.6) for all three cases of the SK model. The order L_p increases for the three membranes is $L_{p(seawater)} < L_{p(brackish\ water)} < L_{p(nanofiltration)}$. This order is in agreement with the membranes manufacturer data for the typical product flux at the same operating pressure ΔP (Table 3.2).

The Onsager reciprocal relation $\sigma_1 = \sigma_2$ is verified in all three cases of the SK model and for all three membranes, except for the 1:1 salts for the nanofiltration membrane when σ_1 is 27% lower than σ_2.The large majority of the authors using the SK model assume that the Onsager reciprocal relation is verified and deal with only one parameter $\sigma = \sigma_1 = \sigma_2$ in the SK model equations. However, according to Mason et al. (1972), the coefficients σ_1 and σ_2 are equal only if proven to be so experimentally.

According to Mason and Lonsdale (1990), σ_1 represents the effectiveness of a salt to develop an osmotic pressure across the membrane whereas σ_2 describes the effectiveness of

the membrane to separate salt and water in the volume flow of the product. Assuming that for a membrane the salt is transported entirely due to diffusion, $\sigma_2 = 1$ because there is no convective flux for the salt. The reflection coefficient, σ_1, can be lower than 1 because the membrane is not rejecting the salt 100%, since there is a salt diffusive flux. The higher the membrane rejection, the closer σ_1 is to 1. Therefore $\sigma_1 = \sigma_2$ only in ideal membranes with a salt rejection of 100% and $\sigma_1 < \sigma_2$ for any non-ideal membranes. The differences in the two coefficients σ_1 and σ_2 are smaller for membranes with higher diffusion fluxes. This is illustrated in Figure 5. 5 using data from Tables 4.3, 4.5 and 4.7.

As shown in Sections 5.2.1 through 5.2.3, when the concentration polarization is considered, all three membranes are diffusion dominant in regards to the salt transport. This explains that $\sigma_1 = \sigma_2$ (within the experimental error-Table G.6) for all membranes and all salts except for 1:1 salts in nanofiltration membrane. The percentage of J_{diff}/J_{total} is lowest for the 1:1 salts in the nanofiltration membrane (55%) which explains that σ_1 is lower than σ_2.

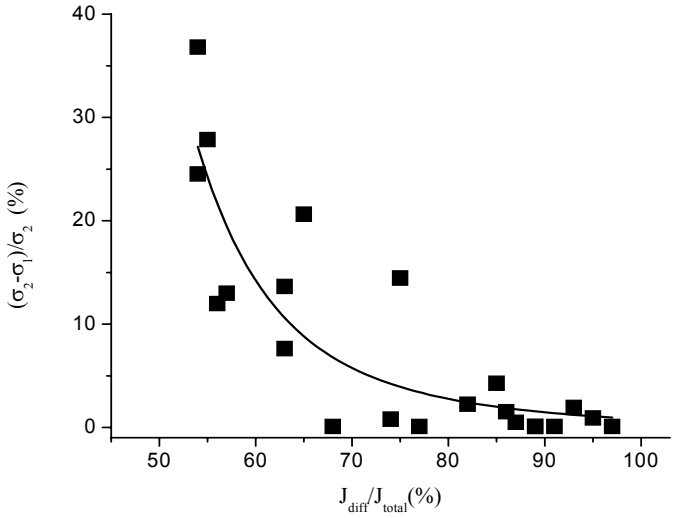

Figure 5. 5 Dependence of the relative difference of σ_1 and σ_2 on the percentage of the diffusive flux of the total flux for all membranes when concentration polarization is considered.

5.2.5 Conclusions on the SK model

Neglecting the concentration polarization in the SK model leads to the erroneous result that convection is the main mechanism of transport in all three membranes. This case is disregarded from any further discussion in this Chapter.

Two cases of calculating the concentration at the membrane wall are considered: 1) when σ_1=1 and 2) combining the film theory with the Sherwood correlation. Both methods lead to close results for the salt transport parameters for the brackish water membrane as well as for the nanofiltration membrane. It results that the diffusion is the dominant flux in the transport of salt across the membranes (68% to 72% for the CG membrane and 65% to 74% for the CK membrane). The salt –water coupling coefficient has a certain trend of increasing among the six salts which can be explained by the hydrated radii of the salts. The contribution of the diffusive flux to the total flux is on average lower for the 1:1 salts than for the 1:2 salts which is a consequence of the differences in the salt-water coupling coefficient for the 1:1 salts and 1:2 salts.

Only the first case of calculating the concentration at the membrane wall (i.e. when σ_1=1) is acceptable for the seawater membrane. In this case, the diffusion flux is dominant at a higher percentage than for the brackish water and nanofiltration membrane (85% on average over all salts). The salt –water coupling coefficient is equal for the six salts which can be explained by the high rejection of this membrane (R>99.5%).

The hydraulic permeability, L_P, is equal within the experimental error for the two cases of calculating the concentration at the membrane wall. The Onsager reciprocity relation $\sigma_1 = \sigma_2$ is valid only for high J_{diff}/J_{total}, i.e for all membranes and all salts in this research except for the 1:1 salts in NF membrane.

5.3 Comparison of the SK and KS models

The differences of the results from the transport models, Spiegler-Kedem and Kimura-Sourirajan, are analyzed in this Section. The discussion refers first to the salt transport and next to the water transport. The objective is to prove that the two models lead to identical salt and water permeability coefficients for the membranes with high percentage of the salt diffusive flux.

5.3.1 Comparison of salt transport parameters, P_{RO} and $(D/K\delta)_{RO}$

As mentioned before, the first case of the Spiegler-Kedem model neglects the concentration polarization and leads to erroneous results for all three membranes. For the seawater membrane, the third case of the SK model also leads to erroneous results. The discussion below considers only the valid cases of the SK model, which are 1) for the seawater membrane, the second case of the SK model when the concentration polarization is calculated for $\sigma_1 = 1$ and 2) for the brackish water membrane and the nanofiltration membrane, both the second and the third case of the SK model.

The salt transport parameter P_{RO} and $(D/K\delta)_{RO}$ are equal (within the experimental error-Table G.6) for the seawater membrane, AD, for all studied salts. For the brackish water membrane, CG, and the nanofiltration membrane, CK, the discussion has to be divided between 1:1 salts and 1:2 salts. Thus, for the 1:1 salts, the salt transport parameter P_{RO} is 24% to 46% lower than the salt permeability $(D/K\delta)_{RO}$ whereas for the nanofiltration membrane CK, P_{RO} is 22 % to 51% lower than the salt permeability $(D/K\delta)_{RO}$. For the 1:2 salts, the differences between P_{RO} and $(D/K\delta)_{RO}$ are within the experimental error (Table G.6) for both CG and CK. These results can be explained by looking back to the assumptions made in calculating $(D/K\delta)_{RO}$ in the Kimura-Sourirajan model.

The KS model assumes that there is no convective flux of the salt (or no coupling salt-water) and the transport is due to the differences in salt concentrations across the membrane. Salt permeability $(D/K\delta)_{RO}$ can be related to P_{RO} in Equation 5.9 which results by equaling Equations 2.8 and 2.12:

$$\left(\frac{D}{K\delta}\right)_{RO} = P_{RO} + \frac{(1-\sigma_2)J_v C_{avg}}{\Delta C} \tag{5.9}$$

The two salt transport parameters will be equal when the salt-water coupling coefficient, σ_2, is one. This situation is equivalent to the absence of any convective salt flux. The closer σ_2 is to one, the lower the difference between $(D/K\delta)_{RO}$ and P_{RO}. As presented in Table 4.3 and 4.5, the lowest value of σ_2 is 0.989 for the AD membranes which validates the equality of the two parameters P_{RO} and $(D/K\delta)_{RO}$ for this membrane for all salts. For the CG and CK membranes, P_{RO} and $(D/K\delta)_{RO}$ are equal for the 1:2 salts when σ_2 has minimum values of 0.961 and 0.907, respectively.

The largest difference (46%) between P_{RO} and $(D/K\delta)_{RO}$ is achieved for NaCl in CG membrane when σ_2 is 0.885 (Table 4.5). Similar, the largest difference of 51% between P_{RO} and $(D/K\delta)_{RO}$ is achieved for KCl in CK membrane when σ_2 is 0.731 (Table 4.5). Figure 5. 5 presents the differences between P_{RO} and $(D/K\delta)_{RO}$ as function of σ_2. It is observed from Figure 5. 5 that large differences between P_{RO} and $(D/K\delta)_{RO}$ correspond to large values of σ_2, which in turn, correspond to low percentages of the salt diffusive flux. It results that the two parameters P_{RO} and $(D/K\delta)_{RO}$ are equal for high σ_2 when the diffusive flux dominates. Similar results are presented by McCray et al. (1991) for cellulose acetate membranes. The authors found that the differences between P_{RO} and $(D/K\delta)_{RO}$ increase as σ_2 decreases. For

comparison, the variation of $[P_{RO} - (D/K\delta)_{RO}]/P_{RO}$ with σ_2 according to McCray et al. (1991) is also plotted in Figure 5. 6.

5.3.2 Comparison of pure water transport parameters, L_p and A

The hydraulic conductivity of the membranes, L_P, is calculated in two cases of the SK model. First, considering the concentration at the membrane wall equal to the concentration in the bulk solution, and second, calculating the concentration polarization from combining the film theory with the Sherwood correlation. These results are compared with the pure water permeability A for the KS model for all three membranes (Table 4.6).

The hydraulic conductivity, L_p, is equal in both cases of the SK model and equal with the pure water permeability, A, calculated from the KS model. This shows that L_p and A are identical parameters which are intrinsic characteristics of the membranes.

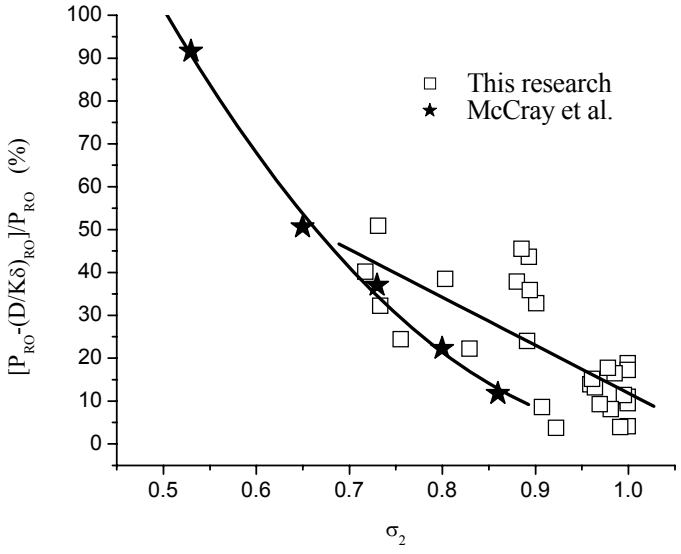

Figure 5. 6 Variation of the difference in the salt permeabilities in the SK and the KS models with the salt-water coupling coefficient.

5.3.3 Conclusions on the comparison of SK and KS models

The two RO models, Spiegler-Kedem and Kimura-Sourirajan, lead to equal salt and water transport parameters for diffusion-controlled membranes for which the diffusive flux is at least 67%. For diffusion-controlled membranes for which the diffusive flux is lower than 67% (such as brackish water membrane and nanofiltration membrane for the 1:1 salts), the salt permeability in the KS model is larger than in the SK. Since low percentage of the diffusive salt flux is directly correlated to low membrane rejection (Figure 5.7, coefficient of correlation of 0.73), it is concluded that KS model is inappropriate to be used for salts with low rejection in a membrane.

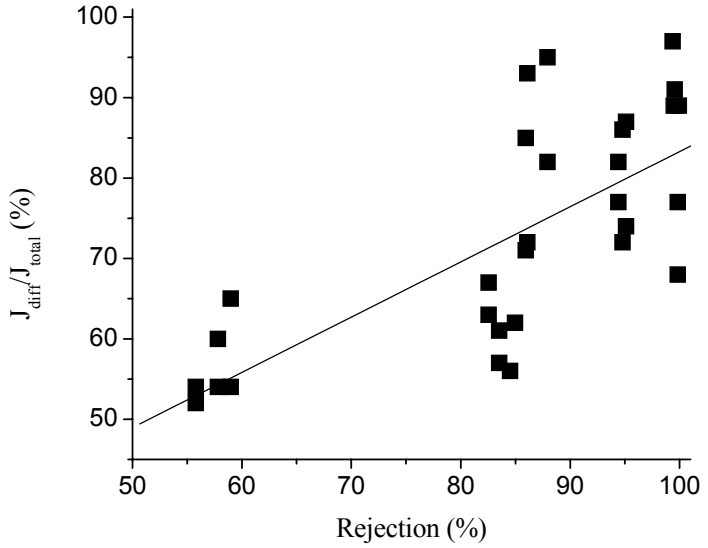

Figure 5. 7 Variation of the salt diffusive flux with membrane rejection.

5.4 Comparison of salt permeability in DO and RO experiments

The salt permeability obtained in Section 5.1.2 from the direct osmosis experiments is compared to the salt permeability from: 1) RO flat sheet membrane experiments-SK model (valid cases only - Section 5.3.1) and 2) RO flat sheet membrane experiments-KS model. The

objective of this section is to demonstrate that the salt permeabilities in the direct osmosis and reverse osmosis experiments are equal for high rejection membranes.

The differences in the salt permeabilities are reported as percentages of the salt permeability in direct osmosis in Table 5.2. The differences are within the experimental error (Table G.6) in all cases except for the salt permeability in the KS model for the 1:1 salts in the brackish water and nanofiltration membranes. The case of 1:1 salts in the KS model for the brackish water and nanofiltration membranes is discussed in Section 5.3 where it is concluded that the KS model is not appropriate to be used for these salts with these membranes.

Table 5. 2 Differences (as percentages) between the salt permeability in direct osmosis experiments and salt permeability from SK and KS models in RO flat sheet membranes.

Seawater membrane AD			
Salts	$P_{RO}^{(2)}$		$(D/K\delta)_{RO}$
LiCl	13		2
NaCl	8		18
KCl	25		28
$MgCl_2$	10		1
$CaCl_2$	7		13
$BaCl_2$	21		0
Brackish water membrane CG			
Salts	$P_{RO}^{(2)}$	$P_{RO}^{(3)}$	$(D/K\delta)_{RO}$
LiCl	16	29	53
NaCl	18	30	55
KCl	16	31	48
$MgCl_2$	20	22	29
$CaCl_2$	17	20	30
$BaCl_2$	16	19	31
Nanofiltration membrane CK			
Salts	$P_{RO}^{(2)}$	$P_{RO}^{(3)}$	$(D/K\delta)_{RO}$
LiCl	23	21	40
NaCl	13	2	32
KCl	27	4	38
$MgCl_2$	14	31	18
$CaCl_2$	19	23	26
$BaCl_2$	19	23	30

Notes: $P_{RO}^{(2)}$ denotes the salt permeability for the second case of the SK model (when the concentration at the membrane wall is calculated for $\sigma_1=1$).
$P_{RO}^{(3)}$ denotes the salt permeability for the third case of the SK model (when the concentration at the membrane wall is from combination of the film theory and Sherwood correlation).

The equality of the salt permeabilities in direct osmosis (zero external pressure) and reverse osmosis (external pressure up to 400 psi) shows that the rate the salt is transported through the membrane does not depend on the external pressure applied. It also shows the validity of the three models used. It leaves the possibility to choose what type of experiment and what model is the most appropriate to use in different circumstances. For example, the SK model is the most laborious model, requiring data from at least three different operation pressures as well as the pre-determination of the concentration at the membrane wall. The

benefit of this model is the quantification of the diffusion and convection fluxes for the salt. The use the KS model requires data at only one operating pressure but also needs a value for pure water permeation that has to be determined by preliminary independent pure water runs. The direct osmosis experiments can be done using lower cost apparatus and with low energy requirements. However, the concentration at the membrane has to be determined also. A summary of the RO and DO models characteristics is presented in Table 5. 3 and 5.4.

Table 5. 3 Comparison of the requirements for the two RO models and the DO model.

Requirements	RO: Spiegler-Kedem	RO: Kimura-Sourirajan	DO
Operating pressure	At least 3	1	N/A
Preliminary water runs	No	Yes	Yes
Other parameters required	Concentration polarization	No	No
Energy/Apparatus costs	High	High	Low
Usage for 1:1 and 1:2 salts	Appropriate for all salts	Inappropriate for salts with low rejection (below 84%)	Appropriate for all salts
Error of the method	High	Medium	Low
Information provided	1.Diffusive and convective salt flux 2. Salt-water coupling coefficient	1. Mechanism of transport 2. Salt and water parameters of transport	Salt and water parameters of transport
Apparatus procurement	Easy	Easy	Custom-made cell
Temperature Control	Easy	Easy	Constant ambient temperature ($\pm 1^{o}C$)

Table 5. 4 Comparison of the salt parameters in the three cases of the Spiegler-Kedem model.

	Case 1	Case 2	Case 3
Characteristics	Absence of concentration polarization	Concentration polarization for $\sigma_1 = 1$	Concentration polarization from film theory and Sherwood correlation
P_{RO}	Adequate for SW and 1:2 salt in BW	Adequate for all membranes	Adequate for BW and NF
J_{diff}/J_{total}	Inadequate for all membranes	Adequate for all membranes	Adequate for BW and NF

Notes: SW, BW and NF represents seawater, brackish water and nanofiltration membranes, respectively.

5.5 Factors controlling the salt permeability in RO and NF membranes

It is shown throughout Chapter 4 that there is a pattern of permeability rate among the six salts, regardless of the experiment, model, the membrane material, and membrane configuration used. The order the salt permeability increases is given by $Mg^{2+} < Ca^{2+} < Ba^{2+} < Li^{+} < Na^{+} < K^{+}$ which is in agreement with the results from the literature (Sourirajan, 1970; Yazdani, 1991). The order is also the same as the lyotropic series.

The objective of this section is to determine what physical and thermodynamic factors determine the order of the salt permeability in the studied membranes. The situations considered for analysis are:

- Direct osmosis (DO) experiments-SE, AD, CG, and CK membrane
- Reverse osmosis (RO)-flat sheet membrane experiments-AD, CG, CK membranes
    a. Spiegler-Kedem model, second case (i.e. for $\sigma_1=1$)
    b. Kimura-Sourirajan model
- Reverse osmosis (RO)-spiral wound membrane experiments-SW30 membrane

Since the salt permeability has different notations in each of these experiments and each model implied for the calculations, in this section is named generically " salt permeability".

5.5.1 Physical parameters

The dependency of the salt permeability in the membrane on several physical parameters of the ions in water is analyzed in this section. The physical parameters considered are the cation ionic radii, the cation hydrated radii and the diffusion coefficient of the salt in infinite dilute solution.

5.5.1.1 Ionic and hydrated radii

Although the selectivity of hyperfiltration membranes is acknowledged not to be based on a sieving mechanism, the most intuitive parameter to be considered in analyzing what factors control the salt permeability is the size of the ions. The studied salts are strong electrolytes in an aqueous solvent and at the concentration of 0.05 mol·L^{-1} they dissociate and exist in the form of independent cations and anions (Cussler, 1997). Any movement of the cation (Li^+, Na^+, K^+, Mg^{+2}, Ca^{+2}, and Ba^{+2}) through the membrane implyes an associate movement of the anion Cl^- in order to maintain electroneutrality. Since all the salts considered in this research have a common anion, it is important to consider the physical properties of the cations in examining the differences in the salt permeabilities.

Figure 5.8 shows the variation of the salt permeability with the ionic radii for direct osmosis (DO) and reveres osmosis (RO) experiments for SE, AD, CG, CK, and SW30 membranes. The plots suggest a rather controversial result: for salts with common anion, the larger the ionic size of the cation, the faster it permeates the membrane. For example, the ionic radii of Li^+ and K^+ are 0.60Å and 1.33Å, respectively, and the permeability of NaCl and KCl in the SW30 membrane are 1.91 x10^{-6} cm·s^{-1} and 2.26 x10^{-6} cm·s^{-1}, respectively.

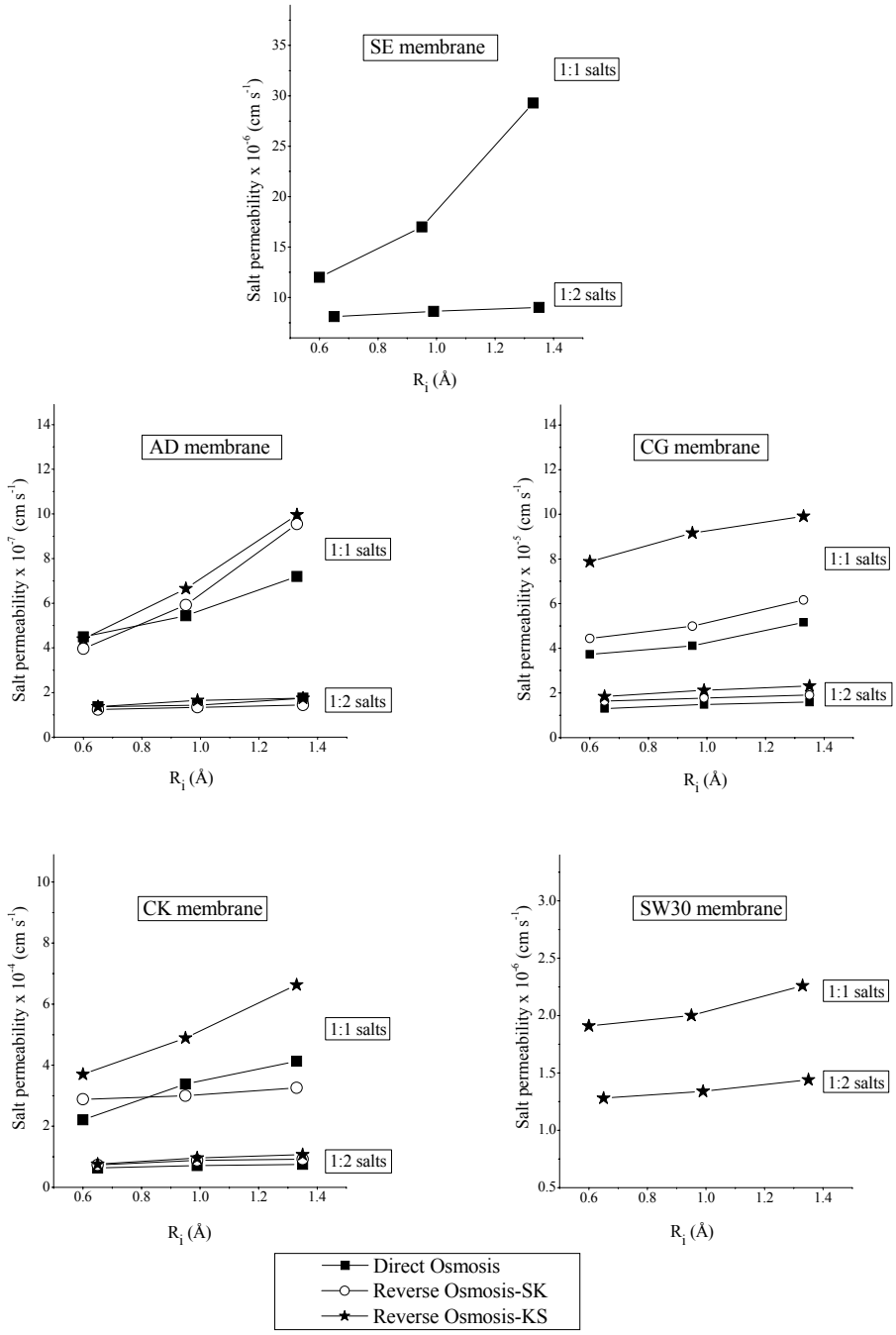

Figure 5. 8 Variation of salt permeability with cation ionic radius of the cation for all salts in direct osmosis and reverse osmosis experiments for AD, CG, CK, and SW30 membranes.

Moreover, there are three pairs of salts with cations of almost the same ionic size (LiCl and $MgCl_2$; NaCl and $CaCl_2$; KCl and $BaCl_2$) which have significant different rate of permeation through membranes. For example, the ionic radii of K^+ and Ba^{+2} are 1.33Å and 1.35Å, respectively, and the permeability of KCl and $BaCl_2$ in the SE membrane are 29.3 $x10^{-7}$ $cm \cdot s^{-1}$ and 9.02 $x10^{-7}$ $cm \cdot s^{-1}$, respectively. Therefore the differences in the ionic radius of the cations can not explain the order the salts move in the studied membranes.

The inconsistencies between the order of the ionic radii and the order of the salt permeability is explained if the ionic radius of a cation is replaced by its hydrated radius. The phenomenon taking place when an ion is introduced in a polar solvent is known as solvation or hydration if the solvent is aqueous. Due to dipolar nature of the water molecules, the dissociated ions form new aggregates consisting of a shell of water molecules known as water of hydration surrounding the ion. The kinetic entity is no longer the bare ion but the ion accompanied by the hydration sphere. However, the water molecules in the hydrate sphere are dynamically exchanged with farther water molecules due to energy fluctuations (Erdey-Gruz, 1974).

The smaller the ionic radius of an ion and the larger the charge, the stronger the interaction with the water molecules because the electric force at the periphery of the ions is larger. Consequently, the hydrated radius is larger. The hydrated radii R_h is related to ionic radii R_i by Equation 5.10:

$$\frac{4}{3}\pi R_h^3 = \frac{4}{3}\pi R_i^3 + n_w\left(\frac{V_w}{N_A}\right) \qquad (5.10)$$

where R_h is the hydrated radii (Å), n_w is the number of water molecules surrounding the ion, known as hydration number, R_i is the ionic radii (Å), V_w is the molar volume of water ($Å^3$), and N_A is Avogadro's number.

There is a considerable discrepancy of the values of the hydration number, n_w, reported in the literature for individual ions. The discrepancies are the result of different methods of measurement of n_w, different assumptions made for the hydration of the chlorine ion, or whether the primary or secondary shell of water molecules is considered. However, the order of hydration remains the same among the studied ions regardless the source considered for the n_w values (Table H.2). Li^+ and Mg^{+2} are the most hydrated of the monovalent and divalent cation series, respectively (Table H.2).

The order the hydrated radii increases among the six cations is the reverse order the ionic radii increases. For example, the ionic radii increase from Li^+ to K^+ whereas the hydrated radii decrease from Li^+ to K^+. This leads to the conclusion that the larger the hydrated radii of the cation, the slower the cation transport across membrane. Figure 5. 9 illustrates the variation of salt permeability with the hydrated radii. Regardless the membrane type (seawater, brackish water or nanofiltration), the type of the experiment (direct osmosis or reverse osmosis), and the membrane configuration (flat sheet or spiral wound), the salt permeabilities are inversely proportional to the hydrated radii of the cations.

5.5.1.2 Diffusibility in solution

It is shown in the previous sections that the mechanism of transport in dense films such as hyperfiltration membranes is diffusion dominant. In Figure 5.10, the salt permeability is plotted against the overall diffusion coefficient of the salt in infinitely dilute solution, D_w, which is calculated based on the diffusion coefficient for ions in infinitely dilute solution using Equation 5.11(Cussler, 1997). The $D_{w,ij}$ is the calculated overall diffusion coefficient

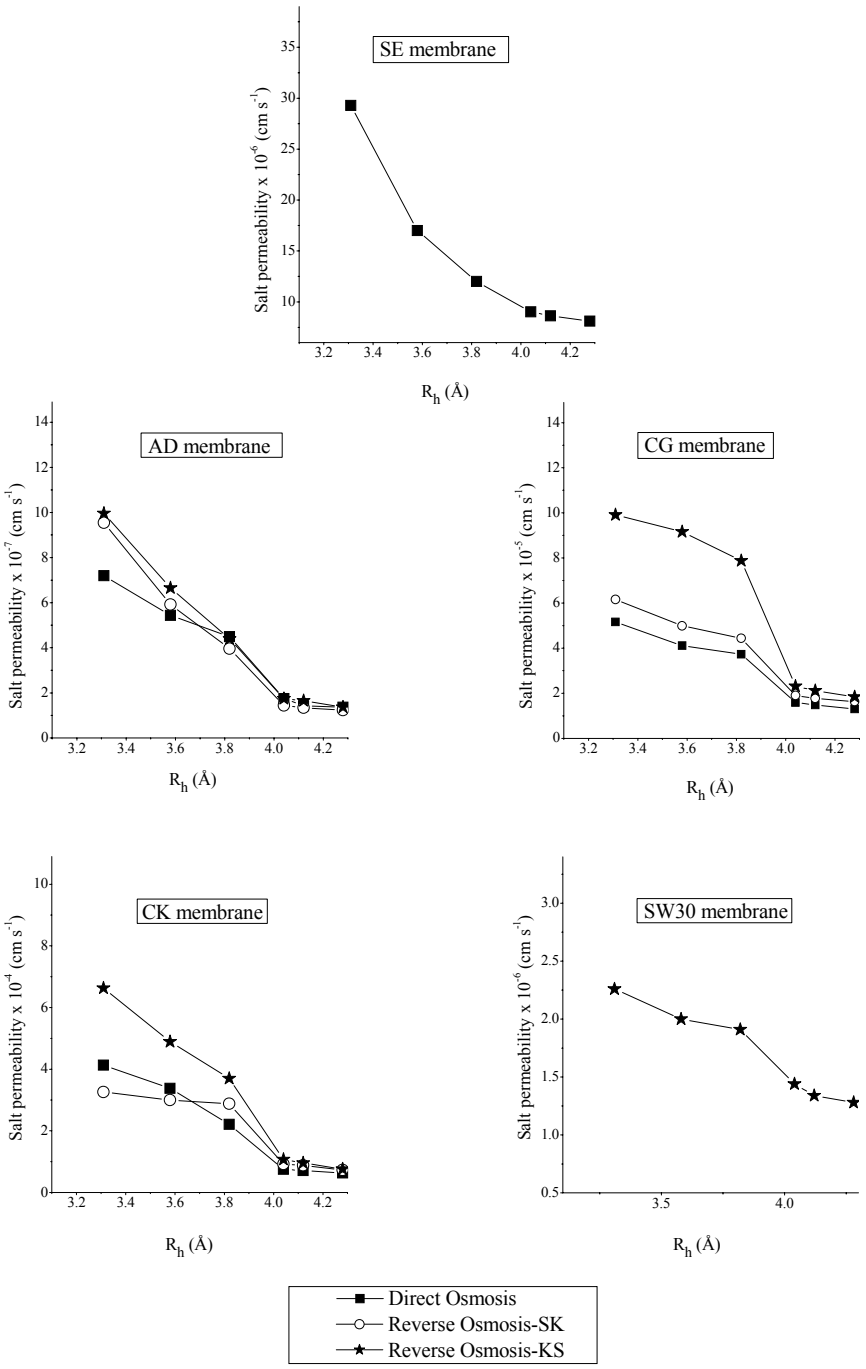

Figure 5. 9 Variation of salt permeability with hydrated radius of the cation for all salts in direct osmosis and reverse osmosis experiments for AD, CG, CK, and SW30 membranes.

is plotted against the overall diffusion coefficient of the salt in infinitely dilute solution, D_w, which is calculated based on the diffusion coefficient for ions in infinitely dilute solution using Equation 5.11(Cussler, 1997). The $D_{w,ij}$ is the calculated overall diffusion coefficient of the "ij" salt in infinitely dilute solutions, $|z_i|$ represents the absolute value of the charge for ion "i", and $D_{w,i}$ represents the tabulated diffusion coefficient for the ion "i" in infinitely dilute solution. It must be emphasized that the diffusion coefficient D from (D/Kδ) characterizes the salt diffusion within the membrane phase and it is different than salt diffusion coefficient, D_w, in infinitely dilute solutions.

$$D_{w,ij} = \frac{|z_i| + |z_j|}{\frac{|z_i|}{D_{w,j}} + \frac{|z_j|}{D_{w,i}}} \tag{5.11}$$

Figure 5.10 shows a linear relationship (average of regression coefficients of 0.93±8%) between the salt permeability and D_w for both 1:1 and 1:2 salts. The diffusion coefficient in water explains the order of permeation among salts with identical valences configuration (i.e. 1:1 salts or 1:2 salts) but does not explain the significant shift up of the 1:1 salts starting at D_w=1.38 x 10^{-5} ($cm^2 \cdot s^{-1}$). The shift up for the 1:1 salts can be explained by the partition coefficient, K, between the membrane and the salt solution. According to Heyde et al. (1974), the membrane/solution partitioning coefficient, defined as 1/K, increases with the decrease in the salt charge. The authors found 1/K equal to 45 and 43 for Na^+ and K^+, respectively, and 1.1 and 6.2 for Mg^{2+} and Ca^{2+}, respectively. The values of 1/K for the monovalent cations are one order of magnitude higher than for the divalent cations and this explains the difference in the salt permeability for salts with similar diffusion coefficients in water.

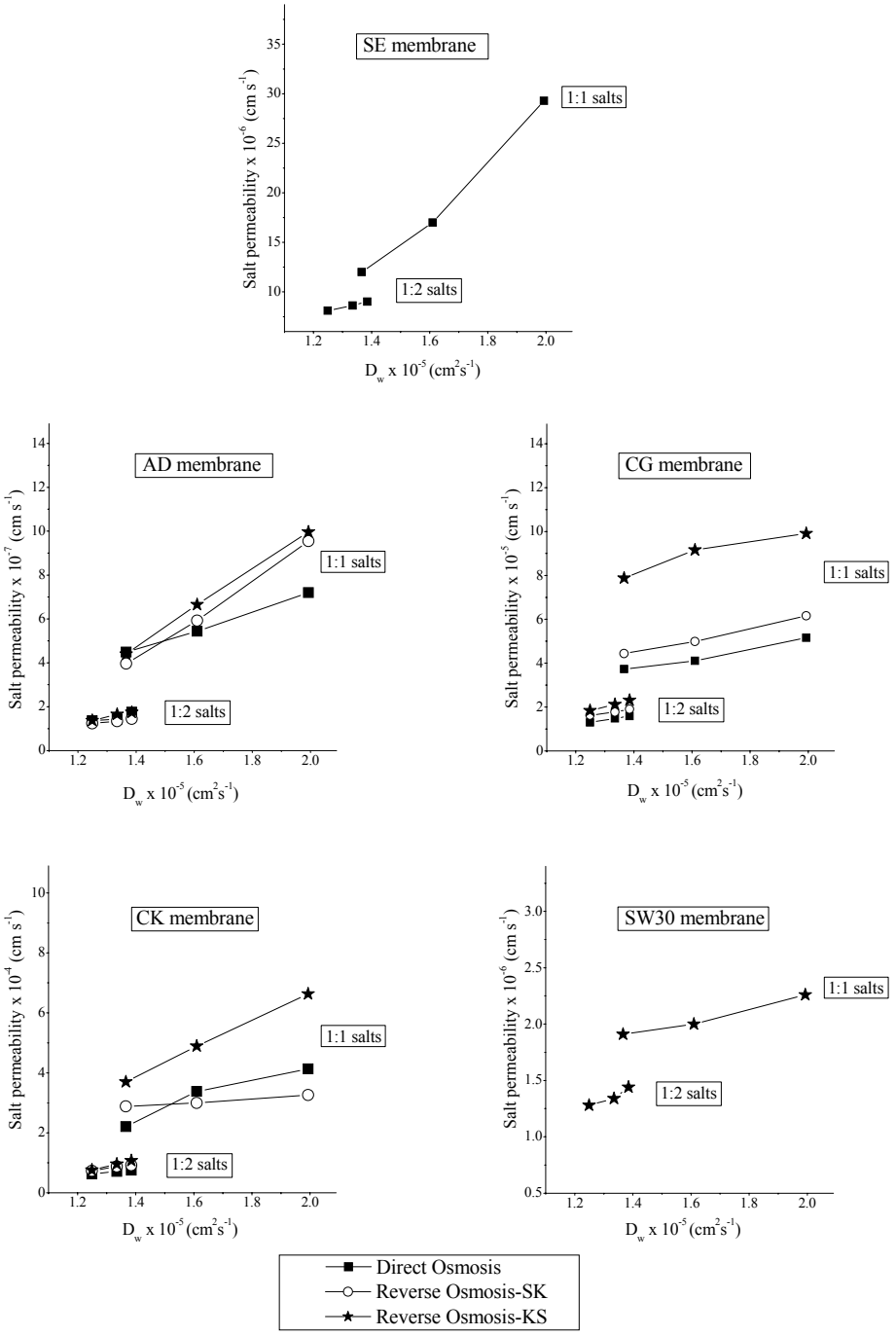

Figure 5. 10 Variation of salt permeability with the diffusion coefficient in infinitely dilute solution for all salts for SE, AD, CG, CK and SW30 membranes.

Among the salts of the same valence configuration (i.e. either 1:1 or 1:2 salts), a highly diffusive salt in solution phase is also highly diffusive in the membrane phase. This suggests that the partition coefficient does not play a significant role in determining the order of salt permeability among the salts with the same valence configuration. The importance of this finding is that D_w (which is found in the literature) can be used as a rough parameter based on which an unknown salt permeability can be estimated from plots similar to those in Figure 5.10. For example, if the salt permeability is experimentally determined for LiCl and NaCl for a certain membrane, the salt permeability for KCl, RbCl and CsCl in that membrane can be roughly estimated from the graph using the published values of D_w for K^+, Rb^+ and Cs^+.

In the DO experiments for the SE membrane (Section 5.1.2), the salt permeabilities for acetate salts are smaller than the salt permeabilities for the chloride salts (considering pairs with the same cation). The differences can be explained by the fact that the values of D_w for the acetate salts are lower than for the chloride salts. The values of D_w for acetate salts are presented in Table H.1.

5.5.2 Thermodynamic parameters

The dependency of the salt permeability in the membrane on several thermodynamic parameters of the ions in water is analyzed in this section. The physical parameters considered are the ionic enthalpy and entropy of hydration as well as the relative Gibbs (free) energy.

5.5.2.1 Enthalpy and entropy of hydration

The process of ion hydration is complemented by changes in the energy of the ion-solvent system. The enthalpy of hydration, ΔH, is a measurement of the interactions between

the ions and the solvent molecules. It is equal to the energy released when a mole of a particular ion dissolves in a large amount of water and forms an infinitely dilute solution. The ΔH has negative values since it measure the energy released to the exterior (water). Similar to the hydrated radii, the enthalpy of hydration is higher (more negative) for smaller cations with large ionic charge, with the largest value corresponding to Mg^{2+} and the smallest corresponding to K^{+}. Unlike for the hydration number, the enthalpy of hydration for a salt is not an equivocal parameter characterizing the degree of hydration. The various methods to measure ΔH of a salt result in variations within few percentages (Erdey-Gruz, 1974).

Figure 5.11 shows the variation of the salt permeability with the cation enthalpy of hydration, ΔH_{cation}. For salts with a common anion, the permeability varies inversely to the enthalpy of hydration of the cation. Cations presenting a large ΔH determine a slow transport of the salts through the membrane. Similar to R_h, enthalpy of hydration of the cation can be used as an indicator of the order the salts with common anion permeate the membranes. Similar results were found by Yazdani (1991) who investigated the transport of salts with a common anion through RO cellulose acetate and thin film composite membranes.

Another way of looking at hydration is from the solvent perspective, i.e. the modifications occurring in the water structure. In the process of hydration, the water molecules transfer from the bulk solvent to the hydration shell, and a considerable ordering in the water structure around each ion takes place. Large monovalent ions such as K^{+} are referred as structure-breaking ions whereas small and/or multicharged ions such as Li^{+}, Na^{+}, and Mg^{2+} are referred as structure making ions (Chang, 2000). The thermodynamic quantity associated with the degree of ordering is the entropy of hydration, ΔS. The ΔS is negative when there is loss of freedom for the water molecules. Figure 5.12 presents the variation of

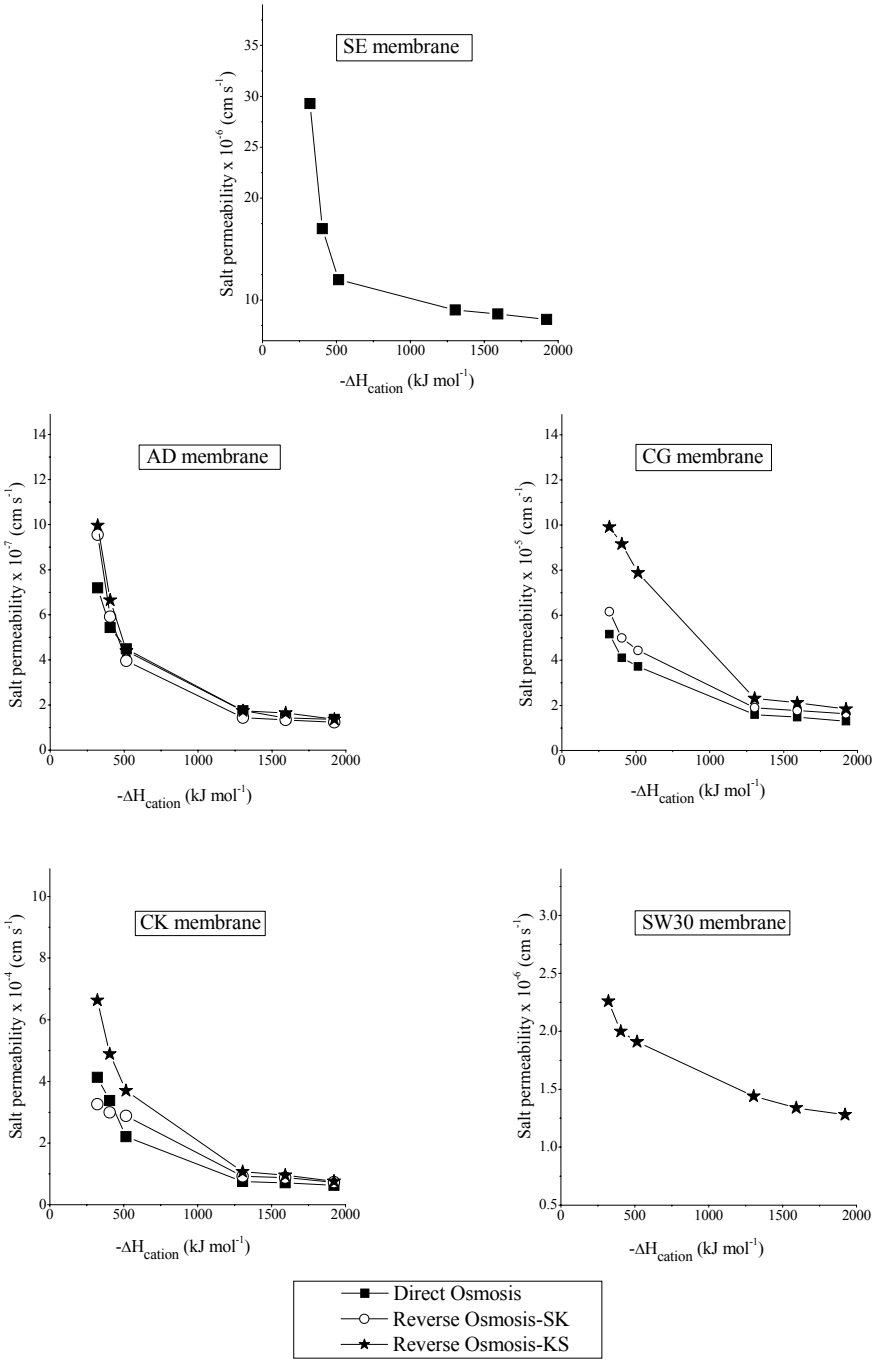

Figure 5. 11 Variation of salt permeability with the cation enthalpy of hydration for all salt in direct osmosis and reverse osmosis experiments for AD, SE, CG, CK and SW30 membranes.

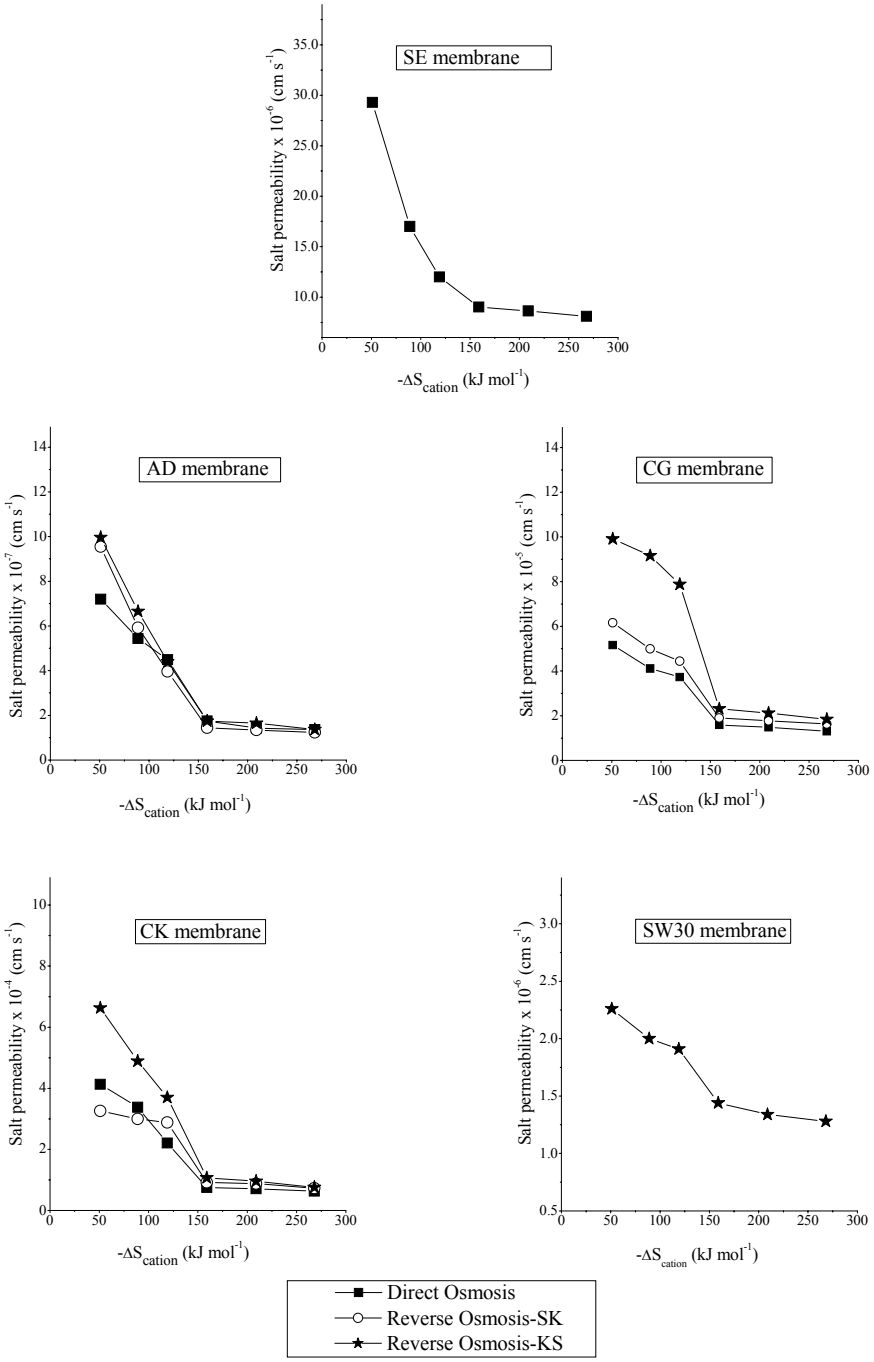

Figure 5. 12 Variation of salt permeability with the cations entropy of hydration for all salt in direct osmosis and reverse osmosis experiments for SE, AD, CG, CK and SW30 membranes.

the salt permeability with the cation entropy of hydration. Similar to ΔH_{cation}, ΔS_{cation} can be used to predict the pattern of permeation for salts with a common anion.

5.5.2.2 Relative free energy $\Delta\Delta G$

The thermodynamic parameter that depends on both the enthalpy and entropy of hydration is the Gibbs (free) energy defined as $\Delta G = \Delta H - T\Delta S$, with T being the absolute temperature. The relative Gibbs energy, $-\Delta\Delta G = (-\Delta G_{mem}) - (-\Delta Gs)$ relates the Gibbs energy of the hydrated ion in the bulk solution, ΔG_S, to that at the solvent-membrane interface, ΔG_{mem}. The relative Gibbs energy depends not only on the ionic species and the solvent but also on the membrane porosity (Matsuura et al., 1975).

The dependence of the salt permeability on the relative free energy is presented only for 1) direct osmosis, the SE membrane, 2) reverse osmosis, Spiegler-Kedem model for σ_1=1 for the AD, CG, and CK membranes, and 3) reverse osmosis, Kimura –Sourirajan model and SW30 membrane element.

The values of $-\Delta\Delta G$ for Li^+, Na^+, K^+, Mg^{2+}, Ca^{2+}, and Ba^{2+} in chloride solutions of 0.05 mołL^{-1} for SE, AD, CG, CK, and SW30 membranes are calculated following the procedure described in the literature (Matsuura et al., 1975) using Equations 5.12 through 5.14.

$$-\Delta\Delta G_i = \left(-\frac{E_{mem}}{R_i + \Delta_{mem}}\right) - \left(-\frac{E_s}{R_i + \Delta_s}\right) \tag{5.12}$$

$$E \equiv N_A \frac{(Z_i e_0)^2}{2}\left(1 - \frac{1}{\varepsilon_s}\right) \tag{5.13}$$

$$P_{salt} = C \cdot e^{\sum_i \alpha_i \left(\frac{-\Delta\Delta G}{R_g T} \right)_i} \tag{5.14}$$

where $\Delta\Delta G_i$ is the relative free energy (kcal·mol^{-1}) of the ion "i", R_i is the ionic radius (Å), Δ_S and Δ_{mem} are the corrections to the ionic radius in the bulk solution and at the membrane surface, respectively, E_S and E_{mem} are the values of E defined in Equation 5.13 for bulk solution and at the membrane interface, respectively, N_A is Avogadro's number, Z_i is the ionic charge, e_0 is the electron charge, ε_s is the dielectric constant of the solvent, P_{salt} is the salt permeability (cm·s^{-1}), C is a constant depending on the membrane porosity, α_i is the number of moles of the ion "i" in one mole of ionized solute, R_g is the gas constant, and T is the absolute temperature (K) .

E_S and Δ_S are calculated in the literature from the slope and the intercept of the plot of $(-\Delta G_S)_i$ vs. R_i (Friedman, 1973). The data is presented in Table I.1. For a given membrane, the set of parameters E_{mem} and Δ_{mem} is unique for ions with the same sign and magnitude of the charge (i.e. there is one set for monovalent cations, one set for divalent cations, one set for monovalent anions, etc.). In order to determine the set corresponding to monovalent cations, for example, experimental values of the salt permeability for a minimum of three salts with monovalent cations and with a common anion are necessary. In this dissertation, the set of E_{mem} and Δ_{mem} for monovalent cations is determined by applying Equations 5.12 and 5.14 for LiCl, NaCl, and KCl whereas the set of E_{mem} and Δ_{mem} for the divalent cations are determined applying the same equations for $MgCl_2$, $CaCl_2$, and $BaCl_2$. The values of the relative free energy are calculated from Equation 5.12 using E_{mem} and Δ_{mem}. The membrane constant and the $\Delta\Delta G$ for Cl^- are determined by applying Equation 5.14 to any pair of 1:1 and 1:2 salts. The parameters obtained are presented in Table 5.4.

Table 5. 5 The relative free energy for the cations, for Cl^-, and for the salts and the membrane constant.

Seawater membrane SE				
Salts	$-\Delta\Delta G/R_gT$ for cations	$-\Delta\Delta G/R_gT$ for Cl^-	$\Sigma-\Delta\Delta G/R_gT$	C
LiCl	-6.89	-6.8	-13.86	1.26
NaCl	-6.54		-13.52	
KCl	-6.00		-12.97	
$MgCl_2$	-0.31		-14.26	
$CaCl_2$	-0.24		-14.19	
$BaCl_2$	-0.20		-14.15	
Seawater membrane AD				
Salts	$-\Delta\Delta G/R_gT$ for cations	$-\Delta\Delta G/R_gT$ for Cl^-	$\Sigma-\Delta\Delta G/R_gT$	C
LiCl	-5.36	-5.75	-11.11	2.66×10^{-2}
NaCl	-4.96		-10.71	
KCl	-4.48		-10.23	
$MgCl_2$	-0.77		-12.27	
$CaCl_2$	-0.69		-12.20	
$BaCl_2$	-0.62		-12.13	
Brackish water membrane CG				
Salts	$-\Delta\Delta G/R_gT$ for cations	$-\Delta\Delta G/R_gT$ for Cl^-	$\Sigma-\Delta\Delta G/R_gT$	C
LiCl	-2.82	-3.13	-7.30	1.72×10^{-2}
NaCl	-2.71		-7.18	
KCl	-2.50		-6.97	
$MgCl_2$	-0.69		-9.64	
$CaCl_2$	-0.61		-9.55	
$BaCl_2$	-0.54		-9.48	
Nanofiltration membrane CK				
Salts	$-\Delta\Delta G/R_gT$ for cations	$-\Delta\Delta G/R_gT$ for Cl^-	$\Sigma-\Delta\Delta G/R_gT$	C
LiCl	-1.11	-4.47	-5.58	7.69×10^{-3}
NaCl	-1.07		-5.54	
KCl	-0.99		-5.46	
$MgCl_2$	1.07		-7.87	
$CaCl_2$	1.26		-7.69	
$BaCl_2$	1.30		-7.65	
Seawater membrane element SW30				
Salts	$-\Delta\Delta G/R_gT$ for cations	$-\Delta\Delta G/R_gT$ for Cl^-	$\Sigma-\Delta\Delta G/R_gT$	C
LiCl	-1.82	-1.10	-2.91	3.50×10^{-5}
NaCl	-1.77		-2.87	
KCl	-1.65		-2.74	
$MgCl_2$	-1.12		-3.31	
$CaCl_2$	-1.07		-3.27	
$BaCl_2$	-1.00		-3.20	

According to Matsuura et al., (1975), a negative $-\Delta\Delta G_i$ means that an ion requires energy to advance from the bulk phase to the membrane surface and, therefore, is repelled by the membrane surface. On the other hand, an ion with a positive $-\Delta\Delta G_i$ is attracted to the surface. Furthermore, the authors correlated the sign of the relative free energy of an ion to the sign of the charge on the membrane surface. The cations have $-\Delta\Delta G < 0$ for membranes with a positive surface charge and $-\Delta\Delta G > 0$ for membranes with a negative surface charge.

As presented in Table 5.4, all cations studied in this dissertation are repelled by the membranes except for the divalent cations in the nanofiltration membrane. Similar, the anion Cl^- is also repelled by the membrane surface for all five membranes. The SW30 membrane element has a negative surface charge, according to the manufacturer. No information about the surface charge could be obtained from the membrane's manufacturer for the SE, AD, CG, and CK membranes. The surface charge of a membrane is commonly measured in the literature using the zeta potential. Using this method, all the cellulose membrane and polyamide/thin film composite membranes are reported in the literature to have a negative surface charge at pH higher than 5 (Baker et al., 1991; Childress and Elimelech, 1996; Childress and Deshmukh, 1998; Deshmukh and Childress, 2001; Vrijenhoek et al., 2001). Assuming that the surfaces of the five membranes are negatively charged, the repulsion of the anion by the membrane surface is correlated with the surface charge for the five membranes.

The identity of the signs in the relative free energy for cations and anions is in disagreement with Matsuura's findings. The disagreement can be explained as follows: If the membrane repels the anion due to charge similarity, it should attract the cation. However, the two opposing charged ions, cation and anion, are tied together electrostatically in their movements in order to maintain the solution electroneutrality. The cations move back and forth from the bulk solution to the membrane vicinity and whether they prefer one location to

another, depends on whether the interaction between the cations and the membrane sites is stronger or weaker than the interaction between the cation and the anion of its ion pair. The negative $-\Delta\Delta G$ for the cations in Table 5. 4 reflects a stronger interaction of the cation-anion pair than cation-membrane surface. The positive $-\Delta\Delta G$ (divalent cations in the nanofiltration membrane) reflects a weaker interaction cation-anion than cation-membrane surface. Moreover, the membrane surface charge can be reduced by 1) the effect of concentration polarization (in RO) and 2) the adsorption of divalent cations in the membrane surface sites (Deshmukh and Childress, 2001; Vrijenhoek et al., 2001). A reduced negative charge on the membrane surface will favor the dominancy of the cation-anion interaction and therefore, the repulsion of the cation by the membrane.

As shown in Table 5. 4, the values of $\Sigma(-\Delta\Delta G/R_gT)$ increases in the order $Mg^{2+}<Ca^{2+}<Ba^{2+}<Li^{+}<Na^{+}<K^{+}$ which is the same order the salt permeability increases. Similar results are reported by Matsuura et al., (1975) for cellulose acetate membranes and by Dickson et al., (1975) for 1:1 salt in aromatic polyamide membranes. The membrane constant, C, defined by Equation 5. 13, characterizes the membrane porosity and one would expect C to be smallest for the seawater membranes and largest for the nanofiltration membrane. However, no correlation between the values of C and the membrane porosity can be established for the five membranes (Table 5. 4). The value of C for the nanofiltration membranes is the second lowest, whereas C for the seawater membrane SE is the largest. Inconsistency among the value of C and the membrane porosity is also found in the literature: the values of C for cellulose acetate membranes calculated from Matsuura et al., (1975) are two orders of magnitude lower than the values of C calculated from Dickson et al., (1975) for higher-rejection polyamide acetate membranes.

The relative free energy emerges as a parameter that can be used in predicting the salt permeability in RO and NF membranes. Figure 5. 13 presents the variation of the salt permeability with the relative free energy for the salt, $\Sigma(-\Delta\Delta G/R_gT)$. The very good linearity confirms Equation 5.13 for the studied membranes.

If the values of salt permeability for 2 more other salts with a common cation and two different monovalent anions are known for a membrane, the plots from Figure 5.12 can be used to predict the salt permeability of any 1:1 and 1:2 salts for that particular membrane. For example, if the salt permeability for NaF and NaI are known for the seawater membrane AD (in addition to the salt permeabilities for the six salts needed to draw the plot), the set of E_{mem} and Δ_{mem} for the monovalent anions can be determined, from which the relative free energy for any monovalent anion can be calculated. Since the relative free energy of any monovalent and divalent cation can be determined based of the corresponding sets of E_{mem} and Δ_{mem}, the plot from Figure 5.13 for the AD membrane can be used to determine the salt permeability for any combination of 1:1 and 1:2 salts (ie fluorides, chlorides, bromides and iodides of any alkali and alkaline earth metals).

5.5.3 Conclusions on the factors controlling the salt permeability in RO and nanofiltration membranes

The salt permeability for the six studied salts ranks in the order $MgCl_2<CaCl_2<BaCl_2<LiCl<NaCl<KCl$ regardless the membrane type (RO or NF), the membrane configuration (flat sheet or spiral wound), the model used to calculate the salt permeability, or the type of experiment (DO or RO). This order cannot be explained by the ionic radius of the cation because the ionic radius of K^+ is larger than of Na^+ and Li^+ and similar, the ionic radius of Ba^{2+} is larger than of Ca^{2+} and Mg^{2+}. Moreover, the pairs (Li^+ and

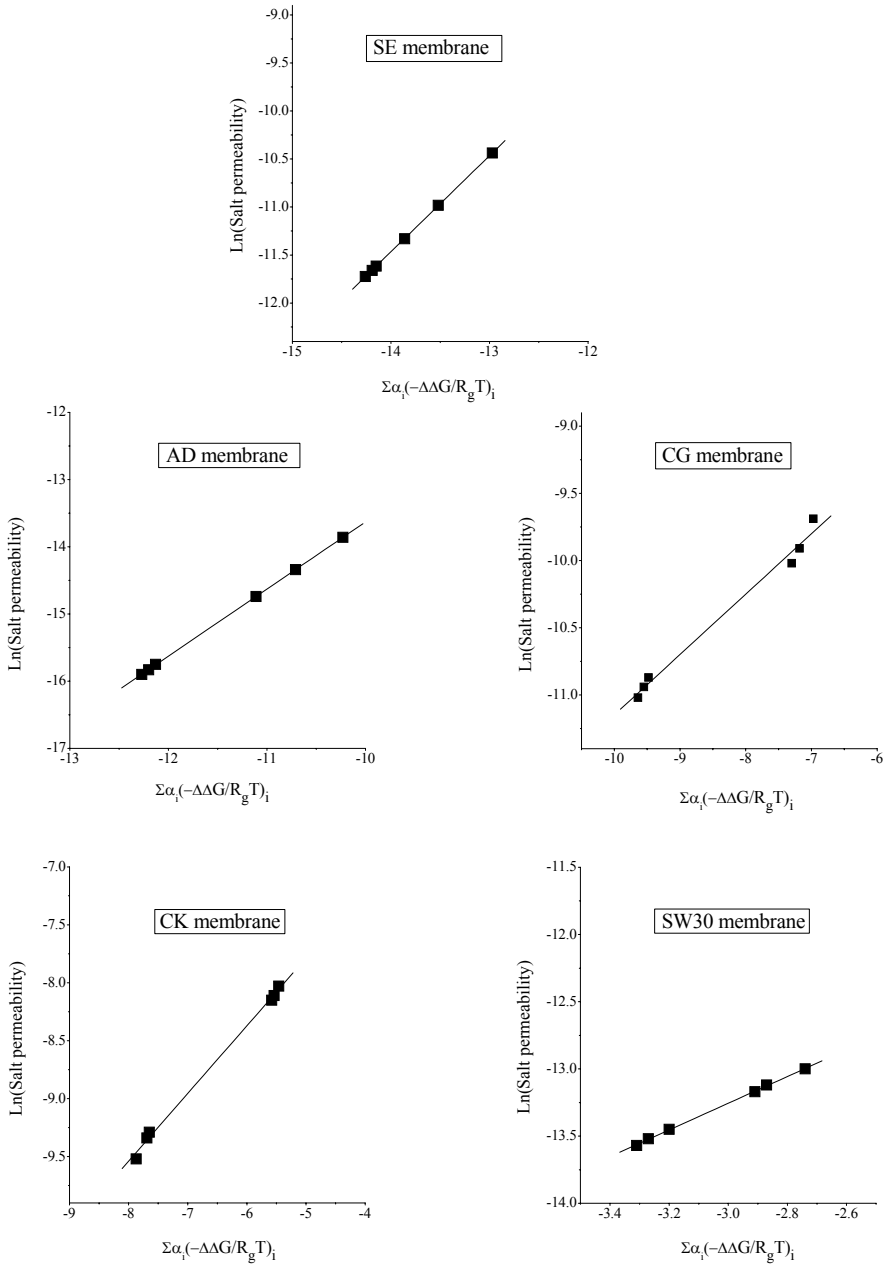

Figure 5. 13 Variation of the salt permeability with the relative free energy for all salts in direct osmosis and reverse osmosis experiments for the SE, AD, CG, CK and SW30 membranes.

Mg^{2+}), (Na^{+} and Ca^{2+}), and (K^{+} and Ba^{2+}) have close value of the ionic radii, however, the salt permeabilities are significantly slower for the divalent cations than for the monovalent cations.

There is a strong interaction of the solute ions with water molecules (ion-dipole interaction), and one should consider the effective radii of the ions, which take into account the water molecules bounded around the charged ions in a 3-dimensional space. The degree of hydration is a function of both size and charge, being higher for small ions with large charge. There are several ways of describing the degree of hydration. The hydrated radii explain the order of salt permeation, however, it is a parameter not uniquely defined, in that its values vary with the method of measurement. The enthalpy of hydration as well as the entropy of hydration represent more precise quantifications of the degree of hydration and can be used in a qualitative evaluation of the permeation rate for a salt in RO and NF membranes by performing comparative studies.

Unlike the entropy and enthalpy of hydration, the relative free energy takes in consideration not only the interaction ion-solvent in the bulk solution but the interactions at the membrane surface. It is a function of ionic species as well as on the membrane material. The relative free energy permits the calculation of salt permeability based on several preliminary data. The free energy, as well as the enthalpy and entropy of hydration have the limitations of not providing any insight into the actual mechanism of salt transport in the membrane.

The salt permeability increases with the increase of the salt diffusion coefficient in infinitely dilute solutions. The diffusion coefficient of a salt in infinite dilute solution can be used as an indicator of the order the salt permeates through the membrane for either 1:1 or 1:2 salts. However, the salt diffusion coefficient in water fails to describe the differences between

the 1:1 and 1:2 salts. These differences are attributed to the differences of the partitioning coefficient for the 1:1 and 1:2 salts.

CHAPTER 6

CONCLUSIONS

In this Chapter, the experimental results of this dissertation are summarized. The importance and the implications of these results with respect to the theoretical and engineering aspects are emphasized. The Chapter concludes the findings of the direct osmosis experiments, followed by the reverse osmosis experiments and by a parallel between the two processes. Last, this Chapter concludes on the factors controlling the salt permeability.

6.1 Direct osmosis (DO) experiments

The results from the direct osmosis experiments show that the concentration at the membrane wall is lower than the concentration in the bulk solution. The effect of salt depletion at the membrane wall is more pronounced for nanofiltration membranes for which the concentration at the membrane wall is found about ten times less than the concentration in the bulk solution. Disregarding the effect of dilution for the salt solution at the membrane surface results in lower salt permeabilities than the salt permeabilities when the dilution is considered.

In this research, concentration at the membrane wall is calculated based on the measured pure water flux and the pure water permeability of the membrane, which is determined from a reverse osmosis experiment. A new equation is desired to calculate the concentration at the membrane wall without the need of pure water permeability, which requires an extra RO experiment. This research shows that the pure water flux in DO depends only on the valence of the salt (such as 1:1, 1:2 etc), which implies that the pure water flux and the salt flux do not interact with each other inside the membrane. Demonstrating that the

salt and water fluxes are uncoupled in direct osmosis can be used as an initial premise in developing a new theoretical method for the calculation of the salt permeability in DO.

Figure 6.1 presents the cases for which the salt permeability measured in DO experiments is equal to the salt permeability in RO experiments. The SW, BW and NF represent the seawater, brackish water and nanofiltration membrane, respectively, and (1:2) represents the 1:2 salts. The coefficient $(D/K\delta)_{DO}$ represent the salt permeability in direct osmosis experiments, $P_{RO}^{(1)}$ is the salt permeability in the RO Spiegler-Kedem model when the concentration polarization is neglected, $P_{RO}^{(2)}$ is the salt permeability in the RO Spiegler-Kedem model when the concentration polarization is calculated for the reflection coefficient equal unity, $P_{RO}^{(3)}$ is the salt permeability in the RO Spiegler-Kedem model when the concentration polarization is calculated by combining the film theory with the Sherwood correlation, and $(D/K\delta)_{RO}$ is the salt permeability in RO Kimura-Sourirajan model. The implications of this equality are presented in Section 6.3, Comparison of DO and RO processes.

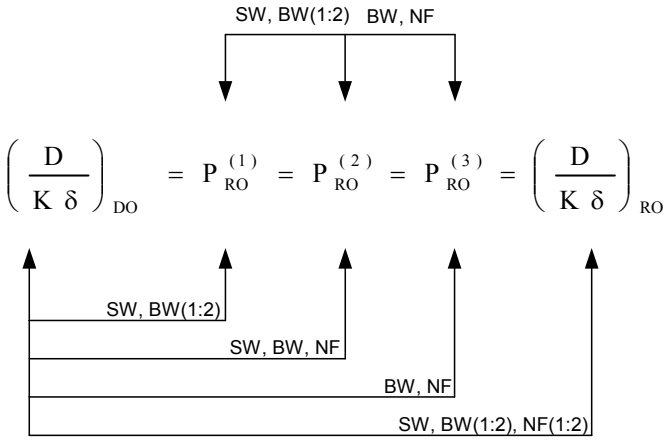

Figure 6. 1 The equality of salt permeability in DO and RO experiments.

6. 2 Reverse osmosis (RO) experiments

a) Spiegler-Kedem model

The first case of the Spiegler-Kedem models neglects the concentration polarization and leads to erroneous result that the convection is the dominant transport mechanism of salt through the hyperfiltration membranes. The second case of the Spiegler -Kedem model (reflection coefficient σ_1=1) is adequate to calculate both the salt permeability and the percentage of the diffusive salt flux of the total salt flux for all three membrane types, seawater, brackish water and nanofiltration membranes. However, this case requires an additional experiment with pure water in order to determine the hydraulic permeability of the membrane. The third case of the SK model is appropriate to calculate both the salt permeability and the percentage of the diffusive salt flux of the total salt flux only for brackish water and nanofiltration membranes. The third case requires information about the test cell geometry as well as the Reynolds number. As summarized in Figure 6.1, the salt permeabilities for the three cases of the Spiegler-Kedem model are equal for all salts in seawater membrane and 1:2 salts in brackish water membrane (R>94%). This implies that for situations when the rejection coefficient is higher than 94%, the first case of the Spiegler-Kedem model should be used in calculating the salt permeability since it requires fewest number of parameters.

The results from Spiegler-Kedem model demonstrate that the mechanism of salt transport in RO processes is diffusion dominant for both reverse osmosis and nanofiltration membranes. However, convective flux can contribute as much as 32% to the total flux for seawater membranes and as much as 46% in the case of brackish water and nanofiltration membranes. The diffusive flux is more important for the 1:2 salts than for 1:1 salts in brackish water and nanofiltration membrane. The importance of the diffusion mechanism has

practical applications to the membrane manufacturing. The diffusive properties of the salts should be considered in developing the polymers and processes for membranes in order to achieve a desired salt selectivity.

The two salt parameters, the reflection coefficient, σ_1 and the salt-water coupling coefficient, σ_2, in the Spiegler-Kedem model are assumed equal in the literature. The results of this dissertation show that the two parameters are equal only for membranes/salts with a diffusive salt flux of at least 65% of the total salt flux (Figure 5.5), which in turn corresponds to a rejection coefficient higher than 86% (Figure 5.7). This implies that the number of unknown parameters in the Spiegler-Kedem model cannot be reduced to three (L_P, σ, and P_{RO}), as presented in the literature, unless the rejection is higher than the threshold value of 86% found in this work.

b) Kimura Sourirajan model

The two RO models, Spiegler-Kedem and Kimura-Sourirajan, are used interchangeably in the literature to characterize the salt transport in hyperfiltration membranes. It is shown in this dissertation that the two RO models are equivalent only for membranes/salts with a rejection coefficient of at least 86% (all salts in seawater membrane, and only 1:2 salts in brackish water and nanofiltration membranes). The use of the Kimura-Sourirajan model for rejection coefficients lower than 86% results in overestimating the salt permeability coefficient and consequently, to over-designing a membrane separation system.

6.3 Comparison of DO and RO processes

The equality of the salt permeability for DO and RO experiments validates the equation derived in Section 5.1.2 for the salt permeability in the DO processes. It also allows one to choose the most convenient experimental set-up and, independently, the most convenient model (for RO) to determine the salt permeability. The decision for choosing the

best option depend on many factors, such as the membrane type, the rejection coefficient, the parameters needed for analysis, the sequence of performing the experiments for a number of salts, the time schedule, the availability of operators, the possibilities of temperature control, and the available budget. The implications of these decision factors are briefly discussed below:

- Membrane type/Rejection coefficient and parameters needed for analysis

If the salt permeability needs to be determined, the valid experiments and models one can choose from are presented in Figure 6.1. The DO experiments are appropriate for all hyperfiltration membranes, whereas the Kimura-Sourirajan model is appropriate only for membranes/salts with rejection higher than 86%. The first case of the Spiegler-Kedem model can be used to calculate the salt permeability for situations when rejection is higher than 94%. The second and the third cases of the Spiegler-Kedem model can be used to calculate the salt permeability for all hyperfiltration membranes, regardless the rejection coefficient. In choosing the most appropriate RO model, one should consider that The Spiegler –Kedem model requires the run for each salt to be carried out at several operating pressures, whereas the Kimura-Sourirajan model needs only one operating pressure per salt. However, the Kimura-Sourirajan model requires additional runs with DI water to determine the pure water permeability.

If the pure water permeability is needed and DI water is available, both RO models can be used since the equations defining DI water transport are identical. However, the situations when only the pure water permeability is needed are not often; in most of the practical cases, the pure water permeability needs to be obtained whenever the salt permeability is sought. The advantage of using either the first or the third case of the

Spiegler-Kedem model is that the salt and water permeability can be obtained simultaneous with no additional DI water run which will be required if the Kimura Sourirajan is used to calculate both the salt and water permeability. If the percentage of the diffusive salt flux of the total salt flux has to be calculated, the only analysis available for the seawater membranes is the second case of the Spiegler-Kedem model. For brackish water and nanofiltration membranes, both the second and the third cases of the Spiegler-Kedem model can be used.

- Sequence of salts

It is observed that unlike in RO, concentration polarization does not develop in DO. Moreover, the salt concentration at the membrane wall in DO is lower than the salt concentration in the bulk solution. This phenomenon suggests that DO experiments would be preferred to RO experiments when the salt permeability for a sequence of several salts is required. In RO processes, the membrane is susceptible to scaling, fouling and compaction, and the salt permeability of a particular salt is influenced by the history of the membrane exposure, and therefore may require using a new sheet of membrane for each experiment.

- Time schedule

The duration of the experimental work required to determine the parameters of the Spiegler-Kedem model is at least 9-10 hours per desired salt. Additionally, at least one run of 3 to 4 hours must be conducted for the pure water permeability if the second case of the model is considered. The Kimura-Sourirajan model requires only one operating pressure, which shortens the experimental time for one salt to 3 hours, plus 3-4 hours for a pure water experiment. The length of the DO runs in this research were of 10 hours, however the time can be shortened to only few hours if conductivity probes with high accuracy in the range of DI water conductivity are used. The high accuracy conductivity sensors can detect the small increases in the DI water conductivity occurring in the first hours of the DO experiments.

- Operators availability

The most involvement of the experiment operator is needed for the Spiegler-Kedem model because each run has to be performed at several operating pressures. The Spiegler-Kedem model also requires the intervention of the operator because the system needs to be cleaned between different salts and the feed solution changed. The DO experiments are the least soliciting and the intervention of the operator is required only in the beginning and at the end of the run, assuming automatic data logging.

- Temperature control

Transport parameters in hyperfiltration membranes are temperature sensitive. Preliminary data is required to perform theoretical temperature corrections and these corrections can introduce additional errors in the calculations of the transport parameters. The temperature control should be preferred to temperature correction whenever is possible. In RO, elevated temperatures can be reached in the water, especially at high operating pressure, therefore the use of a cooling system is often necessary. In DO, the increase in the system temperature is less than few degrees, and the temperature can be controlled by maintaining constant ($\pm 1^{O}C$) ambient temperature.

- Capital and operating costs

The costs involved for running RO experiments are considerably higher than for DO experiments. In this research, the costs of the apparatus used to perform the RO experiments exceeded $10,000, whereas only approximately $1,500 was needed to procure the DO apparatus. However, the DO experiment requires a test cell which is not commercially available and has to be custom fabricated. The design of the DO cell is relatively simple and inexpensive materials, such as acrylic, can be used. The energy consumption to perform a RO experiment is considerably higher than to perform a DO experiment.

6.4 Factors controlling the salt permeability

The order of the salt permeability among the six studied salts is the same regardless the experiment type (DO or RO), the membrane type (seawater, brackish water or nanofiltration), the membrane configuration (flat sheet or spiral wound), or the model chosen (Spiegler-Kedem or Kimura-Sourirajan). The order of the salt permeability is in perfect agreement with the lyotropic series which confirms the physicochemical nature of the transport mechanisms taking place in the membranes.

The order of separation for strong electrolytes with common anion in hyperfiltration membranes can be explained by the different degrees of the hydration for the cations. Any parameter quantifying the hydration of the cation (hydrated radii, enthalpy of hydration or entropy of hydration) can be used for a rough estimation of the salt permeability. Comparing the hydration parameter of the salt with the hydration parameter of a salt with a known permeability, the permeability of the first salt can be estimated from plots similar to those presented in Figures 5.9, 5.11 or 5.12. If a more precise prediction of the salt permeability is desired, the relative free energy theory can be used, although it requires many more known values of the permeabilities for other salts. The prediction of the salt permeability based on the tabulated values of the physical or thermodynamic properties of the salt and the known values of salt permeability of other salts can reduce significantly the experimental work especially when the salt permeability is required for a large number of salts.

6.5 Summary

This work proves that the diffusion is the dominant transport process in hyperfiltration membranes. The equality of the salt permeability in DO and RO experiments represents a significant finding which allows the selection of the most appropriate experiment and model to calculate salt permeability. This research shows that the permeation of salts

with a common anion is controlled by the cation hydration. Any parameter quantifying the cation hydration as well as the relative free energy can be used for prediction of a unknown salt permeability based on known salt permeability of other salts.

CHAPTER 7

RECOMMENDATIONS

This research has shown that the concentration at the membrane wall in direct osmosis is lower than the concentration in the bulk solution. The concentration at the membrane wall was calculated in this dissertation based on the pure water permeability of the membrane, which was determined from reverse osmosis experiments. A new method of determining the concentration at the membrane wall which should not require additional RO experiments, has to be developed. The starting point in determining the equation which will allow the calculation of the concentration at the membrane wall in DO is to consider that at steady state, all the salt fluxes across the membrane are balanced. The resulting equation will be similar to the equation used to calculate the concentration polarization factor in RO from the thin film theory.

Another limitation of the DO research is the consideration of the salt and water fluxes as independent in the membrane. The results of this dissertation confirmed this assumption, however further studies need to consider the implications of a coupling between salt and water fluxes across the membrane. The coupling effect might be relevant for high salt fluxes, such as 1:1 salts in nanofiltration membranes.

The Spiegler-Kedem model and the Kimura-Sourirajan model were selected for the membrane transport analysis in this dissertation because they are widely applied in the literature. Other models which include both diffusive and convective salt fluxes need to be explored. These models include solution-diffusion-imperfection, the frictional model and the finely-porous model. The solution-diffusion-imperfection model considers that water and salt are transported by diffusion and convection in the membrane pores and is most suitable for

membranes with larger pores, such as nanofiltration membranes. The frictional model assumes that the driving forces for any species are balanced by the frictional forces exerted by the other components, including the membrane. The importance of the salt diffusive and convective fluxes can be determined by comparing the friction coefficients between salt-water and salt-membrane. The finely-porous model includes the hindering effects of the diffusion and convection fluxes due to the very small size of the pores (less than 0.5 nm).

An aspect that was not emphasized in this research is the surface charge on the membranes. Some authors consider that the membrane surface charge plays a more important role in the mechanism of salt separation for NF membranes than for RO membranes. This research has to be extended to models that include the effects of the membrane surface charge, such as the Nernst-Plank model. This model describes the transport of ions across the membrane as a result of diffusion and convection, but the diffusive flux is considered to be due to both concentration and electrical potential gradients. The drawbacks of the model are that the membrane surface charge and the thickness of the membrane skin layer need to be known.

Calculating the concentration polarization by combining the thin film theory and Sherwood correlation lead to erroneous results in the case of seawater membrane in this research. It is believed that the use of the Sherwood correlation from the literature might be inadequate. A more accurate dimensionless correlation can be obtained if a term relating the Reynolds number and the salt and water permeation rate are considered. The coefficients of such correlation have to be determined experimentally for the specific test cell used. The experimental method of determining these empirical coefficients of correlation is described by Prabhakar and Ramani (1994) and Ramani (1992).

The measurements of the zeta potential in the literature show that the membrane surface charge depends on the pH of the feed water. A common pattern for variation of surface charge with pH shows that at low pH, the surface charge is positive and decreases with the increase of the pH range. A shift in the sign of the charge occurs at pHs between 3 and 5 while at higher pHs, a negative charge increases with an increase in pH. Moreover, cellulose acetate membranes are subject to hydrolysis at low pH which results in modification in the membrane water contents and the nature of the water-polymer binding. Additional investigation is required to determine the effects of the feed water pH on the transport properties of the membranes.

In verifying the relative free energy theory, it was found that the chloride ion, which is negatively charged, was attracted to the membrane surface of all five membranes studied. According to the literature data, the membrane surface charge is also negative and the attraction of the co-ion by the membrane surface was explained by the co-ion/counter-ion dragging effect. In order to maintain solution electroneutrality, the co-ion which is attracted to the membrane, pulls the counter-ion, and the two ions move together due the dragging effect. The investigation needs to be continued in two directions: first, the assumption made about the negative surface charges on all five membranes needs to be confirmed. This can be done by measuring the charge using a surface zeta potential method. Second, additional experiments with the same salts but positively charged membranes can test the validity of the cation-anion dragging effect.

It was shown in this study that the salt permeability increases with the increase in the salt diffusivity in infinite dilute solution. The plot of the salt permeability for 1:1 and 1:2 salts versus salt diffusivity in infinite dilution presents a significant ”shift “ up of the 1:1 salts compared to the 1:2 salts. Since the salt permeation through the membrane is function of both

diffusion and adsorption, the "shift" suggested that the partition coefficient of the salt between the feed solution phase and membrane phase is different for 1:1 salts than for 1:2 salts. This assumption can be verified experimentally by determining the partition coefficient for the 1:1 and 1:2 salts. Two methods are currently used in the literature to determine the solution-membrane partition coefficient: 1) by using an adsorption/desorption experiment and 2) by using a DO experiment and time the lag method.

The findings of this research are limited to single solutions of strong electrolytes at relatively low concentrations, where they exist in dissociated form. The research needs to be extended to the following categories of solutes: 1) strong electrolytes in dilute solutions for salts with a common cation and different anions; 2) strong electrolytes at higher concentrations; 3) weak electrolytes and non-electrolytes at varying concentrations; and 4) mixture of salts, also at varying concentrations. Each category of solutes is described below:

- Strong electrolytes in dilute solutions for salts with a common cation and different anions. This research has proved that for strong chlorides salts, the salt permeability in the membrane increases with the increase of salt diffusivity in water. However, some studies (Krinke, 1988) have shown that although the diffusivity of nitrate salts is lower than of chloride salts in water, the salt permeability of nitrates is higher than the salt permeability of the chlorides. Therefore, the differences in the salt permeabilities in membrane for salts with common cation and different anions cannot be explained by the differences in the salt diffusivity in water.
- Strong electrolytes at high concentration. Due to electrostatic attraction of the oppositely charged ions at high concentrations, ion-pairs are formed. The factors controlling the salt permeabilities in such cases need to be investigated.

- Weak electrolytes and non-electrolytes. Weak electrolytes in solvent are partly dissociated and partly in their molecular form. Non-electrolytes, such as organic molecules, exist only in the molecular form. The neutral molecules do not hydrate in water and therefore, none of the thermodynamic parameters quantifying the hydration can be used to explain the relative order of permeation for those salts.

- Mixture of salts. The most important application of the RO processes is desalination of seawater and brackish water. These water sources contain among other components, mixture of inorganic salts. It has been shown that the concentration polarization for individual salts changes substantially with the presence of other salts (Srinivasan and Tien, 1970). The equations of transport in membranes are complex for multicomponent systems with more than one anion and more than one cation. The Spiegler-Kedem model is valid only for binary systems and it cannot be used for mixture of salts. One alternative is the use of Nernst -Plank model which for a mixture of n ions requires (3n+2) equations. Another option is the use of the artificial neural network model described by Bowen et al. (2000).

REFERENCES

Baker, R.W., 2000. Membrane Technology and Applications. McGraw-Hill, Menlo Park.

Baker, R.W. et al., 1991. Membrane Separation Systems. Noyes Data Corporation, New Jersey.

Belfort, G., 1984. Synthetic Membrane Processes. Academic Press, Orlando.

Bhanushali, D., Kloos, S. and Bhattacharyya, D., 2002. Solute transport in solvent-resistant nanofiltration membranes for non-aqueous systems: experimental results and the role of solute-solvent coupling. Journal of Membrane Science, 208: 343-359.

Bhattacharya, S. and Hwang, S.T., 1997. Concentration polarization, separation factor and Peclet number in membrane processes. Journal of Membrane Science, 132: 73-90.

Bitter, J.G.A., 1991. Transport Mechanism in Membrane Separation processes. Plenum Press, New York.

Bockris, J.O.M. and Reddy, A.K.N., 1970. Modern Electrochemistry. Vol I. Plenum, New York.

Bowen, W.R., Jones, M.G.J., Welfoot, J.S. and Yousef, H.N.S., 2000. Predicting salt rejections at nanofiltration membrane using artificial neural networks. Desalination, 129: 147-162.

Burgess, J., 1988. Ions in Solution. Basic Principles of Chemical Interactions. Ellis Horwood, Chichester.

Carter, J.W., Hoyland, G. and Hasting, A.P.M., 1974. Concentration polarization in reverse osmosis flow systems under laminar conditions. Effect of surface roughness and fouling. Chemical Engineering Science, 29: 1651-1658.

Chang, R., 2000. Physical Chemistry for the Chemical and Biological Sciences. University Science Books, Sausalito.

Chaudry, M.A., 2002. Water and ions transport mechanism in hyperfiltration with symmetric cellulose acetate membranes. Journal of Membrane Science, 5204: 1-14.

Childress, A.E. and Deshmukh, S.S., 1998. Effect of humic substances and anionic surfactants on the surface charge and performance of reverse osmosis membranes. Desalination, 118: 167-174.

Childress, A.E. and Elimelech, M., 1996. Effect of solution chemistry on the surface charge of polymeric reverse osmosis and nanofiltration membranes. Journal of Membrane Science, 119: 253-268.

Conway, B.E., 1981. Ionic Hydration in Chemistry and Biophysics. Elsevier Sceintific Publishing Company, Amsterdam.

Cussler, E.L., 1997. Diffusion-Mass Transfer in Fluid Systems. Cambridge University Press, Cambridge.

Deshmukh, S.S. and Childress, A.E., 2001. Zeta potential of commercial RO membranes: influence of source water type and chemistry. Desalination, 140: 87-95.

Diawara, C.K., Lo, S.M., Rumeau, M., Pontie, M. and Sarr, O., 2003. A phenomenological mass transfer in nanofiltration of halide ions for selective deflourination of drinking water. Journal of Membrane Science, 219: 103-112.

Dickson, J.M., Matsuura, T. and Blais, P., 1975. Reverse osmosis separation of some organic and inorganic solutes in aqueous solutions using aromatic polyamide membranes. Journal of Applied Polymer Science, 19: 801-819.

Elimelech, M., Zhu, X., Childress, A.E. and Hong, S., 1997. Role of membrane surface morphology in colloidal fouling of cellulose acetate and composite aromatic polyamide reverse osmosis membranes. Journal of Membrane Science, 127: 101-109.

Erdey-Gruz, T., 1974. Transport Phenoma in Aqueous Solutions. Akademiai Kiado, Budapest.

Fang, H.H.P. and Chian, E.S.K., 1975. Criterion of ion separation by reverse osmosis. Journal of Applied Polymer Science, 19: 2889-2895.

Fang, H.H.P. and Chian, E.S.K., 1976. Removal of dissolved solids by reverse osmosis. AICHE Symposium Series: Physical, chemical, wastewater treatment, 73(166): 137-143.

Friedman, H.L., 1973. Water-A Comprehensive Treatise. Plenum, New York.

Frommer, M.A., Murday, J.S. and Messalem, R.M., 1973. Solubility and diffusivity of water and of salts in an aromatic polyamide film. European Polymer Journal, 9: 367-373.

Gekas, V. and Hallstorm, B., 1987. Mass transfer in the membrane concentration polarization layer under turbulent cross flow : I. Critical literature review and adaptation of existing Sherwood correlations to membrane operations. Journal of Membrane Science, 30(2): 153-170.

Gilron, J., Gara, N. and Kedem, O., 2001. Experimental analysis of negative salt rejection in nanofiltration membranes. Journal of Membrane Science, 185: 223-236.

Glueckauf, E., 1976. The distribution of electrolytes between cellulose acetate membranes and aqueous solution. Desalination, 18: 155-172.

Heyde, M.E., Peters, C.R. and Anderson, J.E., 1974. Factors influencing revese osmosis rejection of inorganic solutes from aqueous solution. Journal off Colloid and Interface Science, 50(3): 467-487.

Johnson, H.K., 1975. Reverse osmosis rejection of heavy metal cations. Desalination, 16: 205-224.

Jonsson, G. and Benavente, J., 1992. Determination of some transport coefficients for the skin and porous layer of composite membrane. Journal of Membrane Science, 69: 29-42.

Kessler, J.O. and Moody, C.D., 1976. Drinking water from sea water by forward osmosis. Desalination, 18(3): 297-306.

Krinke, S.L., 1988. The Effect of Ion Species on Concentration Polarization. Master Thesis, University of South Florida.

Lonsdale, H.K., Cross, B.P., Graber, F.M. and Milstead, C.E., 1971. Permeability of cellulose acetate membranes to selected solutes. Journal of Macromolecular Science-Part B:Physics., 5(1): 167-188.

Lonsdale, H.K., Merten, U. and Riley, R.L., 1965. Transport properties of cellulose acetate osmotic membranes. Journal of Applied Polymer Science, 9: 1341-1362.

Mallevialle, J., Odendaal, P.E. and Wiesner, M.R. (Eds), 1996. Water Treatment Membrane Processes. McGraw-Hill.

Marinas, B.J. and Selleck, R.E., 1992. Reverse osmosis treatment of multicomponent electrolyte solutions. Journal of Membrane Science, 72: 211-229.

Mason, E.A. and Lonsdale, H.K., 1990. Statistical-mechanical theory of membrane transport. Journal of Membrane Science, 51: 1-81.

Mason, E.A., Wenndt, R.P. and Bresler, E.H., 1972. Test of the Onsager relation for ideal gas trasport in membranes. Journal of Chemical Society. Faraday Transactions II., 68: 1938-1945.

Matsuda, M. and Kamizawa, C., 1984. Precise measurement of membrane constants of cellulose acetate membranes by direct osmosis tests. Desalination, 49(3): 367-378.

Matsuura, T., Pageau, L. and Sourirajan, S., 1975. Reverse osmosis separation of inorganic solutes in aqueous solutions using porous cellulose acetate membranes. Journal of Applied Polymer Science, 19: 179-198.

McCray, S.B., Vilker, V.L. and Nobe, K., 1991. Reverse osmosis cellulose acetate membranes.II. Dependence of transport properties on acetyl content. Journal of Membranes Science, 59: 317-330.

Mori, K. et al., 2000. Diffusional characteristics of sodium chloride in symmetrical cellulose acetate membranes measures by an unsteady-state dialysis method. Desalination, 127: 225-249.

Mulder, M., 2003. Basic Principles of Membranes Technology. Kluwer Academic Publishers, Dordrech.

Petrotos, K., B., Peter C. Quantick, P.C. and Petropakis, H., 1999. Direct osmotic concentration of tomato juice in tubular membrane – module configuration. II. The effect of using clarified tomato juice on the process performance. Journal of Membrane Science, 160(2): 171-177.

Petrotos, K.B. and Lazarides, H.N., 2001. Osmotic concentration of liquid foods. Journal of Food Engineering, 49(2-3): 201-206.

Petrotos, K.B., Quantick, P. and Petropakis, H., 1998. A study of the direct osmotic concentration of tomato juice in tubular membrane – module configuration. I. The effect of certain basic process parameters on the process performance. Journal of Membrane Science, 150(1): 99-110.

Pontie, M., Buisson, H., Diawara, C.K. and Essis-Tome, H., 2003. Studies of halide ions mass transfer in nanofiltration-application to selective deflourination of brackish drinking water. Desalination, 157: 127-134.

Prabhakar, S. and Ramani, M.P.S., 1994. A new concept of mass transfer coefficient in reverse osmosis-practical applications. Journal of Membrane Science, 86: 145-154.

Ramani, M.P.S., 1992. Mass transport mechanism on the high-pressure side in reverse osmosis: an analysis. Chemical Engineering Science, 47(15-16): 4099-4105.

Rautenbach, R. and Albrecht, R., 1989. Membrane Processes. John Wilet & Sons.

Rutgers, A.J. and Hendrikx, Y., 1962. Ionic hydration. Trans. Faraday. Soc., 58: 2184-2191.

Sablani, S.S., Goosen, M.F.A., Al-belushi, R. and Wilf, M., 2001. Concentration polarization in ultrafiltration and reverse osmosis: a critical review. Desalination, 141: 269-289.

Schaep, J., Van der Bruggen, B., Vandecasteele, C. and Wilms, D., 1998. Importance of ion size and charge in nanofiltration. Separation and Purification Technology, 14: 155-162.

Sherwood, T.K., Brian, P.L.T. and Fisher, R.E., 1967. Desalination by reverse osmosis. Industrial and Engineering Chemistry Fundamentals, 6(1): 1-12.

Soltanieh, M. and Gill, W.N., 1981. Review of reverse osmosis membranes and transport models. Chemical Engineering Communications, 12: 279-363.

Sourirajan, S., 1970. Reverse Osmosis. Academic Press, New York.

Spiegler, K.S., 1966. Thermodynamics of hyperfiltration (Reverse Osmosis): criteria for efficient membranes. Desalination, 1: 311-326.

Srinivasan, S. and Tien, C., 1970. A simplified method for the prediction of concentration polarization in reverse osmosis operation for multicomponent systems. Desalination, 7: 133-145.

Strathmann, H.K. and Michaels, A.S., 1977. Polymer-water interaction and its relation to reverse osmosis desalination efficiency. Desalination, 1: 311-326.

Sutzkovere, I., Hasson, D. and Semiat, R., 2000. Simple technique for measuring the concentration polarization level in a reverse osmosis system. Desalination, 131: 117-127.

Taniguchi, M. and Kimura, S., 2000. Estimation of transport parameters of RO membranes for seawater desalination. AIChE Journal, 46(10): 1967-1973.

Taylor, J.R., 1997. An Introduction to Error Analysis. University Science Book, Sausalito.

Urama, R.I. and Marinas, B.J., 1997. Mechanistic interpretation of solute permeation through a fully aromatic polyamide reverse osmosis membrane. Journal of Membrane Science, 123: 267-280.

Van Gauwbergen, D. and Baeyens, J., 1998. Modeling reverse osmosis by irreversible thermodynamics. Separation and Purification Technology, 13: 117-128.

Vrijenhoek, E.M., Hong, S. and Elimelech, M., 2001. Influence of membrane surface properties on initial rate of colloidal fouling of reverse osmosis and nanofiltration membranes. Journal of Membrane Science, 188: 115-128.

Weast, R.C., 1967. Handbook of Physics and Chemistry. Chemical Rubber Pub. Co., Cleveland.

Yazdani, K., 1991. Studies in Separation of Ionic Species by Reverse Osmosis Membranes. Ph.D. Dissertation, University of South Florida.

APPENDICES

APPENDIX A: DIAGRAMS OF THE TEST CELLS

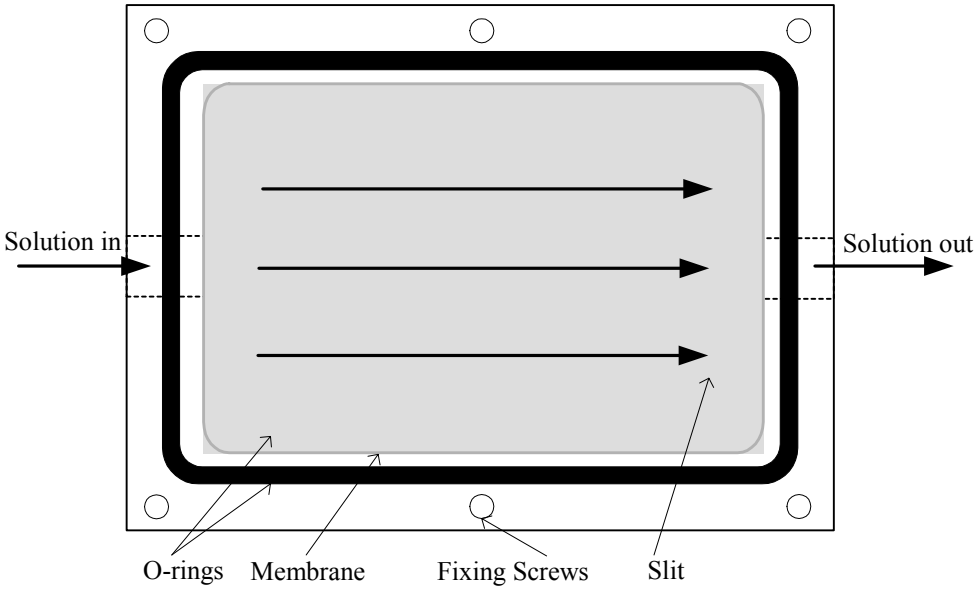

Figure A. 1. DO test cell - top view of the salt solution chamber.

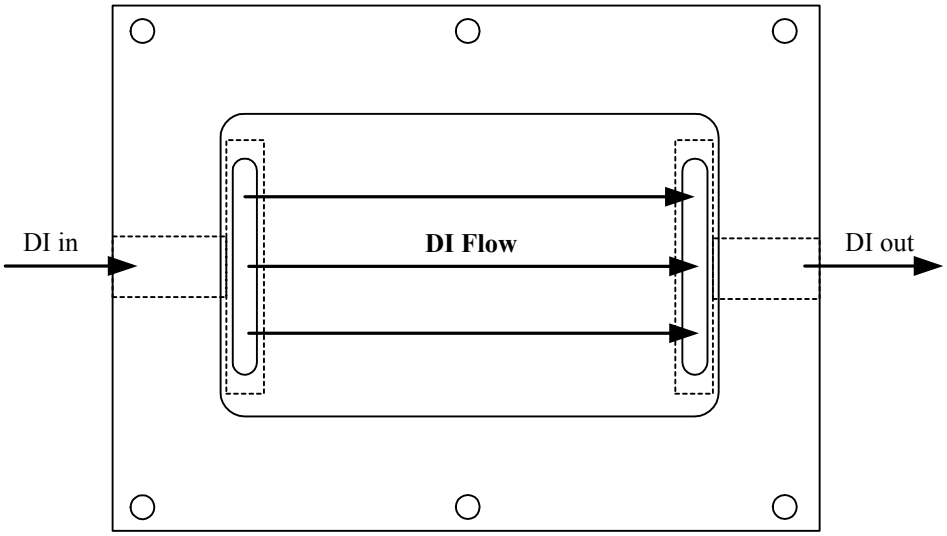

Figure A. 2. DO test cell - top view of the DI water chamber.

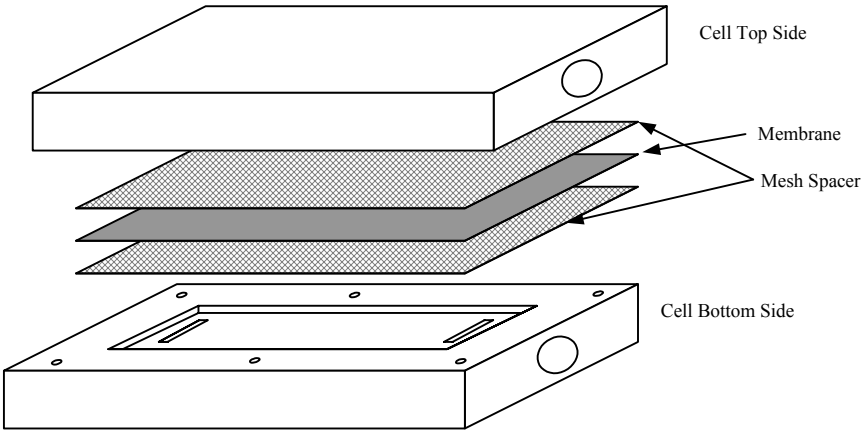

Figure A. 3. DO test cell – assemble view.

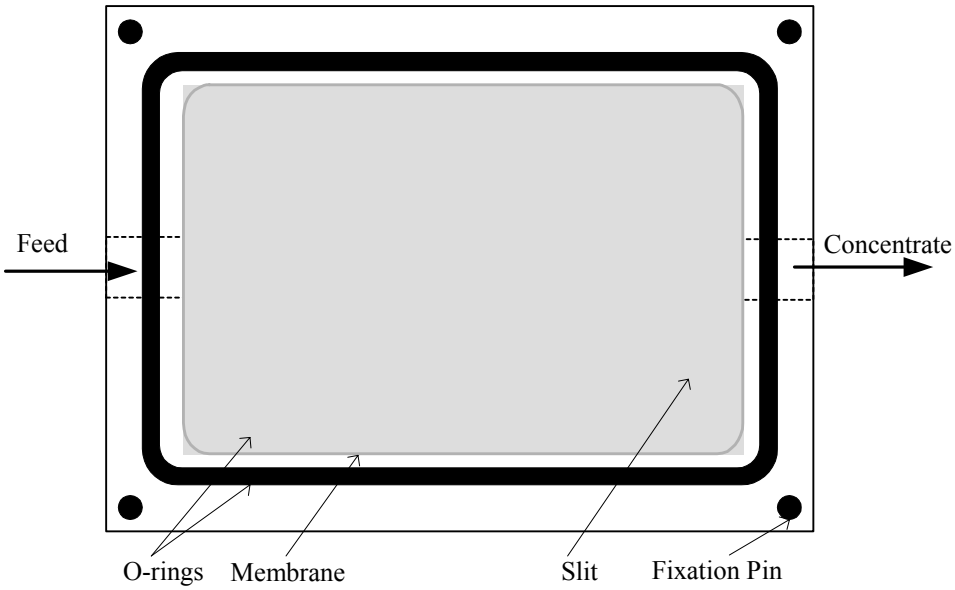

Figure A. 4. RO flat sheet cell - bottom side.

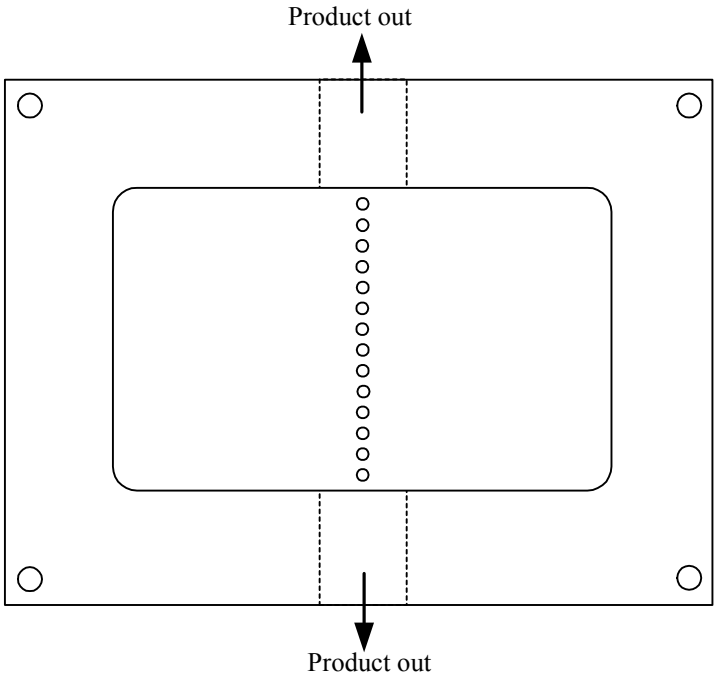

Figure A. 5. RO flat sheet cell - top side.

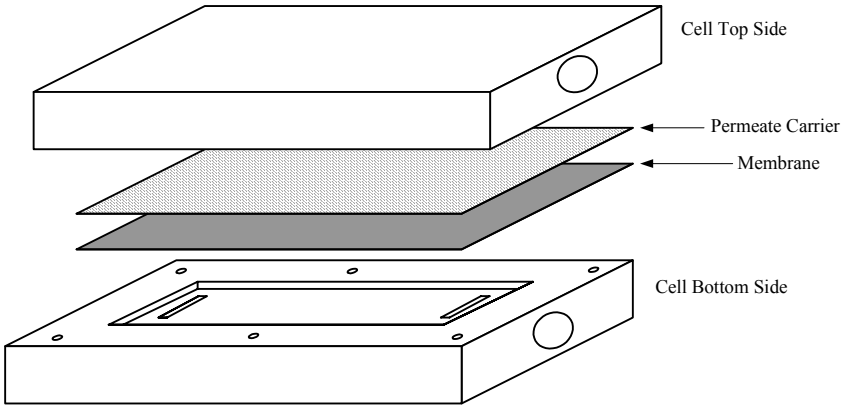

Figure A. 6. RO flat sheet cell –assemble view.

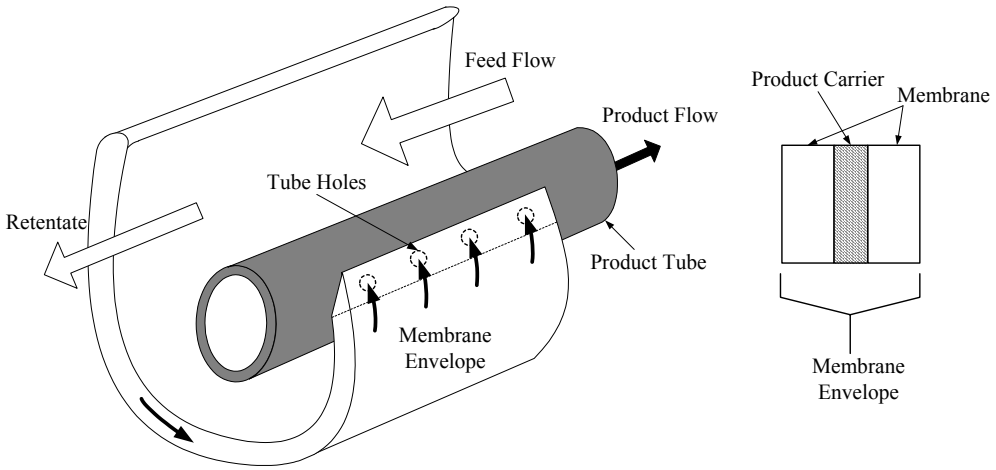

Figure A. 7. Diagram of a spiral wound membrane configuration.

APPENDIX B: EQUATIONS OF THE SALT FLUX IN DO

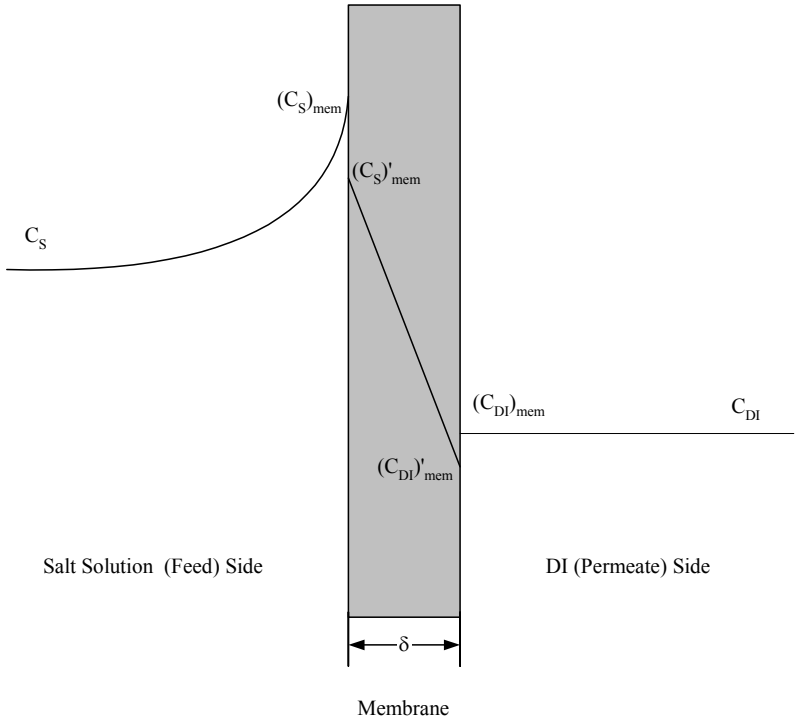

Figure B. 2 Diagram of the salt concentrations across the membrane.

Starting with Fick's law of diffusion represented by Equation B.1,

$$J_S = -D\frac{dC}{dx} \tag{B.1}$$

and using the approximation from Equation B.2 and Equation B.3 in the case of a membrane

$$\frac{dC}{dx} \cong \frac{\left(C_{DI}\right)'_{mem} - \left(C_s\right)'_{mem}}{\delta} \tag{B.2}$$

$$\frac{\left(C_{DI}\right)'_{mem}}{\left(C_{DI}\right)_{mem}} = \frac{\left(C_S\right)'_{mem}}{\left(C_S\right)_{mem}} = \frac{1}{K} \tag{B.3}$$

Equation B.1 becomes Equation B.4:

$$J_s = \left(\frac{D}{K\delta}\right)_{DO}\left((C_s)_{mem} - (C_{DI})_{mem}\right) = \left(\frac{D}{K\delta}\right)_{DO}\left((C_s)_{mem} - C_{DI}\right) \tag{B.4}$$

Using the approximation from Equation B.5 as well as the Equations B.6 and B.7 representing the variation of concentration in time in the solution vessel and in the DI vessel, respectively, Equation B.4 becomes Equation B.8:

$$(C_s)_m \cong C_s \tag{B.5}$$

$$(C_s)_t = (C_s)_{t=0} - \alpha t \tag{B.6}$$

$$(C_{DI})_t = (C_{DI})_{t=0} + \beta t \tag{B.7}$$

$$J_s = \left(\frac{D}{K\delta}\right)_{DO}\left[(C_s - C_{DI})_{t=0} - (\alpha+\beta)t\right] \tag{B.8}$$

$$J_s \equiv \frac{dn}{Sdt} \tag{B.9}$$

Equation B.8 is integrated in time from t = 0 to t = τ, and considering $(D/K\delta)_{DO}$ constant in time, as well as the definition of the molar flux presented in Equation B.9, it results Equation B.10 and Equation B.11

$$\int_{n_{t=0}}^{n_{t=\tau}} \frac{dn}{S} = \left(\frac{D}{K\delta}\right)_{DO}\left[\int_{t=0}^{t=\tau}(C_s - C_{DI})_{t=0}\,dt - \int_{t=0}^{t=\tau}(\alpha+\beta)t\,dt\right] \tag{B.10}$$

$$\frac{\Delta N}{S} = \left(\frac{D}{K\delta}\right)_{DO}\left[(C_s - C_{DI})_{t=0}\tau - \frac{1}{2}(\alpha+\beta)\tau + (\alpha+\beta)\tau^2\right] \tag{B.11}$$

Equation B.10 can be rearranged as Equation 12 which was used in calculating $(D/K\delta)_{DO}$ in the diffusion runs:

$$\left(\frac{D}{K\delta}\right)_{DO} = \frac{\Delta N}{S\left[(C_s - C_{DI})_{t=0}\tau - \frac{1}{2}(\alpha+\beta)\tau + (\alpha+\beta)\tau^2\right]} \tag{B.12}$$

The difference in the total number of moles diffused during a run was calculated using Equation B.13 and Equation B.14:

$$\Delta N = N_{t=\tau} - N_{t=0} = (C_{DI})_{t=\tau}(V_{DI})_{t=\tau} - (C_{DI})_{t=0}(V_{DI})_{t=0} \cong (C_{DI})_{t=\tau}(V_{DI})_{t=\tau} \tag{B.13}$$

$$C_{DI} = \frac{\Gamma_{DI}}{\lambda_{salt}} \tag{B.14}$$

where $(V_{DI})_{t=0}$ and $(V_{DI})_{t=\tau}$ are the volume in the DI water vessel in the beginning and at the end of the experiment, respectively, Γ_{DI} is the conductivity of the DI water, and λ_{salt} is the salt specific conductivity.

APPENDIX C: SALT AND WATER TRANSPORT IN DO

Table C. 1 Comparison of salt permeability for all membranes at 0.05 mol·L^{-1} in direct osmosis experiments.

Salt	$(D/K\delta)_{DO}$ x10^{-7} (cm·s^{-1})			
	SE	AD	CG	CK
LiCl	4.51	1.5	67.1	118
NaCl	6.53	2.2	77.1	133
KCl	8.73	2.6	96.9	165
$MgCl_2$	4.30	0.83	21.9	56.1
$CaCl_2$	5.14	0.91	31.6	63.3
$BaCl_2$	5.99	1.0	33.4	65.5

Table C. 2 Comparison of salt permeability at different concentration for chlorides for the SE membrane in direct osmosis experiments.

Salt	$(D/K\delta)_{DO}$ x 10^{-7} (cm·s^{-1})					
	C_s = 0.01 mol·L^{-1}	C_s = 0.02 mol·L^{-1}	C_s = 0.05 mol·L^{-1}	C_s = 0.1 mol·L^{-1}	C_s = 0.15 mol·L^{-1}	C_s = 0.2 mol·L^{-1}
LiCl	5.27		4.51	3.94		3.37
NaCl	6.75	6.58	6.53	6.13	4.59	3.82
KCl	9.17	8.84	8.73	8.08	7.90	7.02
$MgCl_2$	5.98		4.30	3.74		
$CaCl_2$	6.72		5.14	4.36		
$BaCl_2$			5.99			

Table C. 3 Comparison of salt permeability at different concentration for acetates for the SE membrane in direct osmosis experiments.

Salt	$(D/K\delta)_{DO}$ x 10^{-7} (cm·s^{-1})	
	C_s = 0.05 mol·L^{-1}	C_s = 0.1 mol·L^{-1}
LiAc	4.46	3.29
NaAc	5.28	3.70
KAc	6.05	4.11
$MgAc_2$	3.77	2.75
$CaAc_2$	4.16	3.36

Table C. 4 Comparison of salt permeability for chlorides and acetates at two concentrations for the SE membrane in direct osmosis experiments.

Cation	$(D/K\delta)_{DO}$ x 10^{-7} ($cm \cdot s^{-1}$) At C_s = 0.05 $mol \cdot L^{-1}$		$(D/K\delta)_{DO}$ x 10^{-7} ($cm \cdot s^{-1}$) At C_s = 0.1 $mol \cdot L^{-1}$	
	Chlorides	Acetates	Chlorides	Acetates
Li^+	4.51	4.46	3.94	3.29
Na^+	6.53	5.28	6.13	3.70
K^+	8.73	6.05	8.08	4.11
Mg^{+2}	4.30	3.77	3.74	2.75
Ca^{+2}	5.14	4.16	4.36	3.36

Table C. 5 Comparison of pure water flux for all membranes at 0.05 $mol \cdot L^{-1}$ in direct osmosis experiments.

Salt	$J_{w, DO}$ x 10^{-6} ($g \cdot s^{-1} \cdot cm^{-2}$)							
	SE		AD		CG		CK	
		CV (%)		CV (%)		CV (%)		CV (%)
LiCl	4.75	2.7	5.64	15.1	17.8	0.7	7.26	21.2
NaCl	5.45		7.18		18.5		5.27	
KCl	4.91		7.55		18		5.36	
$MgCl_2$	6.95	0.02	11.7	3.7	31.3	0.1	18.1	0.7
$CaCl_2$	7.02		11.5		31.3		17.9	
$BaCl_2$	6.98		10.5		31		17.4	

Note: CV represents the coefficient of variation calculated as the standard deviation divided to the average.

Table C. 6 Comparison of pure water flux at different concentration for chlorides for the SE membrane in direct osmosis experiments.

Salt	$J_{w, DO}$ x 10^{-6} ($g \cdot s^{-1} \cdot cm^{-2}$)					
	C_s = 0.01 $mol \cdot L^{-1}$	C_s = 0.02 $mol \cdot L^{-1}$	C_s = 0.05 $mol \cdot L^{-1}$	C_s = 0.1 $mol \cdot L^{-1}$	C_s = 0.15 $mol \cdot L^{-1}$	C_s = 0.2 $mol \cdot L^{-1}$
LiCl	1.80		4.75	6.75		8.75
NaCl	1.80	3.22	5.45	6.83	8.72	8.82
KCl	2.25	3.03	4.91	7.05	8.05	10.1
$MgCl_2$	2.47		6.95	10.1		
$CaCl_2$	2.20		7.02	10.0		
$BaCl_2$			6.98			

Table C. 7 Comparison of pure water flux for chlorides and acetates at two concentrations for the SE membrane in direct osmosis experiments

Salt	$J_{w,DO}$ x 10^{-6} ($g \cdot s^{-1} \cdot cm^{-2}$)			
	Cs = 0.05 $mol \cdot L^{-1}$	CV (%)	Cs = 0.1 $mol \cdot L^{-1}$	CV(%)
LiCl	4.75	6.7	6.75	0.9
NaCl	5.45		6.83	
KCL	4.91		7.05	
LiAc	4.32		6.35	
NaAc	4.02		6.60	
KAc	4.07		6.90	
$MgCl_2$	6.95	0.7	10.1	0.9
$CaCl_2$	7.02		10.0	
$MgAc_2$	6.68		9.48	
$CaAc_2$	6.57		9.58	

Note: CV represents the coefficient of variation calculated as the standard deviation divided to the average.

APPENDIX D: SALT REJECTION COEFFICIENT IN RO

Table D. 2 Average over pressure of salt rejection in RO experiments.

Salts	R (%)			
	AD	CG	CK	SW30
LiCl	99.56	84.52	58.99	99.38
NaCl	99.46	83.5	57.82	99.36
KCl	99.36	82.54	55.81	99.24
$MgCl_2$	99.93	95.10	87.92	99.48
$CaCl_2$	99.83	94.78	86.07	99.42
$BaCl_2$	99.82	94.40	85.95	99.40

APPENDIX E: FILM THEORY AND SHERWOOD CORRELATION

E.1 Film theory

In RO membranes, the salt accumulates at the membrane surface, in the region called boundary layer where the concentration is higher than the concentration in the bulk, C_{feed}. The maximum value of the concentration in the boundary layer is at the membrane wall C_{mem}. Due to the differences in the concentrations, the salt diffuses from the boundary layer back to the bulk side. The diffusion is characterized by the diffusivity coefficient D (Figure E.1).

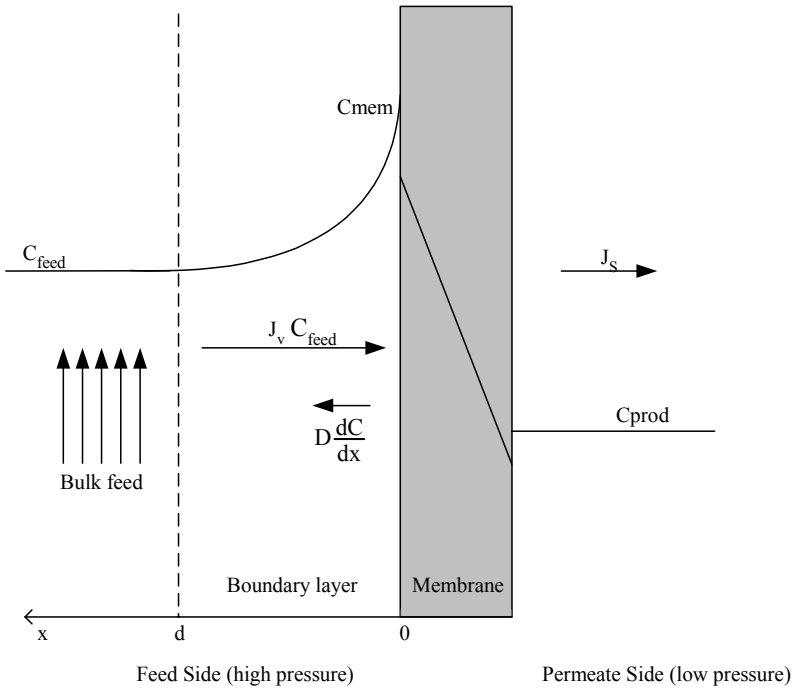

Figure E.1 Schematic diagram of the salt fluxes across RO membranes.

At steady state, the salt convective flux $J_v C_{feed}$ is balanced by the flux of salt that permeates the membrane J_S and the salt diffusive flux from the membrane wall to the bulk (Equation E.1). The boundary conditions are given in Equation E.2.

$$J_S = J_v C_{feed} - D\frac{dC}{dx} \tag{E.1}$$

$$\begin{cases} x = 0 \rightarrow C = C_{mem} \\ x = d \rightarrow C = C_{feed} \end{cases} \tag{E.2}$$

Integrating Equation E.1 with the boundary conditions E.2 it results Equation E.3. The ratio d/D is called the mass transfer coefficient k.

$$\frac{C_{mem} - C_p}{C_{feed} - C_p} = \exp\left(\frac{J_v d}{D}\right) = \exp\left(\frac{J_v}{k}\right) \tag{E.3}$$

E.2 Sherwood correlation

The feed flow in the RO flat sheet cell is in laminar regime with a Reynold number of 667. This is in agreement with findings from the literature for flow in plate module configurations (Prabhakar and Ramani, 1994). In fully developed laminar flow when the concentration boundary layer is developing, the Sherwood correlation is given by Equation (E.4) (Belfort, 1984).

$$k = 0.186\left(\mathrm{Re}\,\mathrm{Sc}\,\frac{d_h}{L}\right)^{0.33} \tag{E.4}$$

where Reynolds number $R_e = vd_h/\nu$ with v = flow velocity (0.313 ms^{-1}), d_h = hydraulic diameter (1.98 x 10^{-3} m), ν = kinematic viscosity (9.27 x 10^{-7} $m^2 s^{-1}$), Schmidt number $S_c = \nu/D$, D = diffusivity coefficient (m^2/s), and L is the length of the flow channel (0.146 m).

APPENDIX F: CONCENTRATION AT THE MEMBRANE WALL FOR SE MEMBRANE AND CORRECTED SALT PERMEABILITIES IN DO

Table F. 1 Concentration at the membrane wall for the SE membrane at different bulk concentrations in direct osmosis experiments.

Salt	C_{mem}^{DO} (mol·L^{-1})					
	C_s = 0.01 mol·L^{-1}	C_s = 0.02 mol·L^{-1}	C_s = 0.05 mol·L^{-1}	C_s = 0.1 mol·L^{-1}	C_s = 0.15 mol·L^{-1}	C_s = 0.2 mol·L^{-1}
LiCl	0.006		0.015	0.021		0.028
NaCl	0.006	0.010	0.017	0.022	0.028	0.028
KCl	0.007	0.010	0.016	0.022	0.026	0.032
LiAc			0.014	0.020		
NaAc			0.013	0.021		
KAc			0.013	0.022		
$MgCl_2$	0.005		0.022	0.032		
$CaCl_2$	0.005		0.022	0.032		
$BaCl_2$			0.022			
$MgAc_2$			0.021	0.030		
CaAc2			0.021	0.030		

Table F. 2 Corrected salt permeability at 0.05 mol·L^{-1} in direct osmosis experiments.

Salts	$(D/K\delta)_{DO}$ x 10^{-7} (cm·s^{-1})			
	SE	AD	CG	CK
LiCl	12	4.49	373	2211
NaCl	17	5.44	411	3383
KCl	29.3	7.20	516	4134
$MgCl_2$	8.1	1.36	130	629
$CaCl_2$	8.63	1.43	148	714
$BaCl_2$	9.02	1.75	159	749

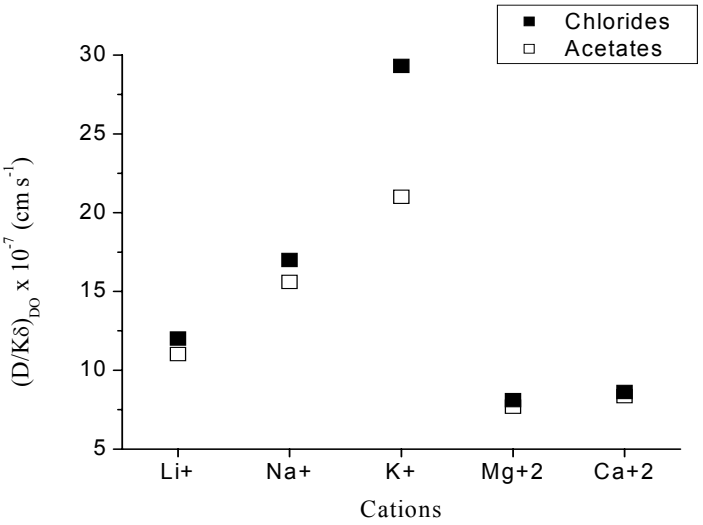

Figure F. 1 Comparison of salt permeability for chlorides and acetates at 0.05 mol·L^{-1} bulk solution concentration after correction in SE membrane in diffusion experiments.

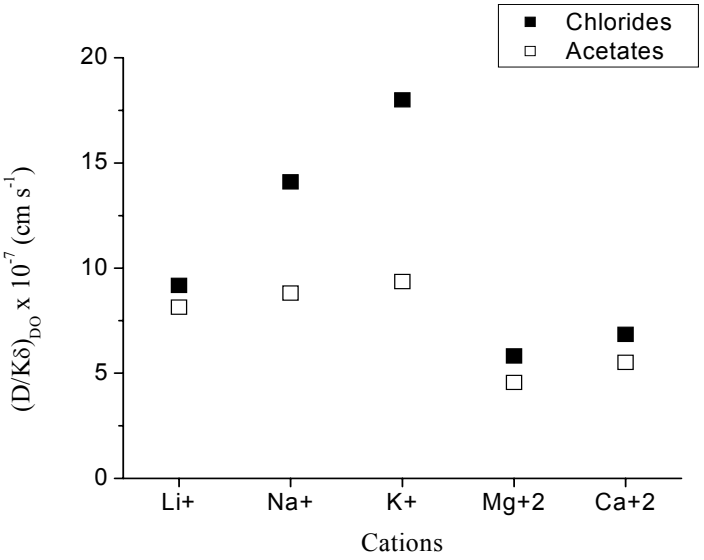

Figure F. 2 Comparison of salt permeability for chlorides and acetates at 0.1 mol·L^{-1} bulk solution concentration after correction in SE membrane in diffusion experiments.

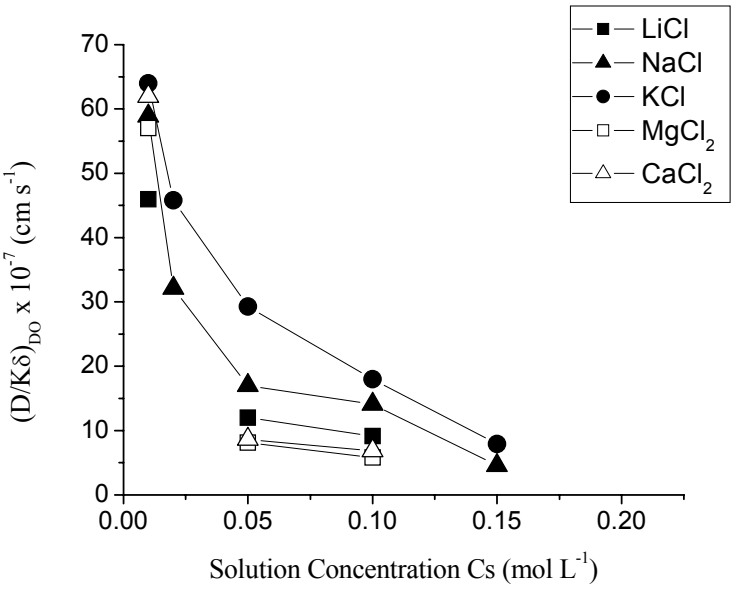

Figure F. 3 Variation of salt permeability with bulk solution concentration after correction in SE membrane for chlorides in diffusion experiments.

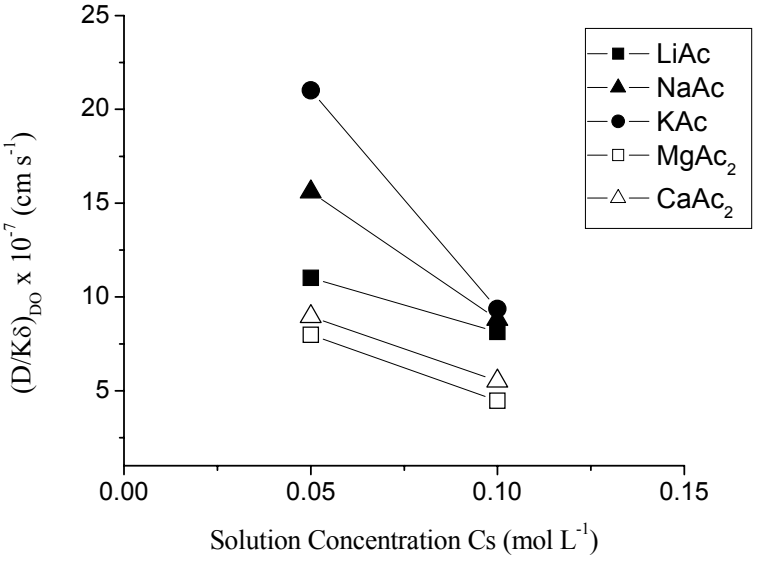

Figure F. 4 Variation of salt permeability with bulk solution concentration after correction in SE membrane for acetates in diffusion experiments.

APPENDIX G: EXPERIMENTAL ERRORS

Table G. 1 Experimental errors for direct osmosis experiments.

Parameter	Equation/Direct measurement	Instrument Nr. (Table 3.1)	Experimental error e
S	Direct measurement	2	≈0 %
τ	Direct measurement	8	≈0 %
C_{DI}, C_S	Direct measurement	3	1 %
T	Direct measurement	10	0.3 %
m_w	Direct measurement	9	≈0 %
Water Volume V_w	Direct measurement	9	≈0 %
$J_{w,\,DO}$	Eq. (3.1)		≈0 %
A'	Same as A in Table G.2		0.45 %
C_{mem}^{DO}	Eq. (5.3)		1.75 %
ΔN	Eq. (B.13)		1 %
$(D/K\delta)_{DO}$	Eq. (5.5)		3.75 %

Table G. 2 Experimental errors for the first case of the SK model in RO flat sheet membrane experiments.

Parameter	Equation/Direct Measurement	Instrument Nr. (Table 3.1)	Experimental error
C_{prod}	Direct measurement	3 and 4	1 %
C_{feed}	Direct measurement	4	1 %
ΔP	Direct measurement	7	0.25 %
Product volume	Direct measurement	12	0.2 %
Product flowrate Q_P	Product volume/time		0.2 %
J_v	Q_P/S		0.2 %
A	$J_v/\Delta P$		0.45 %
ΔC	C_{feed}-C_{prod}		2%
C_{avg}	½ (C_{feed}+C_{prod})		2%
$P_{RO}^{(1)}$	Eq. (2.10)		8.6 %
$\sigma_2^{(1)}$	Eq. (2.10)		5.6 %
$J_{diff}/J_{total}^{(1)}$	$P_{RO}\cdot\Delta C/(C_{prod}\cdot J_v)$		12.8 %
$\sigma_1^{(1)}$	Eq. (2.9)		7.0 %
$L_p^{(1)}$	Eq. (2.9)		8.3 %

Note: $^{(1)}$ Denotes the parameters in the first case of the SK model.

Table G. 3 Experimental errors for the second case of the SK model in RO flat sheet membrane experiments.

Parameter	Equation/Direct Measurement	Experimental error e
C_{mem}^{max}	Eq. (4.7)	2.2 %
ΔC	$C_{mem}^{max} - C_{prod}$	3.2 %
C_{avg}	$\frac{1}{2}(C_{mem}^{max} + C_{prod})$	3.2 %
$P_{RO}^{(2)}$	Eq. (2.10)	9.1%
$\sigma_2^{(2)}$	Eq. (2.10)	4 %
$J_{diff}/J_{total}^{(2)}$	$P_{RO}\cdot\Delta C/(C_{prod}\cdot J_v)$	13.5 %

Notes: 1. $^{(2)}$ Denotes the parameters in the third case of the SK model.
2. C_P, C_F, ΔP, Product volume, Q_P, J_w, J_P, and A are the same as in table G.2.

Table G. 4 Experimental errors for the third case of the SK model in RO flat sheet membrane experiments.

Parameter	Equation/Direct Measurement	Instrument Nr. (Table 3.1)	Experimental error
Volume product	Direct measurement	12	0.2 %
Channel height h	Direct measurement	2	1 %
Channel length L	Direct measurement	2	≈0 %
Channel width l	Direct measurement	2	≈0 %
Channel cross Area	$h\cdot l$		1 %
d_h	$2hl/(h+l)$		2 %
Velocity v	$Q_F/h\cdot l$		4 %
k	Eq. (4.8)		2.64 %
C_{mem}^{k}	Eq. (4.9)		5.84 %
ΔC	$C_{mem}^{k} - C_{prod}$		6.84 %
C_{avg}	$\frac{1}{2}(C_{mem}^{k} + C_{prod})$		6.84 %
$P_{RO}^{(3)}$	Eq. (2.10)		10.4 %
$\sigma_2^{(3)}$	Eq. (2.10)		6.6 %
$J_{diff}/J_{total}^{(3)}$	$P_{RO}\cdot\Delta C/(C_{prod}\cdot J_v)$		18.4 %
$\sigma_1^{(3)}$	Eq. (2.9)		6.2 %
$L_p^{(3)}$	Eq. (2.9)		6.8 %

Notes: 1. $^{(3)}$ Denotes the parameters in the third case of the SK model.
2. C_{prod}, C_{feed}, ΔP, Q_P, and J_v are the same as in Table G.2.

Table G. 5 Experimental errors for KS model in RO flat sheet membrane experiments.

Parameter	Equation/Direct Measurement	Experimental error
R	$1-C_{prod}/C_{feed}$	2 %
Jv	Eq. (2.13)	3.2 %
C_{mem}	Eq. (2.14)	2.5 %
$(D/K\delta)_{RO}$	Eq. (2.15)	8.7 %

Note: C_{prod}, C_{feed}, ΔP, Q_P, $J_{v,}$ and A are the same as in Table G.2.

Table G. 6 Total error for the salt and water parameters in all experiments.

Parameter	Experimental error e	Standard deviation of duplicates STD	Total error $E^{(*)}$
A	0.5 %	12.3 %	13.1 %
$(D/K\delta)_{DO}$	3.8 %	13.2 %	13.7 %
$(D/K\delta)_{RO}$	8.7 %	16.6 %	18.7 %
$J_{diff}/J_{total}^{(1)}$	12.8 %	11.1 %	16.9 %
$J_{diff}/J_{total}^{(2)}$	13.5 %	11.9%	18 %
$J_{diff}/J_{total}^{(3)}$	18.4 %	5.3 %	19.1 %
$L_p^{(1)}$	8.3 %	8.9 %	12.2 %
$L_p^{(3)}$	6.8 %	13.1 %	14.8 %
$P_{RO}^{(1)}$	8.6 %	9.7 %	13 %
$P_{RO}^{(2)}$	9.1 %	15.2 %	17.7 %
$P_{RO}^{(3)}$	10.4 %	12.9 %	16.6 %
$\sigma_1^{(1)}$	7.0 %	6.7 %	9.7 %
$\sigma_1^{(3)}$	6.2 %	8.8 %	10.8 %
$\sigma_2^{(1)}$	5.6 %	3.8 %	6.8 %
$\sigma_2^{(2)}$	4 %	12.9 %	13.5 %
$\sigma_2^{(3)}$	6.6 %	4.6 %	8.0 %

Notes: 1. $^{(1)}$ Denotes the parameters in the second case of the SK model
2. $^{(2)}$ Denotes the parameters in the second case of the SK model.
3. $^{(3)}$ Denotes the parameters in the third case of the SK model.
4. $^{(*)}$ Calculated as $E(\%) = \sqrt{e^2(\%) + STD^2(\%)}$ (Taylor, 1997). It does not include the operator's error and the systematic errors.

APPENDIX H: PHYSICAL AND THERMODYNAMIC PROPERTIES OF IONS

Table H. 1 Physical parameters of cations.

Cation	R_i (Å) [(1)]	R_h (Å)[(1)]	D_w x10^{-5} ($cm^2 \cdot s^{-1}$)[(2)]	D_w x10^{-5} ($cm^2 \cdot s^{-1}$)[(3)]	$-\Delta H_{cation}$[(4)] ($kJ \cdot mol^{-1}$)	$-\Delta S_{cation}$[(5)] ($kJ \cdot mol^{-1}$)
Li^+	0.60	3.82	1.37	1.06	515	119
Na^+	0.95	3.58	1.61	1.20	405	89
K^+	1.33	3.31	1.99	1.40	321	51
Mg^{2+}	0.65	4.28	1.25	0.92	1922	268
Ca^{2+}	0.99	4.12	1.34	0.97	1592	209
Ba^{2+}	1.35	4.04	1.39	0.99	1304	159

Notes: [(1)] (Conway, 1981)
[(2)] For chloride salts (Sourirajan, 1970)
[(3)] For acetate salts (Cussler, 1997)
[(4)] (Burgess, 1988)
[(5)] (Chang, 2000)

Table H. 2 Hydration number calculated from different methods.

Cation	From Mobility[(1)]		From Activity[(2)]	From Entropy[(3)]	From Diffusion[(3)]	From Water Transport[(4)]
	Min	Max				
Li^+	3.5	7	7.1	5	5	22
Na^+	2	4	3.5	4	3	13
K^+	-	-	1.9	3	1	7
Mg^{2+}	10.5	13	13.7	13	9	36
Ca^{2+}	7.5	10.5	-	10	9	29
Ba^{2+}	5	9	-	8	8	28
Cl^-	-	-	-	3	-	5

Notes: [(1)] (Conway, 1981)
[(2)] (Bockris and Reddy, 1970)
[(3)] (Burgess, 1988)
[(4)] (Rutgers and Hendrikx, 1962)

APPENDIX I: FREE ENERGY PARAMETERS

Table I. 1 The corrections of ionic radii, the parameter E, and the ionic free energy in the bulk solution.

Cation	$\Delta_S^{(1)}$ m x 10^{-10}	$E_S^{(1)}$ m·kJ·mol^{-1}	$\Delta G_s^{(1)}$ kJ·mol^{-1}
Li^+	0.89	762	-517
Na^+	0.89	762	-412
K^+	0.89	762	-338
Mg^{2+}	1.01	3124	-1907
Ca^{2+}	1.01	3124	-1594
Ba^{2+}	1.01	3124	-1321

Note: (1) [Friedman, 1973 #35]

Table I. 2 The corrections of ionic radii and the parameter E at the membrane surface, the free energy at the membrane surface.

Seawater membrane SE			
Cation	Δ_{mem} (m x 10^{-10})	E_{mem} (m·kcal·mol^{-1} x 10^{10})	ΔG_{mem} (kcal·mol^{-1})
Li^+	0.84	171	-118
Na^+			-95
K^+			-78
Mg^{2+}	1.01	746	-449
Ca^{2+}			-373
Ba^{2+}			-316
Seawater membrane AD			
Cation	Δ_{mem} (m x 10^{-10})	E_{mem} (m·kJ·mol^{-1} x 10^{10})	ΔG_{mem} (kcal·mol^{-1})
Li^+	0.86	174	-119
Na^+			-96
K^+			-79
Mg^{2+}	1.01	745	-449
Ca^{2+}			-373
Ba^{2+}			-316
Brackish water membrane CG			
Cation	Δ_{mem} (m x 10^{-10})	E_{mem} (m·kJ·mol^{-1} x 10^{10})	ΔG_{mem} (kcal·mol^{-1})
Li^+	0.87	177	-120
Na^+			-97
K^+			-81
Mg^{2+}	1.01	745	-449
Ca^{2+}			-373
Ba^{2+}			-316

Table I. 2 (continued) The corrections of ionic radii and the parameter E at the membrane surface, and the free energy at the membrane surface.

Nanofiltration membrane CK			
Cation	Δ_{mem} ($m \times 10^{-10}$)	E_{mem} ($m \cdot kJ \cdot mol^{-1} \times 10^{10}$)	ΔG_{mem} ($kcal \cdot mol^{-1}$)
Li^+	0.88	180	-121
Na^+			-98
K^+			-81
Mg^{2+}	1.016	750	-450
Ca^{2+}			-374
Ba^{2+}			-317
Seawater membrane SW30			
Cation	Δ_{mem} ($m \times 10^{-10}$)	E_{mem} ($m \cdot kJ \cdot mol^{-1} \times 10^{10}$)	ΔG_{mem} ($kcal \cdot mol^{-1}$)
Li^+	0.88	179	-121
Na^+			-98
K^+			-81
Mg^{2+}	1.01	744	-449
Ca^{2+}			-373
Ba^{2+}			-316

ABOUT THE AUTHOR

Silvana Melania Stefania Ghiu received her BSc in Physics in 1995 from the University of Bucharest, Romania, with a specialization in Physics and Protection of the Environment. She received her first MSc degree in Atmospheric Physics in 1996 from the same university, and her second MSc in Environmental Science and Policy in 1997 from the Central European University, Hungary.

She is the recipient of George Soros Foundation Fellowship for completion of MSc studies and Channabasappa Memorial Scholarship offered by the International Desalination Association. During her PhD program at University of South Florida, she has authored two publications in Desalination Journal, and five articles in conference proceedings. She has presented papers or posters on RO desalination to nine conferences. Her research interests are in separation technologies with hyperfiltration membranes.